DEVELOPMENT AND EXPERIMENTAL TESTING OF PRESS-BRAKE-FORMED STEEL TUB GIRDERS FOR SHORT SPAN BRIDGE APPLICATIONS

Karl E. Barth, Ph.D.
Gregory K. Michaelson, Ph.D.
Pavlo Kozhokin

VOLUME III: EVALUATION OF MODULAR PRESS-BRAKE-FORMED TUB GIRDERS WITH UHPC JOINTS

Submitted to the AISI Steel Market
Development Institute Short Span
Steel Bridge Alliance

ABSTRACT

EVALUATION OF MODULAR PRESS-BRAKE-FORMED TUB GIRDERS WITH UHPC JOINTS

The Short Span Steel Bridge Alliance (SSSBA) is a group of bridge and culvert industry leaders (including steel manufacturers, fabricators, service centers, coaters, researchers, and representatives of related associations and government organizations) who have joined together to provide educational information on the design and construction of short span steel bridges in installations up to 140 feet in length. From within the SSSBA technical working group, a modular, shallow press-brake-formed steel tub girder was developed. This new technology consists of cold-bending standard mill plate width and thicknesses to form a trapezoidal box girder. The steel plate can either be weathering steel or galvanized steel, each an economical option. Once the plate has been press-brake formed, shear studs are then welded to the top flanges. A reinforced concrete deck is then cast on the girder in the fabrication shop and allowed to cure, becoming a composite modular unit. The composite tub girder is then shipped to the bridge site, allowing for accelerated construction and reducing traffic interruptions.

The use of prefabricated bridge elements and systems has led to the recognition that durable connections are the key components in this type of construction. An ultra-high performance concrete (UHPC), which is a steel fiber reinforced, portland cement-based product with advantageous fresh and hardened properties is used for creating robust connections between the prefabricated components. The use of the UHPC as a joint media is becoming more popular during bridge construction. However, the majority of the prefabricated bridge elements and systems are of traditional structural shapes. Therefore, structural performance of the UHPC joint connecting prefabricated composite tub girders needs to be evaluated.

The scope of this project was to test a bridge model system comprised of two composite modular press-brake-formed tub girders connected with an UHPC joint. This was accomplished by, constructing two modular units and joining them with an UHPC joint. The system was then fatigue loaded simulating 75-year traffic conditions in a rural environment. A Service II limit state moment was induced into the system at predetermined numbers of cycles in order to monitor performance of the specimen. Data obtained from strain gages installed on the webs and bottom flanges was used to determine the actual moments induced into the system, as well as the load distribution factors. Experimental results were used to evaluate reliability of the longitudinal UHPC joint in a composite tub girder system.

TABLE OF CONTENTS

LIST OF TABLES

LIST OF FIGURES

CHAPTER 1: INTRODUCTION

1.1 BACKGROUND / OVERVIEW

The Short Span Steel Bridge Alliance (SSSBA) is a group of bridge and culvert industry leaders (including steel manufacturers, fabricators, service centers, coaters, researchers, and representatives of related associations and government organizations) who have joined together to provide educational information on the design and construction of short span steel bridges in installations up to 140 feet in length. From within the SSSBA technical working group, a modular, shallow press-brake-formed steel tub girder was developed. This new technology consists of cold-bending standard mill plate width and thicknesses to form a trapezoidal box girder. The steel plate can either be weathering steel or galvanized steel, each an economical option. Once the plate has been press-brake formed, shear studs are then welded to the top flanges. A reinforced concrete deck is then cast on the girder in the fabrication shop and allowed to cure, becoming a composite modular unit. The composite tub girder is then shipped to the bridge site, allowing for accelerated construction and reducing traffic interruptions (Michaelson 2014).

The use of prefabricated bridge elements and systems has led to the recognition that durable connections are the key components in this type of construction. An ultra-high performance concrete (UHPC), which is a steel fiber-reinforced, cementitious-based material, is used for creating robust connections between the prefabricated components (FHWA EDC-3 2015). The use of UHPC as a joint media is becoming more popular during bridge construction, however, the majority of the prefabricated bridge elements are of traditional structural shapes. Therefore, structural performance of the UHPC joint connecting two prefabricated composite tub girders needs to be evaluated.

1.2 PROJECT SCOPE & OBJECTIVES

The scope of this project was to test a bridge model system comprised of two composite modular press-brake-formed tub girders connected with an UHPC joint. This was accomplished by, constructing two modular units and joining them with an UHPC joint. The system was then fatigue loaded simulating 75-year traffic conditions in a rural environment. A Service II limit state moment was induced into the system at predetermined numbers of cycles in order to monitor performance of the specimen. Data obtained from strain gages installed on the webs and bottom flanges near the midspan was used to determine the resulting moments induced into the system, as well as load distribution factors. Experimental results were used to evaluate reliability of the longitudinal UHPC joint in a composite tub girder system.

1.3 REPORT ORGANIZATION

A brief overview of the organization of this report is as follows:

- Chapter 2:
    - This chapter provides a general overview of the accelerated bridge construction (ABC) details. It outlines two of the most commonly used substructure systems in ABC, as well as a technology called the “link slab” that allows for an efficient connection of the prefabricated elements and systems of the superstructure. This chapter describes the I-93 Fast 14 project, where the ABC technology allowed fourteen bridges in Medford, MA to be replaced in one summer. Also included in this chapter is an overview of the previously conducted UHPC joint research, and projects where this technology had been used.
- Chapter 3:
    - This chapter contains an overview of the experimental work conducted in the effort to prepare the concrete slab edges for the installation of the UHPC joint.

- Chapter 4:
    - This chapter describes the experimental testing conducted for this research. This includes namely the assembly of two composite modular units, the installation of the UHPC longitudinal joint, and testing methods and procedures.
- Chapter 5
    - This chapter introduces and discusses the results obtained during the testing. Methods used for the data analysis and a general overview of obtained live load distribution factors are described in this section.
- Chapter 6
    - This chapter provides a summary of the project, and recommendations for future work.
- Appendix A
    - This appendix describes calculations of Service II and Fatigue I moments.
- Appendix B
    - This appendix documents the experimental gage data obtained during the testing.

CHAPTER 2: LITERATURE REVIEW

2.1 INTRODUCTION

Presented in this chapter is a general overview of several accelerated bridge construction (ABC) methods. This chapter outlines two of the most commonly used substructure systems in ABC, as well as a technology called the "link slab" that allows for an efficient connection of the prefabricated elements and systems of the superstructure. This chapter also describes the I-93 Fast 14 project, where ABC technology allowed for the replacement of fourteen bridges in Medford, MA in one summer. Finally, in this chapter includes an overview of the previously conducted UHPC joint research, and projects where this technology had been used.

2.2 ACCELERATED BRIDGE CONSTRUCTION

In 2009, the Federal Highway Administration (FHWA) launched the Every Day Counts (EDC) program in cooperation with the American Association of State and Highway and Transportation Officials (AASHTO) to speed up the delivery of highway projects and to address the challenges presented by limited budgets. Since its launch in 2009, the EDC initiative has encouraged the adoption of proven technologies and business practices that enable state and local agencies achieve more, while spending less time and money. The name "Every Day Counts" captures the public's need for better transportation infrastructure delivered faster with less delays (FHWA EDC-2). ABC methods were employed to enable faster transportation infrastructure construction. ABC uses innovative planning, design, materials, and construction methods in a safe and cost-effective manner to reduce the onsite construction time that occurs when building new bridges or replacing and rehabilitating existing bridges (Culmo 2011).

Rapid construction concepts have long been used by the railroad industry to avoid service interruption. However, such innovations in highway bridge construction have been limited. The main reason for this restraint is that the expansion of the country's infrastructure system over the past 50 years involved building bridges and roads where elongated construction time did not represent any significant problems. However, with a significant number of bridges approaching or

surpassing their design life, bridge replacement is becoming a major focus of the bridge construction industry. Many of these bridges are located in congested areas where traditional methods of bridge construction are no longer suitable or economical (Structure 2005).

Utilizing ABC methods can help meet the Every Day Counts objectives. ABC decreases the total project delivery time by reducing on-site construction duration. Shortening the construction duration results in less exposure, and therefore contributes to the safety of the construction workers and the traveling public. Long detours, costly use of temporary structures, remote site locations, and limited construction periods present opportunities where the use of ABC methods can provide more practical and economical solutions to those offered if conventional construction methods were used. The advantages of using ABC are that it improves: site constructability, material quality and product durability, and work-zone safety for the traveling public and contractor personnel. Additional benefits of ABC include minimization of environmental impacts, and reduction of impacts to existing roadway alignment.

Two parameters are used in order to quantify the effectiveness of ABC: onsite construction time and mobility impact time. The onsite construction time is the period of time from when a contractor alters the project site location until all construction-related activity is removed. This includes, but is not limited to, the removal of maintenance of traffic items, construction materials, equipment, and personnel. Mobility impact time is the period of time the traffic flow of the transportation network is reduced due to onsite construction activities (Culmo 2011).

2.3 PREFABRICATED BRIDGE ELEMENTS AND SYSTEMS

There is no one set of techniques that is used in ABC. Instead, there is a family of construction methods that are employed during the majority of ABC projects. Prefabricated bridge elements and systems (PBES) is one strategy that can meet the objectives of accelerated bridge construction. PBES are structural components of a bridge that are built offsite, or near the site of the bridge, and include features that reduce the onsite construction time and mobility impact time that occur from conventional construction methods. Because PBES are built off the critical path and under controlled environmental conditions, improvements in safety, quality, and long-term durability can be better achieved (Culmo 2011).

2.4 SUBSTRUCTURES

2.4.1 Precast Abutments

One of the most commonly used ABC substructure systems is the integral or semi-integral precast abutments. This type of substructure contains voids within its stem formed by the corrugated metal pipes. The voids are aligned with the driven steel piles and grouted to complete the connection as shown in Figure 2.1.

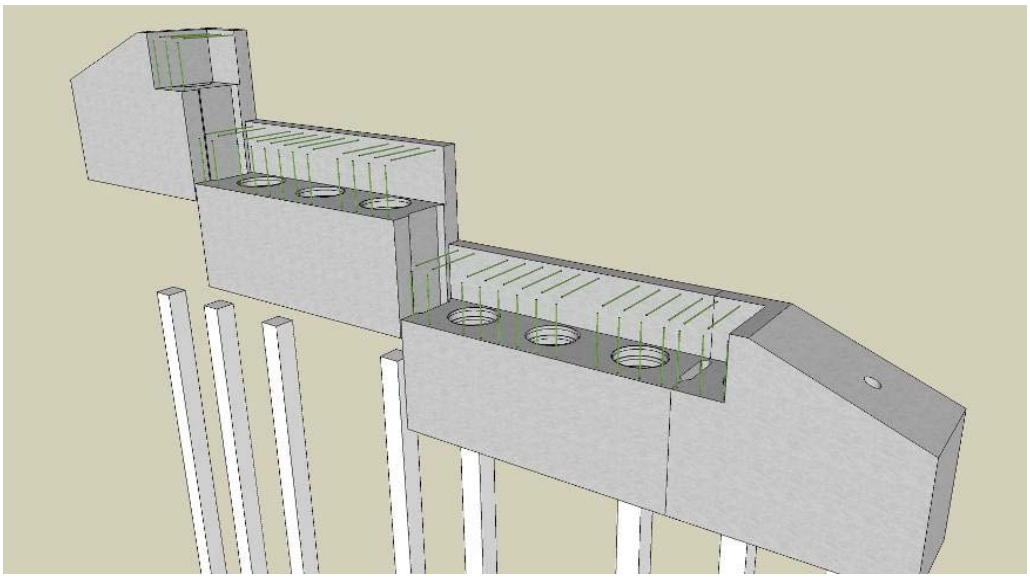

Figure 2.1: Prefabricated Integral Abutment (Culmo, 2011)

There are two major advantages for the use of integral abutments. Integral abutments do not have deck joints, which eliminates one of the most common deterioration areas on bridges. Also, integral abutments transfer the embankment soil forces into the bridge superstructure. The superstructure has tremendous available capacity for axial load; therefore this usually has no effect on the superstructure design. Integral abutments are normally supported on a single row of piles that are designed to move with the bridge during thermal cycles and rotate with the beam ends under live load. The result of this approach is that the abutment does not need a spread footing or multiple rows of piles to resist the overturning soil forces. Several states use semi-integral abutments where the backwall is integral with the beams and is located at the end of the beams.

The backwall is simply cantilevered and lapped behind the abutment stem. Figure 2.2 shows a detail of this approach (Culmo 2011).

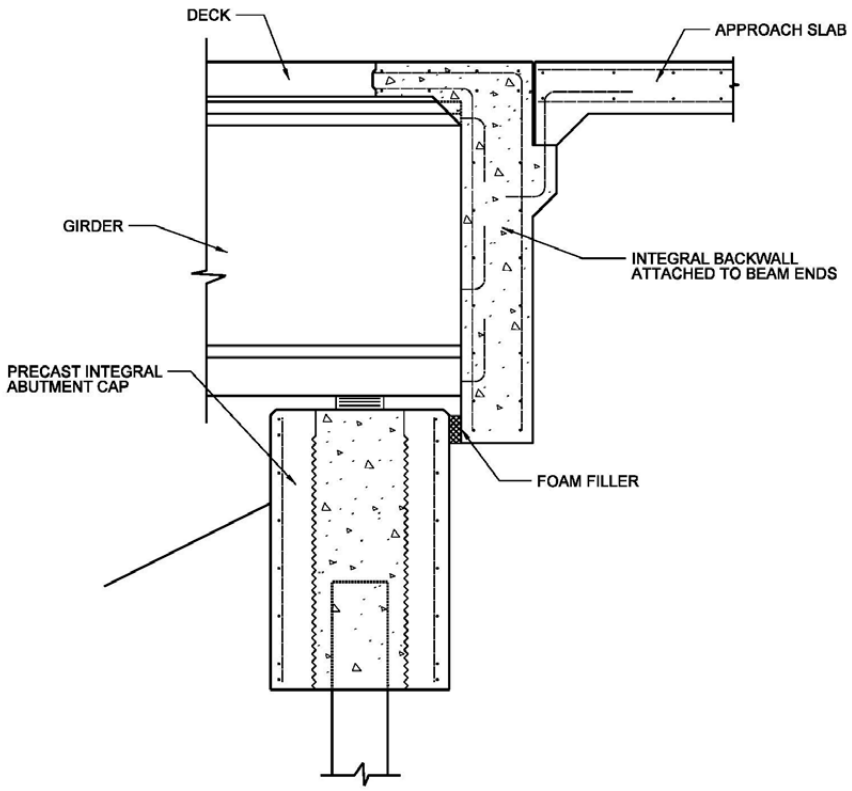

Figure 2.2: Semi-Integral Abutment Detail (Culmo, 2011)

2.4.2 GRS-IBS Substructure System

2.4.3 2.4.2 GRS-IBS Substructure System

Another effective substructure system in ABC is the Geosynthetic Reinforced Soil – Integrated Bridge System (GRS-IBS). GRS technology consists of closely spaced layers of geosynthetic reinforcement and compacted granular fill material. GRS-IBS includes a reinforced soil foundation, a GRS abutment, and a GRS integrated approach. When integrated with a bridge superstructure, the system combines the embankment with the superstructure to act as a single unit with respect to settlement (Culmo 2011).

The GRS – IBS provides an economical solution to accelerated bridge construction. GRS-IBS is a fast, cost-effective method of bridge support that combines the roadway into the superstructure to create a jointless interface between the bridge and the approach. Figure 2.3 shows a cross-section of a GRS abutment.

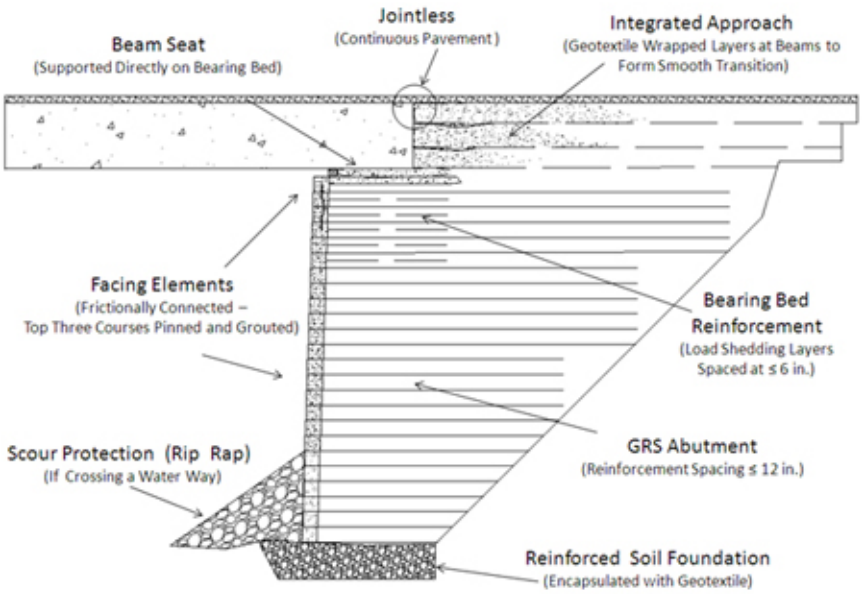

Figure 2.3: GRS-IBS Cross-Section (Adams, 2011)

GRS-IBS consists of three main components: the reinforced soil foundation (RSF), the abutment, and the integrated approach. The RSF is composed of granular fill material that is compacted and encapsulated with a geotextile fabric. It provides embedment and increases the bearing width and capacity of the GRS abutment. It also prevents water from infiltrating underneath and into the GRS mass from a river or stream crossing. This method of using geosynthetic fabrics to reinforce foundations is a proven alternative to deep foundations on loose granular soils, soft fine-grained soils, and soft organic soils. The abutment uses alternating layers of compacted fill and closely spaced geosynthetic reinforcement to provide support for the bridge, which is placed directly on the GRS abutment without a joint and without cast-in-place (CIP) concrete. GRS is also used to construct the integrated approach to transition to the superstructure. This bridge system therefore alleviates the "bump at the bridge" problem caused by differential settlement between bridge abutments and approach roadways (Adams 2011).

According to the FHWA, the GRS abutments built with a reinforcement spacing less than or equal to 12 inches, behave as a composite mass with predictable behavior. These types of abutments can be built to economically support a bridge superstructure bearing directly on the reinforced soil behind the facing blocks. GRS can be used to integrate the superstructure with the approach and substructure to create a jointless bridge system.

A degree of composite behavior results from reinforcement frequency. For larger-spaced reinforced soil systems, the composite behavior is reduced with increased reinforcing spacing. The reinforcing spacing is not the only factor impacting the composite behavior of a GRS substructure. The aggregate size and friction angle are also contributing factors.

A closer reinforcement spacing creates more soil-geosynthetic interaction. In GRS, the reinforcement not only serves to resist tensile forces but also functions to restrain lateral deformation of the soil, increase lateral confinement of the soil, generate apparent cohesion in a granular fill (while maintaining all desirable characteristics of granular soil), suppress dilation of the soil, enhance compaction-induced stresses, increase ductility of the soil mass, and reduce migration of fines, depending on the reinforcement type selected. These added benefits develop because of the close reinforcement spacing. Figure 2.4 illustrates the load-carrying capacity of GRS with a typical spacing of 8 inches.

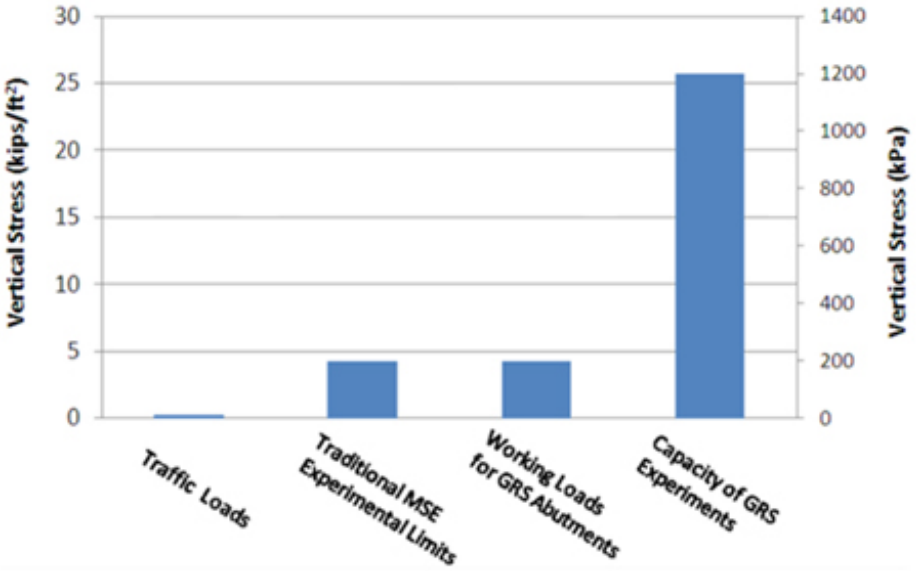

Figure 2.4: Comparison of Surcharges on MSE and GRS structures (Adams, 2011)

As shown in Figure 2.4, the available capacity of a GRS abutment is significantly higher that the traditionally mechanically stabilized earth (MSE) substructures (Adams 2011).

According to the Federal Highway Administration Every Day Counts Final Report (EDC-2) dated March 2015, 31 states had used the GRS-IBS systems, and six states consider GRS-IBS use a mainstream practice. An example of successful implementation of the GRS-IBS is the replacement of the State Route 7A bridge over the Housatonic Railway in Sheffield, MA. MassDOT saved 49 percent of the $1.1 million estimated project cost by using the GRS system versus conventional construction (FHWA EDC-2 2015).

2.5 SUPERSTRUCTURES

Superstructure PBES include beam elements, deck elements, truss/arch systems and others. Cost and performance analysis is used in the design phase to deliver the most cost effective and durable products. A variety of techniques have been developed in an attempts to reduce the project costs.

2.5.1 Link Slab

Two common methods employed in ABC for multiple-span bridges are installation of multiple simple spans between the supports, or the use of continuous-span beams. Conventional simple span bridges require an expansion joint at each pier. It is believed that leakage in this type of joints leads to bridge elements' deterioration. However, simple span construction does not require field splicing, which simplifies the erection of a bridge. A continuous-span beam does not require a deck expansion joint, and it also requires less steel than simple-span beam construction. Leakage in the expansion joints has been addressed by making bridge decks jointless or using concrete pours at the interior joints to eliminate the need for an expansion joint. One method that has been developed in order to eliminate deck joints in simple-span bridges is known as "link slab". A "link slab" is poured over a pier to link two spans. The slab is designed to accommodate for girder rotation. This is accomplished by de-bonding concrete from the steel at the interior

supports. Approximately five percent of the span length is de-bonded on each side of the support as shown in Figure 2.5.

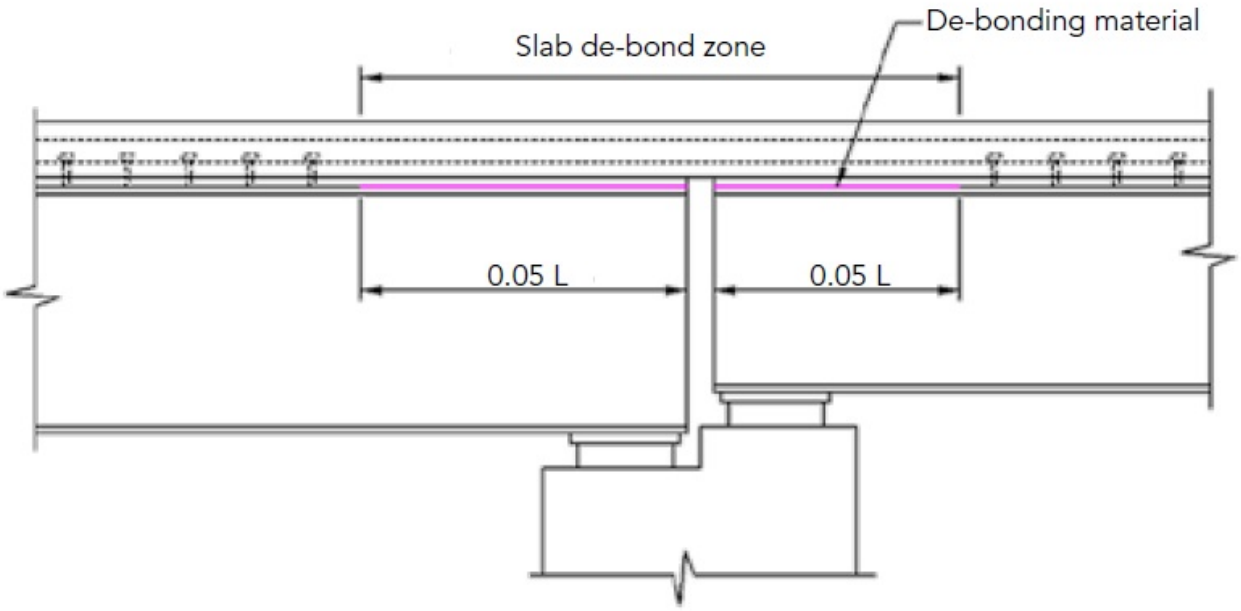

Figure 2.5: Link Slab Configuration (Culmo, 2014)

The link slabs are not a form of continuity; therefore the negative bending moments are far less than those in continuous girder bridges. The reinforcing is designed to resist cracking.

Less steel is required in a continuous-span type construction. However, when costs of erection, splicing, shoring, and reinforcing are compared between the two methods, the simple-span bridge may result in a more economical option, and therefore should be considered during design (Culmo 2014).

2.5.2 I-93 Fast 14

I-93 is a major interstate that takes drivers in and out of Boston. It was built in the 1950's, and did not need major repairs until the summer of 2010 when a bridge deck collapsed in Medford, MA. MassDOT decided to replace fourteen deteriorated bridges in Medford on I-93. ABC techniques were used on this project, allowing for over-the-weekend 55-hour bridge replacement.

Fourteen bridges were replaced over ten weekends (MassDOT). The concept development and preliminary design were completed within two months. There were four alternatives that were considered during the initial design phase. The first alternative was a self-propelled modular transporter bridge to be slid-in place. This option was ruled out due to the difficulty of installing multi-span bridges over a weekend using this method, as well as the congested area of the project. The second alternative was to use precast northeast extreme tee (NEXT) beams. This option was ruled out due to span limitations, difficulty with span-to-depth ratios, weight of the section, and a degree of skew on several bridges. The third alternative was to use new beams with separate precast concrete decks. This option was also ruled our due to skew issues and a concern about construction of a four span bridge in one weekend. The fourth alternative using modular steel stringer/girder systems was accepted. This type of superstructure had the same weight as the existing deck, and was very adaptable for different geometries.

The next step was to select deck connections. The alternatives for the connections were: small closure pours with straight bars and UHPC, medium closure pours with hooked bars and grout, or wider pours with lapped bars and high early strength concrete. The wide pour option was chosen which allowed for reduced width of the precast decks, and allowed room for other adjustments. I-93 Fast 14 was a successful ABC project completed over ten weekends in the summer of 2011 (Culmo).

2.6 ULTRA-HIGH PERFORMANCE CONCRETE (UHPC)

An ultra-high performance concrete (UHPC) is a fiber reinforced, portland cement-based product with advantageous fresh and hardened properties. Through the appropriate combination of advancements in superplasticizers, dry constituent gradation, fiber reinforcements, and supplemental cementitious materials, UHPC is able to deliver performance that far exceeds conventional concrete. The mechanical properties of UHPC include compressive strength greater than 21.7 ksi, and sustained post cracking tensile strength greater that 0.72 ksi. (Graybeal 2014). UHPC can be used in a variety of applications including building a new bridge or rehabilitating an existing one.

2.6.1 Background

Developed in the late 20th century, UHPC has emerged as a capable replacement for conventional structural materials in a variety of applications (Graybeal 2014). The FHWA began investigating the use of UHPC for highway infrastructure in 2001 and has been working with State transportation departments to deploy the technology since 2002. This work has led to the use of UHPC in several bridge applications, including precast, prestressed girders; precast waffle panels for bridge decks; and as a joint material between precast concrete deck panels and girders, and between the flanges of adjacent girders. Countries all over the world have researched and implemented the UHPC technology since the late 20th century. (Graybeal and Russell 2013).

2.6.2 UHPC Properties

The UHPC used most often in North America for both research and in practical applications is a commercial product known as Ductal®. Table 2.1 shows a typical composition of this material.

Table 2.1: Typical Composition of Ductal® (Graybeal and Russell 2013)

Material	lb/yd^3	Percent by Weight
Portland Cement	1,200	28.5
Fine Sand	1,720	40.8
Silica Fume	390	9.3
Ground Quartz	355	8.4
HRWR	51.8	1.2
Accelerator	50.5	1.2
Steel Fibers	263	6.2
Water	184	4.4

Material properties of a widely available, preblended UHPC have been independently assessed through a series of research projects completed by the FHWA. When deployed with 2 percent by volume steel fiber reinforcement and cured in field-type conditions, this UHPC has been observed to exhibit the properties provided in Table 2.2.

Table 2.2: Typical Field-Cast UHPC Material Properties (Graybeal 2014)

Material Characteristic	Average Result
Density	155 lb/ft3 (2,480 kg/m3)
Compressive strength (ASTM C39; 28-day strength)	24 ksi (165 MPa)
Modulus of elasticity (ASTM C469; 28-day modulus)	7,000 ksi (48 GPa)
Direct tension cracking strength (uniaxial tension with multiple cracking)	1.2 ksi (8.5 MPa)
Split cylinder cracking strength (ASTM C496)	1.3 ksi (9.0 MPa)
Prism flexure cracking strength (ASTM C1018; 12-inch (305-mm) span)	1.3 ksi (9.0 MPa)
Tensile strain capacity before crack localization and fiber debond	> 0.003
Long-term creep coefficient (ASTM C512; 11.2 ksi (77 MPa) load)	0.78
Long-term shrinkage (ASTM C157; initial reading after set)	555 microstrain
Total shrinkage (embedded vibrating wire gage)	790 microstrain
Coefficient of thermal expansion (AASHTO TP60–00)	8.2 x10–6 inches/inches/°F (14.7 x10–6 mm/mm/°C)
Chloride ion penetrability (ASTM C1202; 28-day test)	360 coulombs
Abrasion resistance (ASTM C944 2x weight; ground surface)	0.026 oz. (0.73 g) lost
Freeze-thaw resistance (ASTM C666A; 600 cycles)	RDM = 99 percent
Alkali-silica reaction (ASTM C1260; tested for 28 days)	Innocuous

UHPC product is sensitive to mixing deviations, therefore timing and mix proportions must be followed closely. Temperature of the mix increases during the mixing process, which causes a loss of water due to evaporations. Ice cubes were found to be a suitable replacement for water when the mixing operation occurs during warm weather. Tow-behind pan mixers and conventional concrete ready-mix trucks have been used to mix UHPC. Ideal bonding characteristics are observed when the UHPC is cast against a pre-wetted precast concrete panel with an exposed aggregate finish (Graybeal 2014).

2.6.3 Previously Conducted Research

Research conducted by Graybeal was aimed toward the evaluation of structural performance of field-cast UHPC joints connecting precast bridge panels. Figure 2.6 shows a cross section of a longitudinal connection used during testing.

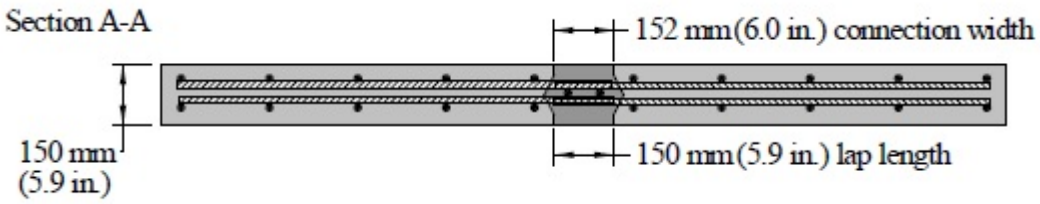

Figure 2.6: UHPC Longitudinal Joint (Graybeal, 2010)

Transverse and longitudinal UHPC joints with different reinforcing configurations were fatigue-loaded with 2 million cycles to a load just below the cracking strength, followed by at least 5 million cycles to a load larger than the cracking strength. Testing results indicated an acceptable field performance (Graybeal 2010).

2.7 Folded Steel Plate Girder with UHPC Closure Pours on GRS Abutment

Nebraska DOT used several ABC tools on a school route bridge installation project in Boone County, Nebraska. Prefabricated trapezoid folded steel plate girders were supported by GRS-IBS abutments, and decks connected with 8-inch UHPC closure pours with straight rebar were used. Two cranes and four trucks were used during placement of the prefabricated girders with the decks. The system was placed in two and a half hours. Three cubic yards of UHPC was mixed and poured to connect the decks. The UHPC showed a compressive strength of 12 ksi in four days, and the 28-day compressive strength was 21 ksi. This project took 30 days, and the cost of the project was $455,000. The contractor found the project interesting, and mentioned that the cost of another similar project would be less, since they have built one already. The contractor also claimed that they could build a similar system within 14 working days (Jaber 2015).

2.8 SUMMARY

This chapter provided an overview of the current ABC developments, and types of prefabricated bridge elements and systems, including sub-contractors and superstructures. A brief summary of the I-93 Fast 14 ABC project was included in this section. Also included in this chapter was an overview of the UHPC product, the testing that had been conducted, and a description of a project where several ABC techniques were used.

CHAPTER 3: SLAB EDGE TREATMENT METHODS

3.1 INTRODUCTION

This chapter provides an overview of two techniques used in order to obtain a concrete slab edge with an exposed aggregate finish. One of the methods used to obtain the desired surface included the application of different kinds of retarder to the formwork. The second method included the use of ¾" stone attached to the formwork in order to create voids on the concrete slab edge. Both techniques were tested on two 6.5-feet long by 3.5-feet wide concrete deck samples, yielding the use of the retarders to be an acceptable method in obtaining a rough edge concrete finish.

3.2 SHEAR-KEY DETAIL DESIGN

The goal of the construction phase of the project was to build a 35-foot long bridge system that consisted of two modular units longitudinally joined with UHPC. Each modular unit consisted of a 35-foot long steel press-brake-formed tub girder with a reinforced concrete deck cast on top. Each deck was 55 inches wide and 6 inches deep. The outside longitudinal edge of each deck was smooth and flat, while the inside edges (where the UHPC joint would be installed) needed to be rough, and had reinforcing bars protruding out of them. In order for the UHPC to develop a good bond with the concrete deck, aggregate on each of the inner longitudinal edges needed to be exposed. Also, the shape of the edges had to be detailed as shown in Figure 3.1. A secondary option for the shear-key detail is shown in Figure 3.2.

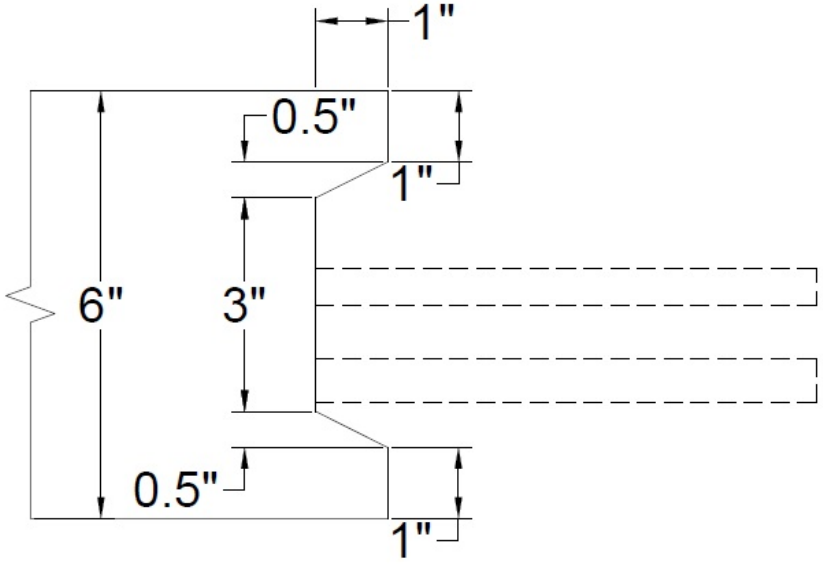

Figure 3.1: Shear-Key Design Detail— Alternative A

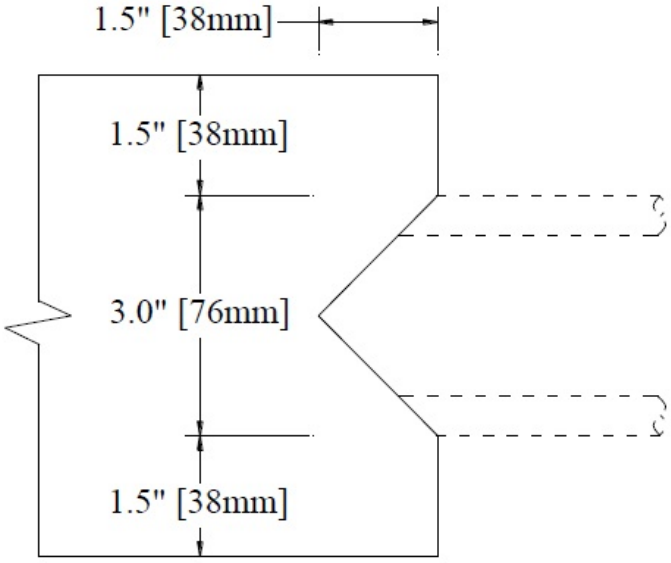

Figure 3.2: Shear-Key Design Detail—Alternative B

According to Zachary B. Haber, a bridge research engineer at Professional Service Industries, Inc., the geometry of the shear-key has minimal effect on the flexural performance of the connection (Haber). Alternative A shown in Figure 3.1 was chosen for the experiment, since

the reinforcing was located along the flat edge, which provided advantage from a constructability point of view over Alternative B shown in Figure 3.2.

Prior to manufacturing the shear-key on the 35-foot model, two small-scale concrete deck samples were poured, and the options for producing an exposed aggregate finish on the slab edges were investigated.

3.3 RETARDER PRODUCT

In order to achieve an exposed aggregate finish, a product called *Altus Series In-Form Retarder* was used. Two types of retarder were used in this experiment: *Altus Series In-Form Retarder* #125 and *Altus Series In-Form Retarder* #250. *Retarded* #125 is typically used with the ½" aggregate size, and *Retarded* #250 is used with the ¾"+ aggregate size.

3.4 FORMWORK PREPARATION

A trapezoidal key block-out was used to create the shape shown in Figure 3.1. A trapezoidal block-out was fabricated from ¾- and ¼ -inch plywood bonded together with Titebond III Ultimate Wood Glue. The form was then cut to meet required dimensions and is shown in Figure 3.3

Figure 3.3: Trapezoidal Key Block-Out

Formwork for two 6.5-feet long by 3.5-feet wide concrete deck samples was designed to have trapezoidal shear-key block outs fastened to each 6.5 ft edge. The side panels with the fastened trapezoidal shear-key block-outs were sanded and coated with Minwax Fast-Drying Polyurethane. Three coats were applied with sanding in-between each coat, and the form work was then allowed 24 hours to dry. After the last coat of Polyurethane dried, holes for penetrating reinforcing bars were drilled. Bars #4 and #5 with respective diameters of 0.5 inches and 0.625 inches were used. The hole diameters were up-sized 1/8 inches from the nominal reinforcing bar diameters for ease of installation and minimal leakage during casting. After the holes were drilled, two of the panels were coated with *Altus Serie*s *In-Form Retarder* #250 (grey) and one panel was coated with *Altus Series In-Form Retarder* #125 (green) as shown in Figure 3.4. Panels coated with *Altus Serie*s *In-Form Retarder* #250 were used for Sample 1 formwork, and the panel coated with *Altus Series In-Form Retarder* #125 was used for the formwork for Sample 2. The retarder was applied two and a half days prior to casting.

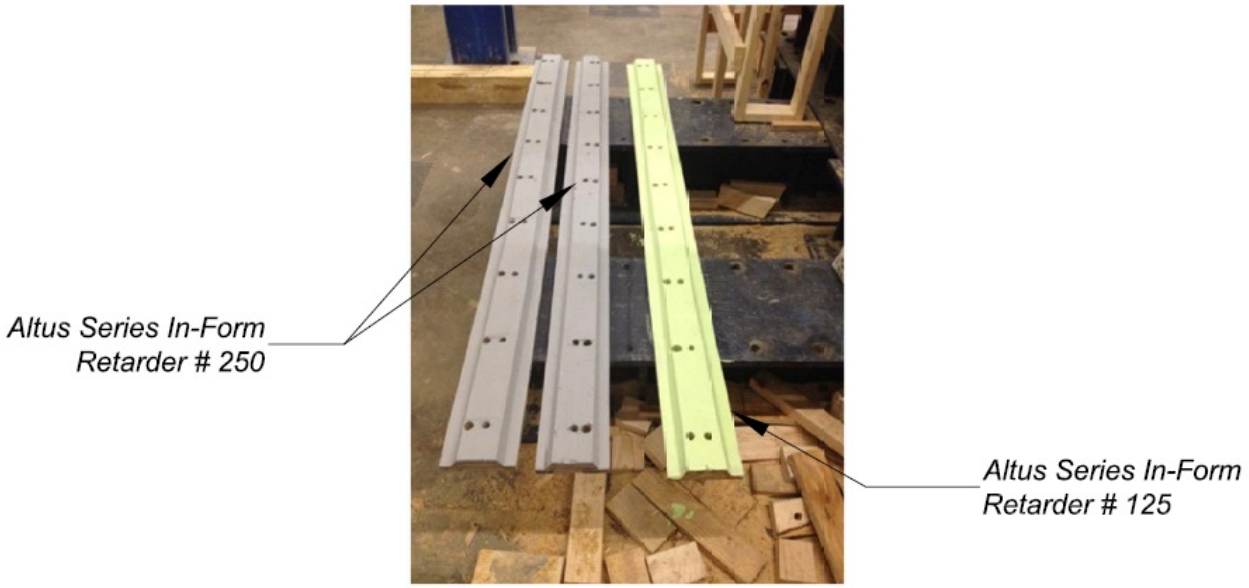

Figure 3.4: Panels Coated With the Altus Series In-Form Retarder

The second panel of Sample 2 did not have holes drilled for protruding reinforcing bars and was coated with BIO-DUR™ Standard Cure, a heavy duty epoxy compound, to allow ¾-inch stone to be glued to the panel's surface as shown in Figure 3.5. The epoxy dried for approximately 20 hours prior to casting and was then coated with machine oil to act as a releasing agent.

Figure 3.5: Sample 2 Formwork Panel Coated With BIO-DUR™ with ¾-inch Stone

Sample 1 had transverse reinforcing bars penetrating both 6.5-feet side panels with the shear-key block-outs as shown in Figure 3.6.

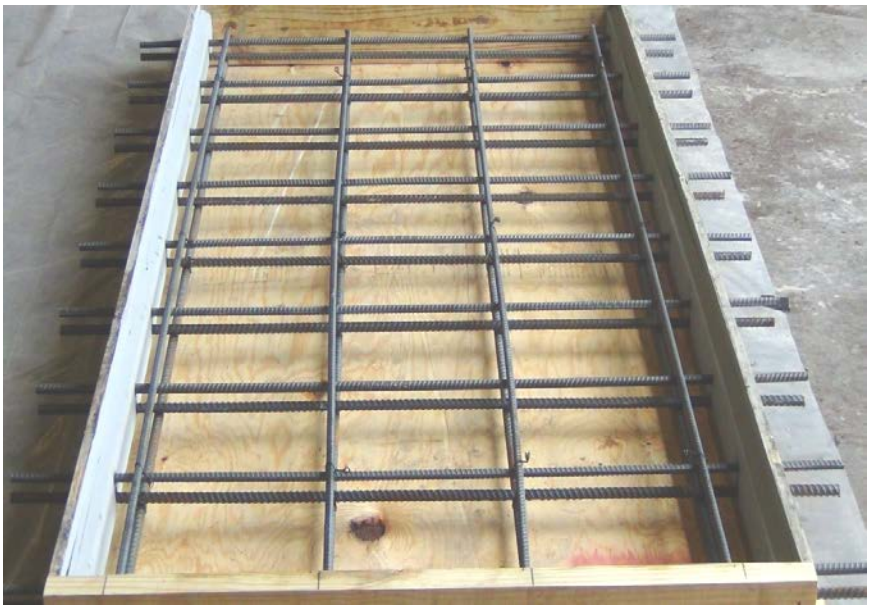

Figure 3.6: Sample 1 Completed Formwork

The side panel of Sample 2 that was coated with *Altus Series In-Form Retarder* #125 had transverse reinforcing bars penetrating it, and the panel with ¾" stone glued to it had no prodruding reinforcing bars as shown in Figure 3.7. Figure 3.8 shows a close-up view of the stone glued panel.

Figure 3.7: Sample 2 Completed Formwork

Figure 3.8: Sample 2 Panel with Attached ¾-inch Stone

Longitudinal rebar was spaced at 12 inches with a 2-inch edge distance. Transverse rebar was spaced at 9 inches with a 3-inch edge distance. Top cover was 2 inches for this rebar layout and bottom cover was 1 inch. Number 5 rebar was used for the bottom reinforcement while #4 rebar was used for the top reinforcement.

3.5 SLAB EDGES TREATMENT

Formwork was removed 24 hours after casting. The greatest challenge was to remove the panels coated with the *Altus Series In-Form Retarder* without breaking the concrete trapezoidal shear-key, as the retarder did not serve as a releasing agent. Figure 3.9 shows Sample 1 immediately after removal of formwork. As seen in Figure 3.9, several areas of the concrete shear-key detail were damaged during the removal of the formwork.

Figure 3.9: Sample 1 after Removal of Formwork

A wire brush attached to a grinder was used to remove concrete paste from the surface layer, exposing the aggregate where the *Altus Series In-Form Retarder* was applied. Figure 3.10 shows Sample 1 with the exposed aggregate.

Figure 3.10: Sample 1 after Wire-Brushing

Figure 3.11 shows the shear-key detail of Sample 2 after wire-brushing the side where the *Altus Series In-Form Retarder* #125 was applied.

Figure 3.11 Sample 2 after Wire-Brushing

The exposed aggregate finish of Sample 1 and Sample 2, where *Altus Series In-Form Retarder* was used, appeared to be very similar. However, the shear-key detail of Sample 1, where *Altus Series In-Form Retarder* #250 was applied, appeared to be more brittle than the shear-key in Sample 2 where *Altus Series In-Form Retarder* #125 was applied.

The removal of the panel coated with BIO-DUR™ Standard Cure and ¾" stone was also challenging, but not nearly as much as the other panels. During casting of Sample 2, concrete was vibrated at different distances from the side of the panel. At one end, the concrete was vibrated right next to the panel, while at the other end the vibrator was held approximately 3.5 inches from the panel. The majority of the aggregate detached from the panel at the end where the concrete was vibrated directly next to the panel as shown in Figure 3.12.

Figure 3.12: Closely Vibrated Concrete

Contrarily, the majority of stones remained attached to the panel at the end where the vibrator was held approximately 3.5 inches away, creating voids in the concrete as shown in Figure 3.13.

Figure 3.13: Vibration Distance Maintained During Casting

3.6 CONCLUSION

This chapter described different options of concrete slab edge treatment methods in the effort to prepare the slabs for UHPC joint installation. Two 6.5-feet by 3.5-feet reinforced concrete samples were built in order to investigate the edge treatment options and to select the optimal option. Upon completion of the experiment, use of *Altus Serie*s *In-Form Retarder* #250 yielded the best results in preparation of the concrete surface. This product was selected to be used during construction of the full-scale model.

CHAPTER 4: EXPERIMENTAL TESTING

4.1 INTRODUCTION

This chapter describes the assembly of a 35-foot simple span bridge model that consisted of two modular units. Each modular unit consisted of a steel-brake-formed tub girder with reinforced concrete decks cast on top. Casting of the UHPC longitudinal joint and testing procedures are also describe in this chapter.

4.2 OVERVIEW OF THE TEST SPECIMEN

4.2.1 Specimen Properties and Dimensions

Through a series of design studies, Michaelson (2014) determined the optimum cross-section using an 84” x 7/16” plate for this press-brake-formed steel tub girder design being used, which was found to have a top flange width of 6 inches and a total girder depth of 23 inches. All plates were bent such that the inside bend radius was equal to five times the thickness of the plate. Once the plates were bent, shear studs were welded to the top flanges. Figure 4.1 shows a cross-sectional view of the press-brake-formed tub girder dimensions. Section properties for the test specimens are summarized in Table 4.1. In addition, Figure 4.2 shows end bearing plates that were utilized at support locations to prevent premature bearing failure during testing (Kelly 2014).

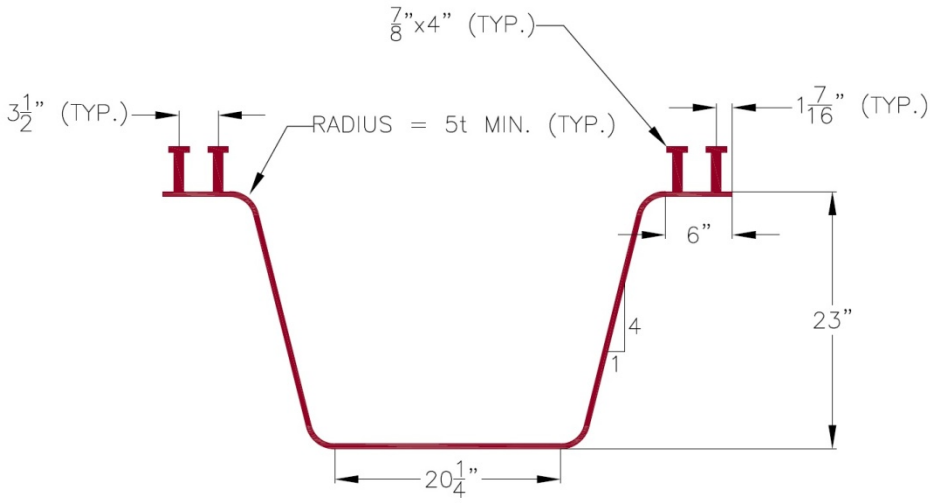

Figure 4.1: Test Specimen Dimensions (Kelly, 2014)

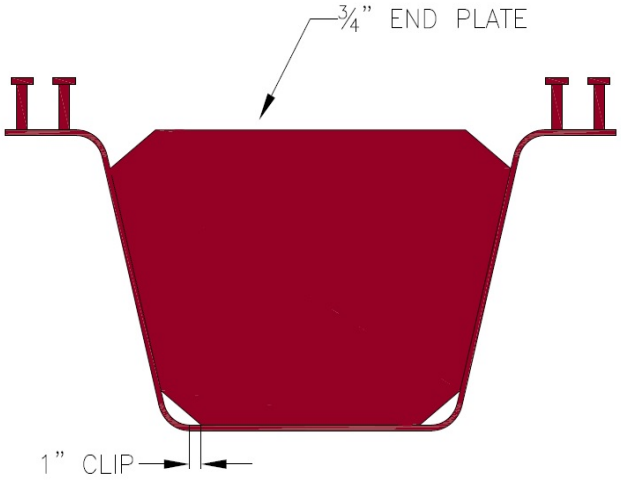

Figure 4.2: End Bearing Plate (Kelly, 2014)

Table 4.1: Press-Brake-Formed Tub Girder Section Properties

Property	Value
A (in^2)	36.75
L (in)	420
E (ksi)	29,000
G (ksi)	11,154
I_x (in^4)	2893.1
I_y (in^4)	8049.6
I_{open} (in^4)	2.3447
I_{closed} (in^4)	69,000
C_w (in^6)	139,952
β_x (in)	-19.704

4.3 LAYOUT OF STRAIN GAGES

Uniaxial strain gages were used to measure the strain in the specimen during testing. Six gages were placed on the top and bottom of the bottom flange to measure tensile strains. In addition, six gages were placed along the quarter points of the flat portion of each web. To avoid bearing effects at load locations, all 18 strain gages were placed along a cross section at a distance *2d* (46 in.) away from the load application, where *d* is the total depth of the steel girder. Figure 4.3 illustrates the layout of the strain gages. Gages installed inside the tubs were covered with plastic to minimize the risk of damage (Figure 4.4).

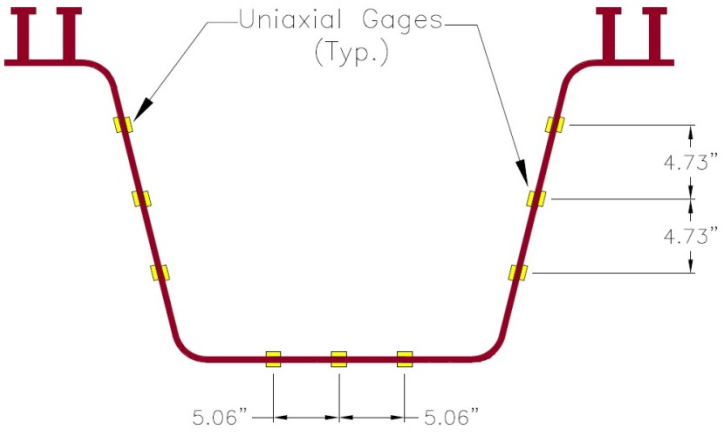

Figure 4.3: Strain Gage Layout

Figure 4.4: Covered Stain Gages

4.4 TEST SPECIMEN ASSEMBLY

4.4.1 Support Assembly

Fatigue testing was conducted on a 35-foot long, simple span bridge model consisting of two modular units. Steel bearing plates and 2-inch-diameter steel rods were used to create simply supported boundary conditions for the test specimen. One end of the girder was pin-supported, and the other end simulated roller supports. The pinned support was comprised of a 2-inch-diameter rod stitch-welded parallel to the top face of the steel bearing plate (Figure 4.5). The roller support consisted of a rod free to move in the longitudinal direction with thin metal strips stitch-welded to the top of the plate to prevent the rod from rolling off (Figure 4.6).

Figure 4.5: Pin Support

Figure 4.6: Roller Support

6- x 24- x 2-inch plates and the 12- x 24- x 2-inch plates were used to support the tub girders. The plates rested on two 24-inch long 6- x 6-ich HSS shapes filled with reinforced concrete. The ¾-inch threaded rods were used to connect the 12- x 24- x 2-inch bearing plates to the support. Each plate was tapped and threaded rods were screwed into the plates. The threaded rods penetrated the composite 6- x 6-inch HSS and the top flange of the wide flange support section that the assembly rested on (Figure 4.7).

Figure 4.7: Threaded Rods Used in the Support

4.4.2 Concrete Formwork

Two 35-feet long steel press-brake-formed tub girders were placed onto the temporary supports, to allow for easier installation of the concrete formwork (Figure 4.8).

Figure 4.8: Initial Tub Girder Placement

Concrete formwork was built in preparation for deck casting. 2- x 4-inch dimensional lumber was cut to fit inside the girders to support the plywood SIF forms after the concrete decks were poured (Figure 4.9).

Figure 4.9: Supports Inside the Girders

2- x 8-inch dimensional lumber was cut to produce 6-inch deep formwork for the concrete deck. The formwork was constructed to allow for a 4.5-inch overhang on the outer edge of each modular unit. The trapezoidal shear key block-outs were mounted to the formwork along the inner edge – the edge where the UHPC joint was going to be installed (Figure 4.10).

Figure 4.10: Shear Key Block-Out Mounted to the Concrete Formwork

4.4.3 Reinforcing Bars Placement

The reinforcing bars were placed in the same manner as in the sample decks described in Chapter 3. Longitudinal rebar was spaced at 12 inches with a 2-inch edge distance. Transverse rebar was spaced at 9 inches with a 3-inch edge distance. The 9-inch transverse spacing was adjusted in several locations due to interference with the shear studs. The reinforcing bars were protruded through the inner edge formwork – the edge with the shear key block-out detail mounted to it. The top concrete cover was 2 inches, and the bottom cover was 1 inch. #5 rebar was used for the bottom reinforcing layer, while #4 rebar was used for top reinforcement. According to the FHWA, the minimum embedment length of a reinforcing bar into an UHPC joint, l_d, shall be 8 times the bar diameter. The nominal diameter of #5 rebar is 0.625 inches, which converted into a minimum required embedded length of 5 inches. The actual length of the portion of rebar embedded into the UHPC joint was 6 inches. The final rebar placement is shown in Figure 4.11.

Figure 4.11: Reinforcing Bars Placement

Along with the reinforcement, hooked bars were placed at 5 feet and 8 feet from each end of the deck in order to have the ability to move the units after the concrete pour.

4.4.4 Formwork Coating

Two days prior to the concrete pour, the inner edge formwork of each unit that had the shear key block-outs attached to than were coated with *Altus Serie*s *In-Form Retarder* #250. Paint brushes were used to coat the formwork (Figure 4.12).

Figure 4.12: Formwork Coated with Altus Series In-Form Retarder #250

Machine oil was applied to the remaining formwork on the day of the pour to ease lumber stripping after concrete hardening.

4.4.5 Concrete Deck Pour

A slump test was conducted according to ASTM C143 when concrete was delivered to the laboratory, and was measured to be 6.25 inches. According to the West Virginia Department of Highway, slump of Class H concrete shall not exceed 7 inches (WVDOH). After it had been determined that the product met the WVDOT standard, 4-inch and 6-inch cylinders were poured for the compression testing.

Next, a concrete bucket hooked to an overhead hoist was used to deliver wet concrete from the truck to the pour location (Figure 4.13).

Figure 4.13: Concrete Bucket Moving Wet Concrete

The concrete was placed into the deck forms and vibrated to minimize voids. Special care was taken to vibrate wet concrete near the shear key block-outs in order for the concrete to take the desired shape. Figure 4.14 shows the concrete deck pour.

Figure 4.14: Concrete Pour

Figure 4.15: Poured Concrete Decks

Two decks were poured within 3 hours and are shown in Figure 4.15. Following a 24-hour curing period, concrete formwork was stripped. Extra caution was used during removal of the formwork in the shear key detail area. Once the block-outs were removed, the joint was inspected for any damages or manufacturing shortcomings. As seen in Figure 4.16, the joint edges were in a good condition with only a few damaged concrete locations.

Figure 4.16: Shear-Key After Formwork Removal

4.4.6 Shear-Keys Surface Treatment

Altus Series In-Form Retarder #250 that was put on the shear-key block outs prior to the concrete pour brittlelized the concrete. A wire brush was used to remove the most outer layer of the cement paste, providing an exposed aggrege finish (Figure 4.17).

Figure 4.17: Shear-Key Detail with Exposed Aggregate Finish

4.5 UHPC JOINT POUR

4.5.1 Concrete Formwork

Once the slab edges were wire-brushed and the layer of cement paste had been removed exposing the concrete aggregate as shown in Figure 4.17, the two modular units were aligned as shown in Figures 4.18 and 4.19. The reinforcing bars were aligned in a manner that the intervals between the rebar coming into the joint from either of the slabs were approximately 4.5 inches. The distance between the slab edges was 6 inches at the top and bottom, and 8 inches in the middle portion of the shear-key detail (Figure 4.20).

Figure 4.18: Aligned Modular Units

Figure 4.19: Close-Up View of the Aligned Modular Units and Reinforcing Bars

Figure 4.20: Shear-Key Cross Section Dimensions

Next, the UHPC joint formwork was constructed. Two layers of insulation foam were placed at the bottom of the joint with a ¾-inch plywood strip supporting the insulation (Figure 4.21).

Figure 4.21: UHPC Joint Bottom Formwork

Insulation foam with plywood strips were placed on each end of the UHPC joint formwork and anchored into the slab with 3/8-inch concrete screws as shown in Figure 4.22.

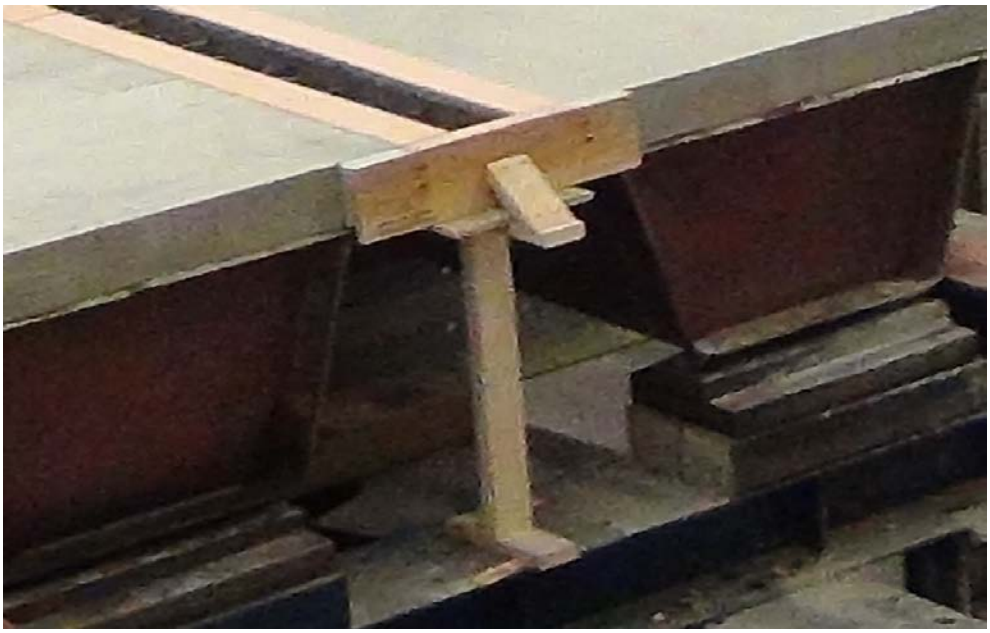

Figure 4.22: UHPC Joint End Formwork

Following the installation of the end formwork, two strips of ½-inch plywood were glued to the existing slabs along the edges of the UHPC joint. This was done in order to overfill the joint during the pour and allow for settlement. Locations of possible mix leaks were caulked. The final setup is shown in Figure 4.23.

Figure 4.23: UHPC Joint Completed Formwork

4.5.2 UHPC Joint Pour

The UHPC mix was prepared in a pan mixer using ice in lieu of water in order to keep the mix fresh for a longer period of time, and to ensure a good bond between the sections of the joint that were poured from different batches. The pan mixer was placed on top of the concrete slabs to ease the product installation (Figure 4.24).

Figure 4.24: IMER 750 Pan Mixer Placed on the Slab

Prior to placement of the UHPC into the formwork, the existing deck edges were wetted to reduce the effect of concrete extracting moisture from the newly placed mix. There were three batches of UHPC prepared. Each batch was tested using the flow table (Figure 4.25), and results are summarized in a quality control sheet and shown in Figure 4.26.

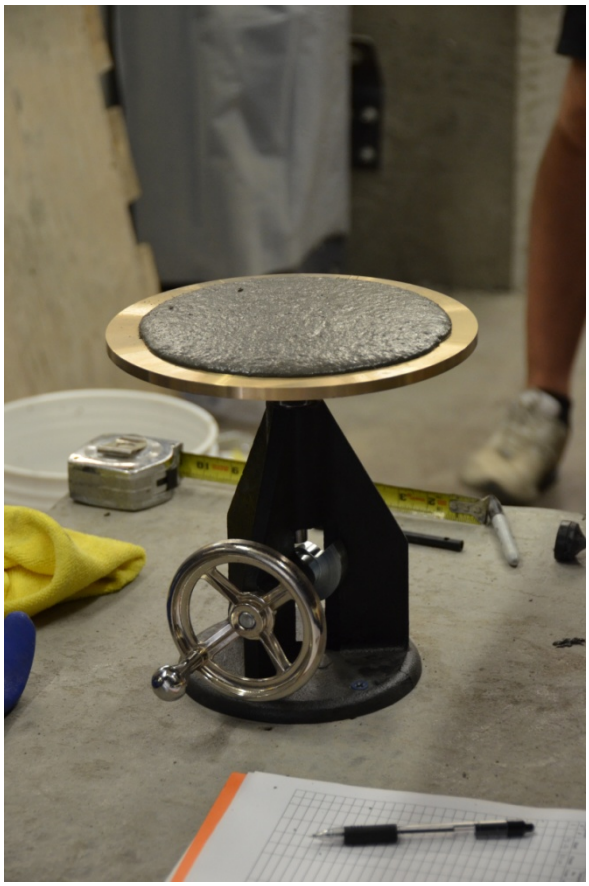

Figure 4.25: Flow Table with UHPC Sample

LAFARGE NORTH AMERICA

JOINT FILL ONSITE QC

JS1000 formulation

Ductal®

Project: 38 ft long joint between precast deck panels
Location: West Virginia University

Date: 13-Aug-15
Tech Rep: Gaston Doiron

Approx. amount used: 0.5 yd3

		Time		Mix Temp	Ambient		Flow		
Batch #	Mixer	Start	Finish	Finish	Temp	Lot #	Static	Dynamic	Comments
1	Imer 750	9:19am	10:00am	82	73	MXIV2114	8.75 in	9.5 in.	used over 90% ice
2	Imer 750	10:30am	10:55am	77	73	MXIV2114	9 in.	9.75 in	used over 90% ice, one extra 50 lbs added after flow test
3	Imer 750	11:31am	12:02pm	79	73	MXIV2114	8.25 in	8.75 in.	used over 90% ice, batch used for cylinders and cubes

Figure 4.26: UHPC Mix Quality Control Sheet

As the mix reached acceptable flow condition in the pan mixer, it was put into a wheel barrel and poured into the formwork as shown in Figure 4.27.

Figure 4.27: Pour of the UHPC Joint

Samples of the mix were poured into 2-inch cubes and 4-inch cylinders for compression testing. Upon the completion of the UHPC pour, the joint was covered with plastic to prevent moisture escape.

48 hours after the pour, the UHPC joint experienced minimal settlement. Figure 4.28 shows the end section of the joint, and Figure 4.29 shows the joint along its length after a two-day period.

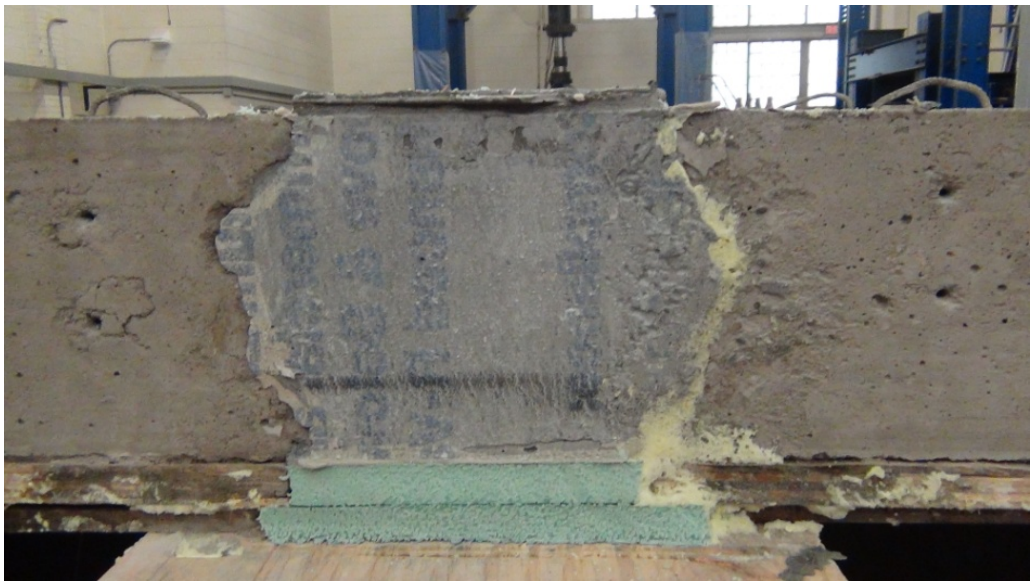

Figure 4.28: UHPC Joint End Section Two Days after the Pour

Figure 4.29: UHPC Joint Two Days after the Pour

Since the joint was approximately 3/8-inch above the slab, a concrete grinder was used to bring the joint level down. Figure 4.30 shows the grinding process, and Figure 4.31 shows the joint after grinding.

Figure 4.30: UHPC Joint Grinding

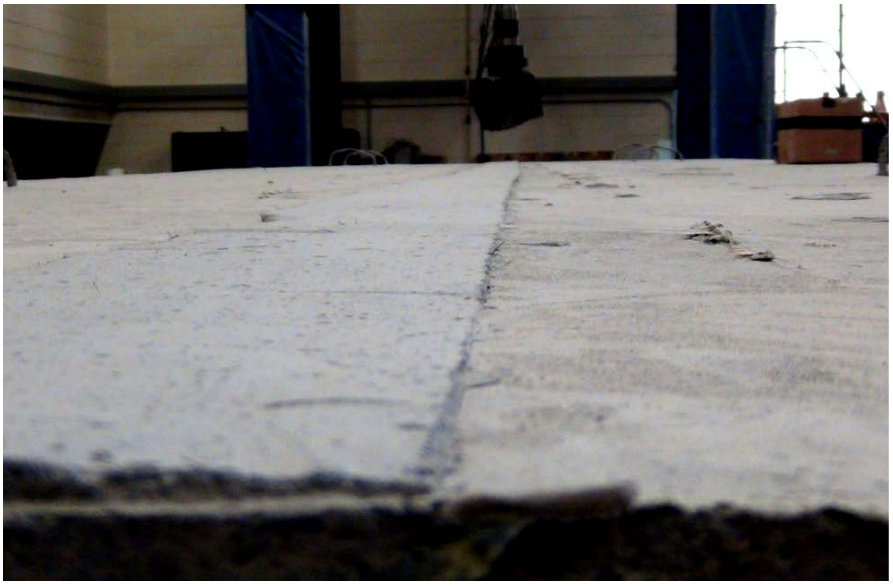

Figure 4.31: UHPC Joint After Grinding

Figure 4.32 shows the completed specimen, and Figure 4.33 shows a typical cross-section of the specimen.

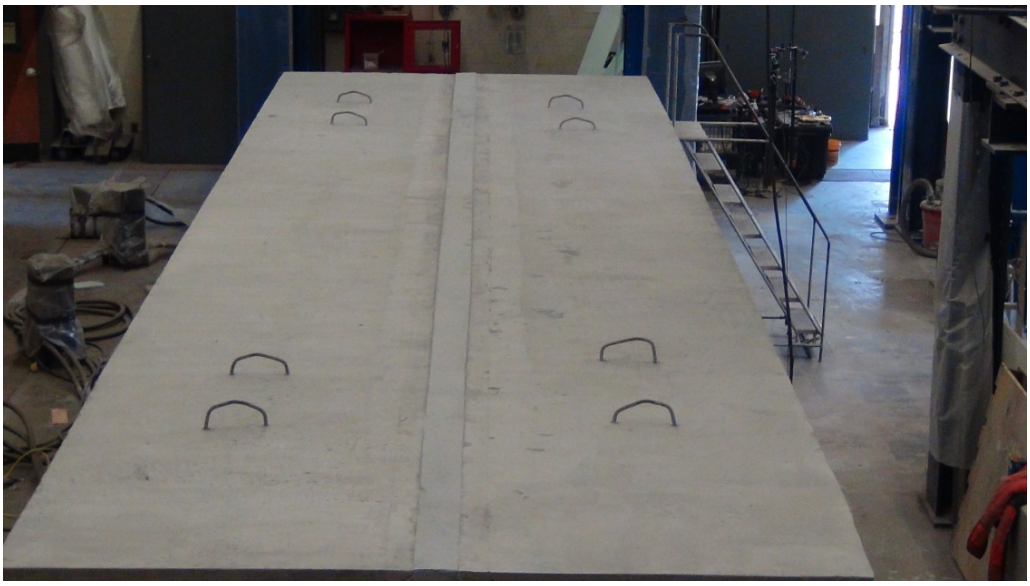

Figure 4.32: Concrete Deck with the UHPC Joint

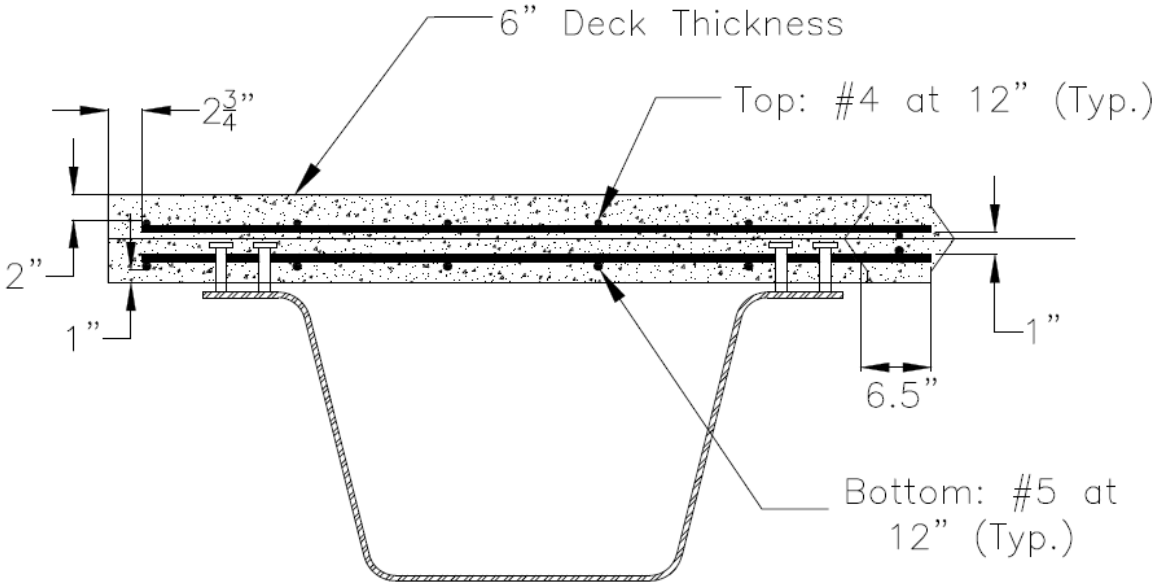

Figure 4.33: Cross-Section of the Specimen

4.6 LOAD CONFIGURATION

The test load was applied to the system at the midspan using an MTS 330-kip servo-hydraulic actuator mounted to a large structural reaction frame as shown in Figure 4.34.

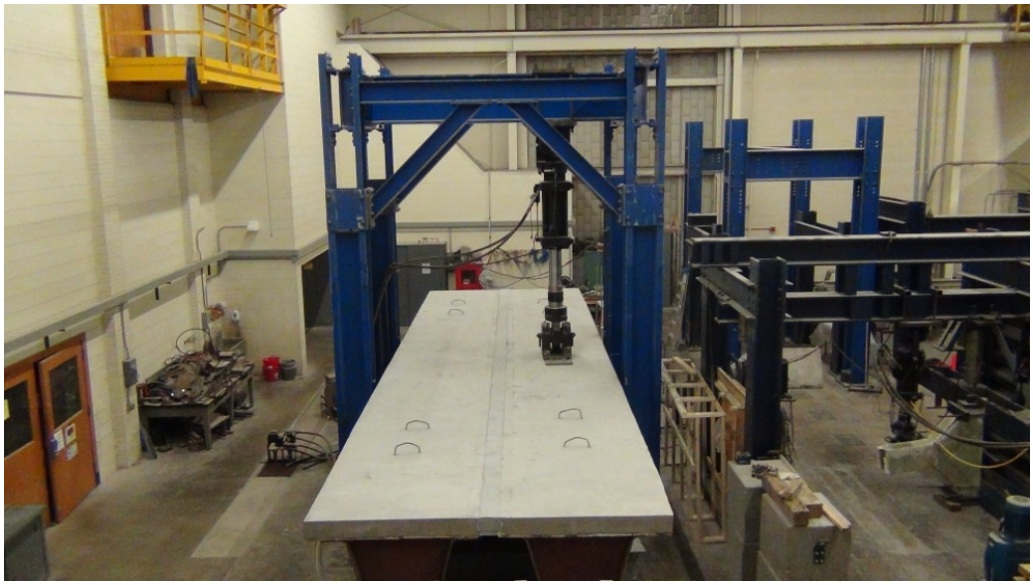

Figure 4.34: Load Applied to the System

A 20- x 10- x 1-inch thick plate was welded to a 20- x 16- x 1-inch thick plate as shown in Figure 4.35, which was attached to the actuator. The smaller plate dimensions were designed to replicate a truck tire contact area (AASHTO). An elastomeric pad was placed between the steel plate and concrete as shown in Figure 4.36.

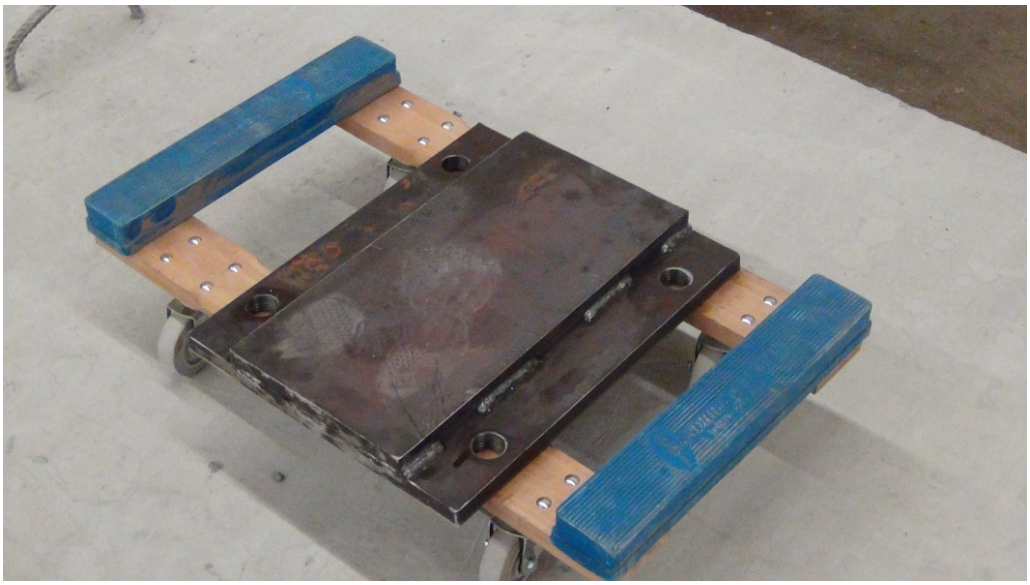

Figure 4.35: Plate System Replicating a Truck Wheel Load

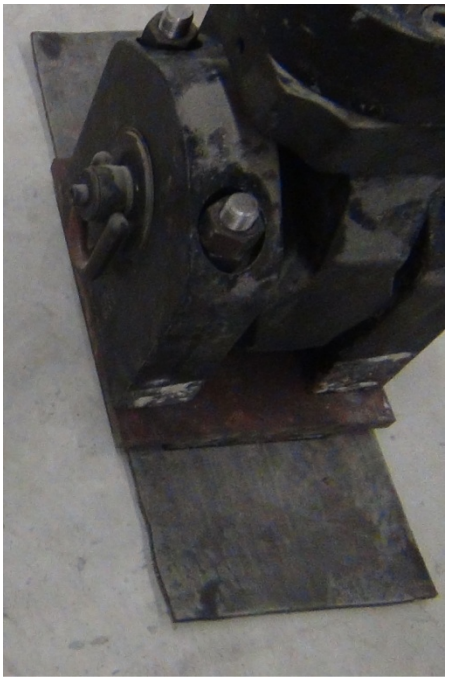

Figure 4.36: Elastomeric Pad Placed Between the Steel Plate and Concrete Deck

4.7 LOAD MAGNITUDE DETERMINATION

4.7.1 Load Determination Overview

One of the steps leading to testing of the specimen was to determine the loads that induce the Service II and Fatigue I moments. Service II load combination is intended to control yielding of steel structures, and is determined using AASHTO Tables 3.4.1-1 and 3.4.1.-2.

$$Service\ II = 1.0DC + 1.0DW + 1.3(LL + IM) \quad \text{Eq. 4-1}$$

Fatigue I load combination is related to infinite load-induced fatigue life, and is also determined using AASHTO Tables 3.4.1-1 and 3.4.1.-2.

$$Fatigue\ I = 1.75(LL + IM) \quad \text{Eq. 4-2}$$

Load factor for Fatigue I in the current AASHTO LRFD edition is 1.5. It is anticipated that the load factor will be increased to 1.75 in the future AASHTO LRFD editions. If the factor will be increased, current testing represents future Fatigue I load combination. It the load factor remains 1.5, current testing may be considered to be conservative.

AASHTO LRFD defines terms in Eqs. 4-1 and 4-2 as follows:

- DC = dead load of structural components and nonstructural attachments
  - Divided into two components: DC1 (applied to the noncomposite section) and DC2 (applied to the composite section)
- DW = dead load of wearing surface and utilities
- IM = vehicular dynamic load allowance
  - Serves to amplify the vehicular components of the HL-93 live load (i.e. the truck and tandem)
  - For the fatigue limit state, IM = 15% (Article 3.6.2)
  - For all other limit states, IM = 33% (Article 3.6.2)
- LL = vehicular live load
  - The HL-93 vehicular live load as defined in Article 3.6.1.2.

        - Combination of either design truck + design lane or the design tandem + design lane (whichever yields the largest force effect).
    - Note that for the fatigue limit state, the fatigue load consists of only one design truck with a fixed rear axle spacing of 30 feet (Article 3.6.1.4.1).

4.7.2 Magnitude of Applied Loads

Procedures used to determine the magnitudes of cyclic and static loads are described in Appendix A. A static load that induced a Service II moment was determined to be 90.78 kips, and a cyclic load inducing Fatigue I moment was found to be 67.43 kips.

4.7.3 Number of Cycles

Several assumptions were made to determine the number of fatigue cycles:

a. The average daily traffic (ADT) was 1000 vehicles.

b. Rural environment.

AASHTO Table C3.6.1.4.2-1 – Fraction of Trucks in Traffic, was used to determine that the average daily truck traffic (ADTT) in rural environment was 10% of the ADT. Only one lane was available to trucks, and therefore a single lane ADTT was equal to ADTT. Using 75-year bridge design life, the number of fatigue cycles was determined as follows:

Number of cycles = 1000(ADT) x 0.10(represents 10%) x 365 (Days/Year) x 75 (Years)

= 2,737,500 Cycles

4.8 TESTING PROCEDURE

4.8.1 Testing Procedure Overview

As discussed in Section 4.3, a total of 18 strain gages were placed along the cross section at a distance *2d* (46 in.) away from the midspan, where *d* is the total depth of the steel girder. Additionally, four linear variable displacement transducers (LVDT) were placed underneath each girder at fifth points to measure vertical deflections. The LVDT placement scheme is shown in Figure 4.37.

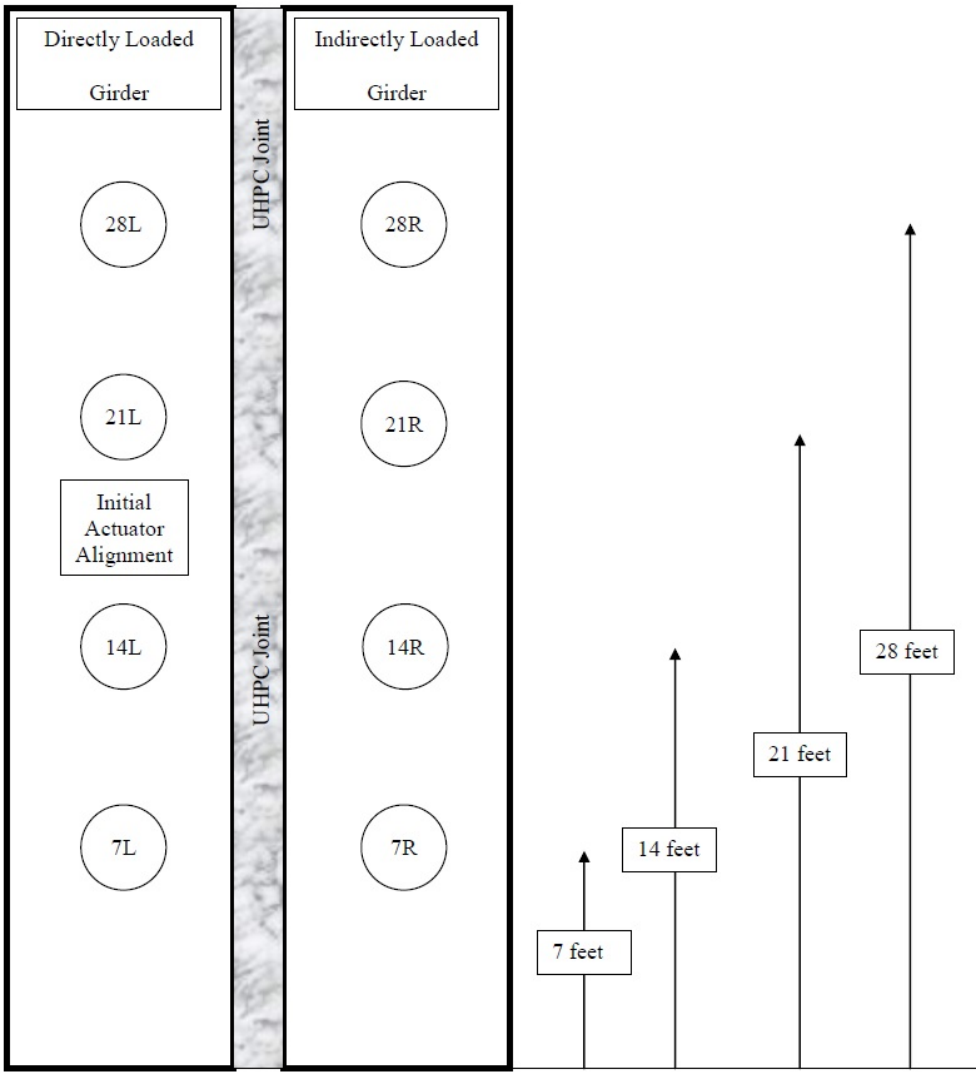

Figure 4.37: Scheme of the LVDT Placement

The fatigue loading frequency was one half of a cycle per second up to 1.5 million cycles. At a 1.5 million mark, an attempt was made to increase the frequency to one cycle per second. The actuator was unable to load the bridge system to 67.93 kips and unload it to 0.5 kips in such a short time interval, and therefore a frequency of three quarters of a cycle per second was used.

A static base test was conducted prior to the start of fatigue testing. The system was loaded with 90 kips two times. The targeted load was reached in nine intervals of 10 kips each, and five strain gage and LVDT readings were taken at each interval. There was a ten minute wait between the loading intervals in order to let the system settle and eliminate vibration effects. The static testing was conducted at a predetermined numbers of cycles following the procedure described above with the exception that the specimen was loaded to 90.78 kips in ten intervals of 9.078 kips. The static testing was scheduled to take place at the following number of cycles: 100,000; 250,000; 500,000; 1,000,000; 1,500,000; 2,000,000; 2,500,000; and 2,800,000. Each cycle set was followed by a thorough UHPC joint inspection to indicate if cracking had occurred.

4.9 CONCRETE DECK FAILURE

After 1,635,000 fatigue cycles, the concrete deck had failed in the location of the direct load application as shown in Figure 4.38.

Figure 4.38: Concrete Deck Failure

The nature of the deck breakdown suggested that a punching shear failure had occurred. Low concrete compressive strength largely contributed to the resulted condition. The deck was grouted as shown in Figure 4.39.

Figure 4.39: Concrete Deck Patch

A new 30- x 18- x ½-inch steel plate was attached to the bottom of the 20- x 16- x 1-inch plate replacing the 20- x 10- x 1-inch plate (Figure 4.40).

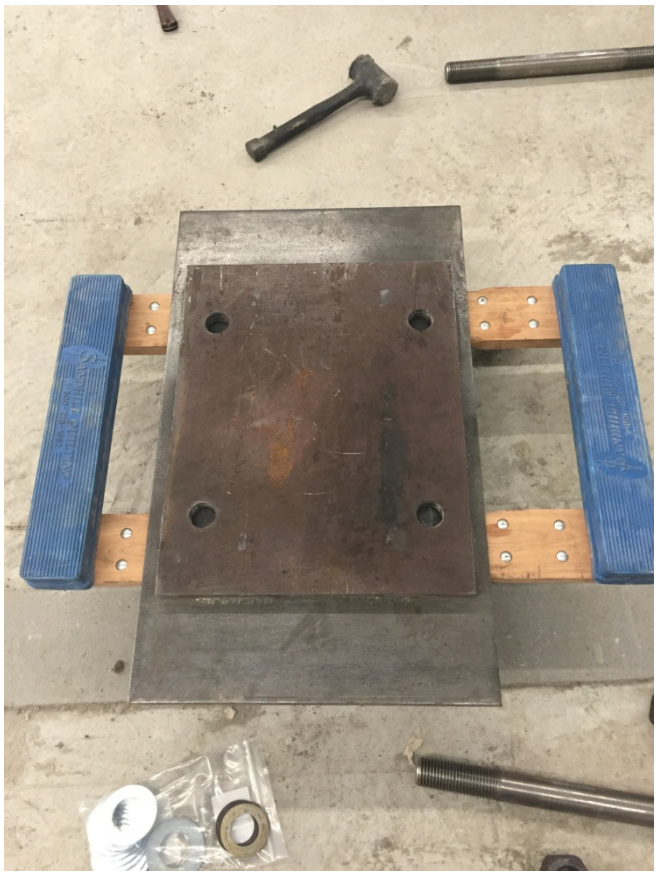

Figure 4.40: Plate with Greater Dimensions Replaced Initial Steel Plate

The testing continued for an additional 27,000 cycles until the patch failed. The actuator was relocated to a position where the load was applied in the middle of the undamaged, initially indirectly loaded girder. Figure 4.41 shows the modified testing configuration.

Figure 4.41: Actuator Aligned with Undamaged Deck

A static base test was conducted with the new actuator alignment. As the fatigue testing continued, a shear crack from the failed deck propagated across the UHPC joint (Figure 4.42).

Figure 4.42: Shear Crack Propagated Across UHPC Joint

Testing was continued as the crack was in transverse and not the longitudinal direction. The system was closely monitored, and the static tests were conducted at the following fatigue cycle intervals: 2,000,000; 2,100,000; 2,200,000; 2,300,000; 2,500,000; 2,700,000; 2,800,000. The only visible crack at the end of 2,800,000 fatigue cycles was the shear crack that had propagated from the damaged deck area.

4.10 SUMMARY

The focus of this chapter was to describe the assembly of a 35-foot simple span bridge model that consisted of two modular units. A reinforced concrete deck was poured on top of each steel press-brake-formed tub girder. Transverse reinforcing was extended from within each deck along one of the longitudinal edges for the UHPC joint installation. Once the UHPC joint was poured, the system cured for approximately 45 days prior to initial testing. Steel plates attached to the MTS 330-kip servo-hydraulic actuator were fabricated to replicate a truck contact area. Low strength of deck concrete contributed to a deck failure after 1,635,000 fatigue cycles. The actuator was re-aligned over the second tub girder to mirror its initial position. As the testing continued with the latter testing alignment, a transverse crack from the deck failure propagated into the UHPC joint. The integrity of the system was not jeopardized and testing continued. Results and methods used to analyze the collected data are presented in Chapter 5.

CHAPTER 5: EXPERIMENTAL TESTING RESULTS

5.1 INTRODUCTION

This chapter describes the results obtained during testing, and the methods used in data analysis. Results of UHPC and deck concrete compression testing are reported. Also, included in this chapter is a description of the procedures used to calculate moments induced into each girded by the applied loads. The last two sections of this chapter provide an overview of the moment distribution factors and deflections obtained from testing.

5.2 CONCRETE STRENGTH

5.2.1 Deck Concrete

As noted in Chapter 4, a slump test was conducted with concrete used to pour the decks. The slump was found to be 6.25 inches, which met the WVDOT requirement of 7 inches maximum. Deck concrete compression testing results are summarized in Table 5.1.

Table 5.1: Concrete Compression Test Results

Age	Strength (psi)
7 days	2,450
28 days	2,952
50 days	3,009

Concrete strength did not meet the minimum requirement of 4,000 psi at 28 days (WVDOT). Low concrete compression strength contributed to the punching shear failure as indicated in Chapter 4.

5.2.2 UHPC Compressive Strength

Compression test results for the UHPC cubes and cylinders are summarized in Table 5.2

Table 5.2: UHPC Cubes and Cylinders Compression Test Results

Age	Cubes Strength (psi)	Cylinders Strength (psi)	% Difference
7 days	18,438	19,511	5.7
14 days	22,123	22,162	0.18
28 days	23,624	27,653	15.7

According to a study performed by Graybeal, the 2-inch cylinders and cubes exhibit the greatest strength variations and least correlation when compared with 3- and 4-inch diameter cylinder strength results (Davis and Graybeal 2008). The obtained cubes and cylinders 7- and 14-day compressive strengths are within reasonable variance, while the 28-day results vary greatly. The difference in results supports Graybeal's observations. An additional factor that could have contributed to the greater variance was the alteration of the testing equipment. The cubes were tested using Instron testing equipment, while a Forney apparatus was used for the cylinders. Despite the differences in the obtained results, the obtained concrete strengths were in the predicted range of 24 ksi.

5.3 MOMENT CALCULATION

5.3.1 Gage Configuration

A method used by Helwig and Fan (2000) was adopted to determine the stresses from the obtained strain data. The longitudinal stresses induced by axial forces and bending moments are distributed linearly across the cross-section of the members. The stress distribution on the cross-section can be expressed using Equation 5-1:

$$f(x,\ y) = a + bx + cy \qquad \text{Eq. 5-1}$$

Where *a*, *b*, and *c* are constants, and *x*, *y* is the coordinate system. Table 5.2 lists the gages with the respective *x*,*y* coordinates. Figure 5.1 shows the strain gage layout according to the x,y coordinates.

Table 5.3: x, y Coordinates of Strain Gages

Gage Coordinates		
Gage	Modular Unit	
	x (in)	y (in)
G01	45.71	5.78
G02	44.53	1.05
G03	43.35	-3.68
G04	34.56	-10.39
G05	29.50	-10.39
G06	24.44	-10.39
G07	15.65	-3.68
G08	14.47	1.05
G09	13.29	5.78
G10	45.29	5.89
G11	44.11	1.16
G12	42.92	-3.57
G13	34.56	-9.96
G14	29.50	-9.96
G15	24.44	-9.96
G16	16.08	-3.57
G17	14.89	1.16
G18	13.71	5.89
G19	-13.29	5.78
G20	-14.47	1.05
G21	-15.65	-3.68
G22	-24.44	-10.39
G23	-29.50	-10.39
G24	-34.56	-10.39
G25	-43.35	-3.68
G26	-44.53	1.05
G27	-45.71	5.78
G28	-13.71	5.89
G29	-14.89	1.16
G30	-16.08	-3.57
G31	-24.44	-9.96
G32	-29.50	-9.96
G33	-34.56	-9.96
G34	-42.92	-3.57
G35	-44.11	1.16
G36	-45.29	5.89

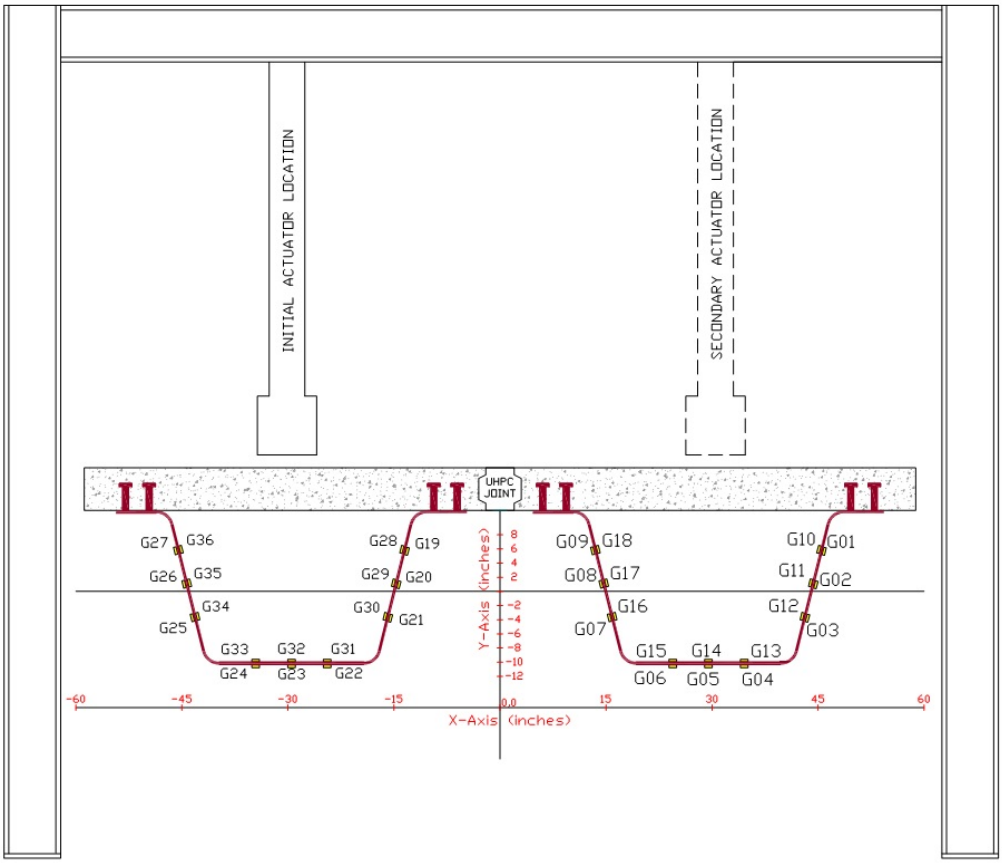

Figure 5.1: Strain Gage Layout Legend

5.3.2 Linear Regression Algorithm

To determine the distribution plane of stress, only three stress readings at three points that are not collinear are required. To reduce errors in physical strain measurements, a three-dimensional linear regression algorithm, based on least square regression was employed. According to the method, constants *b* and *c* in Equation 5-1 can be solved using Equations 5-2 through 5-11.

$$\begin{bmatrix} L_{11} & L_{12} \\ L_{21} & L_{22} \end{bmatrix} \begin{Bmatrix} b \\ c \end{Bmatrix} = \begin{Bmatrix} L_{10} \\ L_{20} \end{Bmatrix} \qquad \text{Eq. 5-2}$$

$$L_{11} = \sum_{i=1}^{n} \left(x_i - \bar{x} \right)^2 \qquad \text{Eq. 5-3}$$

$$L_{22} = \sum_{i=1}^{n} \left(y_i - \bar{y} \right)^2 \quad \text{Eq. 5-4}$$

$$L_{12} = L_{21} = \sum_{i=1}^{n} \left(x_i - \bar{x} \right) \left(y_i - \bar{y} \right) \quad \text{Eq. 5-5}$$

$$L_{10} = \sum_{i=1}^{n} \left(x_i - \bar{x} \right) \left(f_i - \bar{f} \right) \quad \text{Eq. 5-6}$$

$$L_{20} = \sum_{i=1}^{n} \left(y_i - \bar{y} \right) \left(f_i - \bar{f} \right) \quad \text{Eq. 5-7}$$

$$\bar{x} = \frac{1}{n} \sum_{i=1}^{n} x_i \quad \text{Eq. 5-8}$$

$$\bar{y} = \frac{1}{n} \sum_{i=1}^{n} y_i \quad \text{Eq. 5-9}$$

$$\bar{f} = \frac{1}{n} \sum_{i=1}^{n} f_i \quad \text{Eq. 5-10}$$

$$a = \bar{f} - b\bar{x} - c\bar{y} \quad \text{Eq. 5-11}$$

The system was statically loaded twice at the specified cycle intervals. Once the static loading strain gage data was collected, it was sorted to only include the gage readings that displayed consistent results, and to discard the irregular data values. The gages used in the testing did not perform consistently throughout the test. Table 5.4 lists the gages and the cycle intervals at which the static testing was conducted. Zeros denote the strain gage readings that were discarded, while “1’s” indicate the gage readings that were used during the moment evaluation.

Table 5.4: Gage Inclusion Matrix

	Cycle Count													
Gage	Base Test	100,000	250,000	500,000	1,000,000	1,500,000	Secondary Base Test	2,000,000	2,100,000	2,200,000	2,300,000	2,500,000	2,700,000	2,800,000
G01	0	0	0	0	0	0	0	0	0	0	0	0	0	0
G02	1	1	1	1	1	1	1	1	1	1	1	1	1	1
G03	0	0	0	0	0	0	0	0	0	0	0	0	0	0
G04	1	1	1	1	1	1	1	1	1	1	1	1	1	1
G05	1	1	1	1	1	1	0	1	1	1	1	1	1	1
G06	0	0	0	0	0	0	0	0	0	0	0	0	0	0
G07	0	0	0	0	0	0	0	0	0	0	0	0	0	0
G08	1	0	1	1	0	1	1	1	1	1	1	1	1	1
G09	0	0	0	0	0	0	0	0	0	0	0	0	0	0
G10	0	0	0	0	0	0	0	0	0	0	0	0	0	0
G11	0	0	0	0	0	0	0	0	0	0	0	0	0	0
G12	0	0	0	0	0	0	0	0	0	0	0	0	0	0
G13	1	1	1	1	1	1	1	1	1	1	1	1	1	1
G14	1	1	0	1	1	1	1	1	1	1	1	1	1	1
G15	1	1	0	1	1	1	1	1	1	1	1	1	1	1
G16	1	1	0	1	1	1	1	1	1	1	1	1	1	1
G17	1	0	0	1	1	1	1	1	1	1	1	1	1	1
G18	0	0	0	0	0	0	0	0	0	0	0	0	0	0
G19	0	0	0	0	0	0	0	0	0	0	0	0	0	0
G20	1	1	1	1	1	1	1	1	1	1	1	1	1	1
G21	0	0	0	0	0	0	0	0	0	0	0	0	0	0
G22	0	0	0	0	0	0	0	0	0	0	0	0	0	0
G23	0	1	1	1	1	1	1	1	1	1	1	1	1	1
G24	0	0	1	1	1	1	1	1	1	1	1	1	1	1
G25	1	1	1	1	1	1	1	1	1	1	1	1	1	1
G26	0	0	0	0	0	0	0	0	0	0	0	0	0	0
G27	0	0	0	0	0	0	0	0	0	0	0	0	0	0
G28	0	0	0	0	0	0	0	0	0	0	0	0	0	0
G29	0	0	0	0	0	0	0	0	0	0	0	0	0	0
G30	0	0	0	0	0	0	0	0	0	0	0	0	0	0
G31	1	1	1	1	1	1	1	1	1	1	1	1	1	1
G32	1	1	1	1	1	1	1	1	1	1	1	1	1	1
G33	0	0	0	0	0	0	0	0	0	0	0	0	0	0
G34	1	1	1	1	1	1	1	1	1	1	1	1	1	1
G35	1	1	1	1	1	1	1	1	1	1	1	1	1	1
G36	0	0	0	0	0	0	0	0	0	0	0	0	0	0

The inconsistencies in gage performance introduced a degree of uncertainty into system performance analysis. Each gage either performed consistently well or consistently poorly throughout the test. There were only several instances when the readings of a well performing gage had to be discarded due to inconsistency. After the data was sorted, the L_{10} and L_{20} coefficients were calculated, and subsequently the *a*, *b*, and *c* constants of Equation 5-1.

5.3.3 Calculation of Induced Moment

Next, a procedure adopted from Imhoff was used to determine the induced moments. The total moment was calculated by breaking down the load carrying mechanism into three parts: the steel girder bending about its own neutral axis (M_L), the concrete bending about its own neutral-axis (M_u), and the couple induced by the composite action of the deck and girder (Bertoldi). The steel girder properties summarized in Table 4.1, concrete compressive strength of 2,959 psi, and the individual concrete deck dimensions of 59 inches wide and 6 inched deep were used in determining the moments. The modulus of elasticity of the slab concrete was calculated as 3,101 psi, and the slab's moment of inertia was found to be 1062 in^4. Equations 5-12 through 5-15 were used to calculate the total moment.

$$M_L = \left(\sigma_O - \sigma_{CG}\right) S_{steel} \qquad \text{Eq. 5-12}$$

$$M_u = \left(\frac{E_{slab} I_{slab}}{E_{steel} I_{steel}}\right) M_L \qquad \text{Eq. 5-13}$$

$$M_A = \sigma_{CG} A_{steel} \left(d_{steel} - CG + haunch + \frac{t_{slab}}{2}\right) \qquad \text{Eq. 5-14}$$

$$M_{TOTAL} = M_L + M_u + M_A \qquad \text{Eq. 5-15}$$

Where:

S_{steel} = section modulus of the steel girder

E_{slab} = modulus of elasticity of concrete

I_{steel} = moment of inertia of the steel girder

A_{steel} = steel cross-sectional area

d_{steel} = depth of steel girder section

haunch = distance between the steel girder and concrete deck = 0.75 inches

t_{slab} = thickness of concrete slab

5.3.4 Total System Moment

The moments at each of the two girders were calculated, and the obtained values were added to determine the total moment in the system. Since strain readings were taken at a distance 2*d* (46 in) away from the midspan, the values were proportioned to determine the moments at the midspan. The distance between the centers of the supports was 34.5 feet, which was used in the moment calculations. These values were used to back-calculate the applied load using the equation for moment induced by a concentrated load at a midspan. The theoretical loads and experimentally obtained values were plotted, and the least square values are reported in Table 5.5. Along with the R^2 values, Table 5.5 contains the percent error values between the theoretical and back-calculated loads at 90.78 kips (with the exception of N=0 where the system was loaded to 90 kips).

Table 5.5: Least Squares and Percent Errors

Cycle Count	Least Square, R^2	Percent Error, %
Initial Actuator Alignment		
0	0.9988	9.923
100,000	0.9996	10.668
250,000	0.9986	2.54
500,000	0.9991	1.49
1,000,000	0.9986	2.91
1,500,000	0.9991	6.65
Secondary Actuator Alignment		
1,662,000	0.9986	6.02
2,000,000	0.9988	5.65
2,100,000	0.9993	6.65
2,200,000	0.9993	6.33
2,300,000	0.9991	5.85
2,500,000	0.9993	6.66
2,700,000	0.9992	6.46
2,800,000	0.9992	2.03

Tables 5.6 through 5.19 summarize the moments induced into the system during each static test. Also, Figures 5.2 through 5.15 display the plots of the theoretical load versus the experimentally calculated values.

Table 5.6: Initial Base Test Summary

Load Test Summary (N = 0 cycles)					
Applied Load, P (kip)	Tub Girder Moments @ Gage Locations (ft-kip)			Moment @ Midspan (ft-kip)	Back-Calculated Applied Load (kip)
	Directly-Loaded	Indirectly-Loaded	Sum		
0	0	0	0	0	0
10	68.95	30.87	99.82	128.34	14.88
20	117.42	52.42	169.85	218.38	25.32
30	165.25	73.81	239.06	307.36	35.64
40	213.62	95.85	309.48	397.90	46.13
50	261.52	117.58	379.10	487.41	56.51
60	309.86	139.48	449.33	577.71	66.98
70	360.14	161.08	521.23	670.15	77.70
80	410.46	181.50	591.96	761.09	88.24
90	460.82	202.84	663.66	853.28	98.93

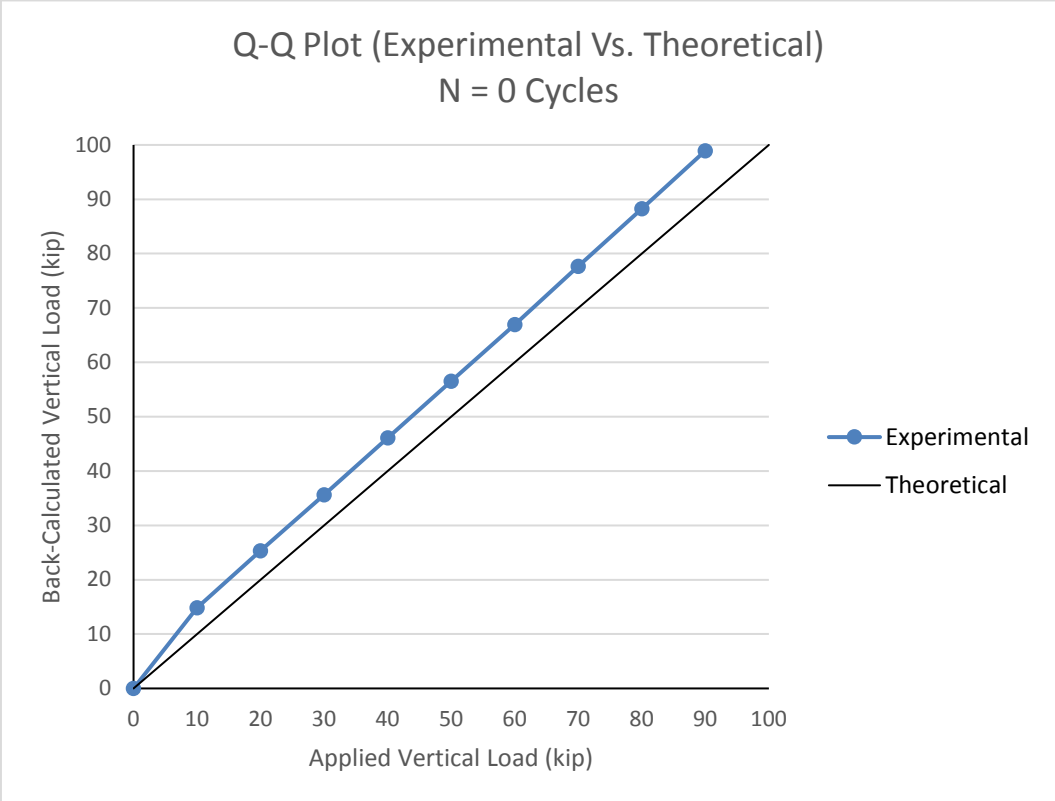

Figure 5.2: Experimental Vs. Theoretical Loads at Base Test

Table 5.7: Load Test Summary at 100,000 Cycles

Load Test Summary (N = 100,000 cycles)					
Applied Load, P (kip)	Tub Girder Moments @ Gage Locations (ft-kip)			Moment @ Midspan (ft-kip)	Back-Calculated Applied Load (kip)
	Directly-Loaded	Indirectly-Loaded	Sum		
0	0	0	0	0	0
9.08	42.09	24.25	66.35	85.30	9.89
18.16	75.97	43.68	119.65	153.84	17.84
27.23	107.32	63.38	170.70	219.47	25.45
36.31	141.72	83.16	224.88	289.13	33.52
45.39	176.19	102.91	279.10	358.84	41.60
54.47	209.56	122.70	332.26	427.19	49.53
63.55	245.99	143.17	389.16	500.35	58.01
72.62	277.45	162.14	439.60	565.20	65.53
81.7	308.53	181.89	490.42	630.54	73.11
90.78	342.13	201.95	544.08	699.53	81.10

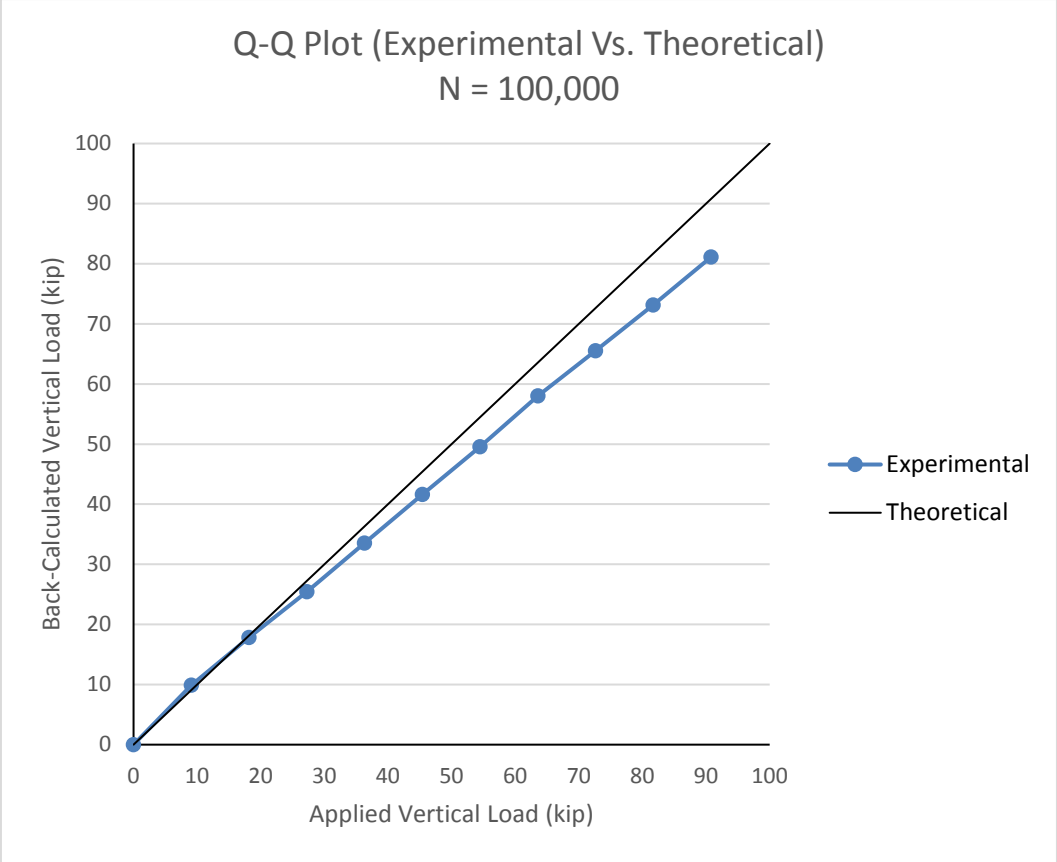

Figure 5.3: Experimental Vs. Theoretical Loads at 100,000 Cycles

Table 5.8: Load Test Summary at 250,000 Cycles

Load Test Summary (N = 250,000 cycles)					
Applied Load, P (kip)	Tub Girder Moments @ Gage Locations (ft-kip)			Moment @ Midspan (ft-kip)	Back-Calculated Applied Load (kip)
	Directly-Loaded	Indirectly-Loaded	Sum		
0	0	0	0	0	0
9.08	56.08	26.31	82.38	105.92	12.28
18.16	94.62	45.05	139.67	179.57	20.82
27.23	132.45	63.08	195.53	251.39	29.15
36.31	171.10	81.14	252.24	324.31	37.60
45.39	210.06	99.95	310.01	398.59	46.21
54.47	247.26	119.08	366.34	471.01	54.61
63.55	284.54	137.31	421.85	542.38	62.88
72.62	320.22	155.40	475.63	611.52	70.90
81.7	357.14	175.02	532.16	684.20	79.33
90.78	398.72	194.82	593.54	763.12	88.48

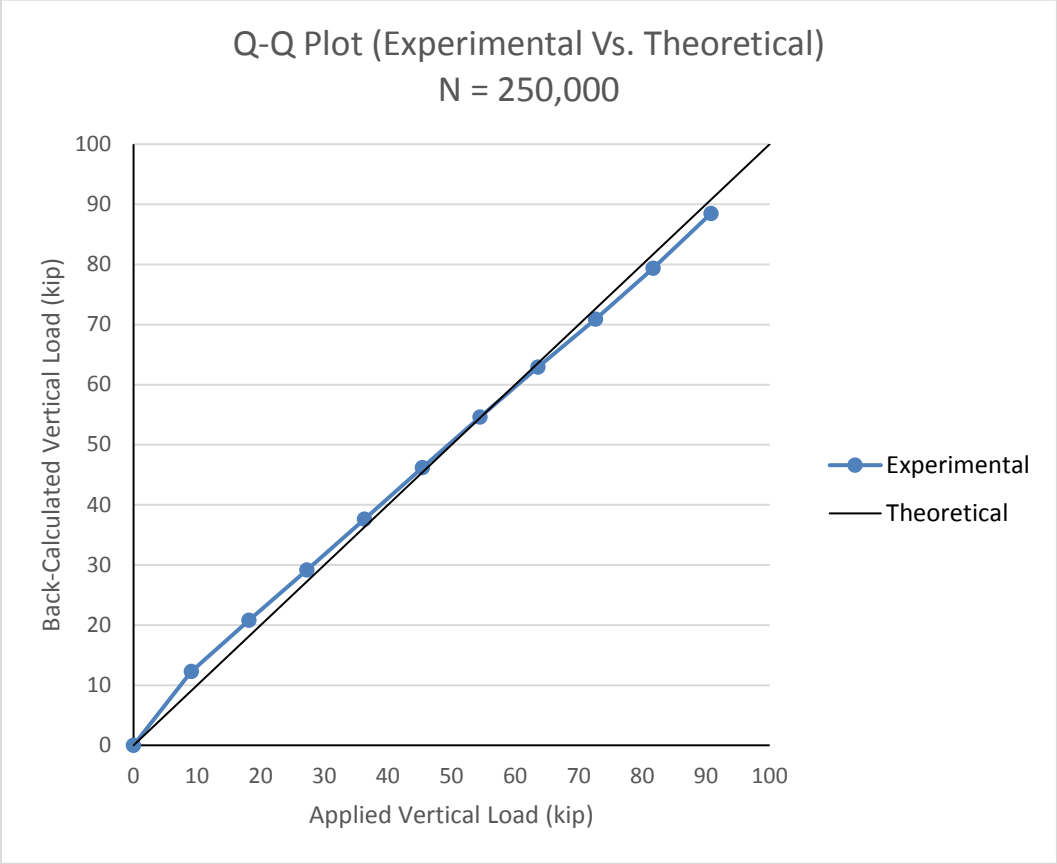

Figure 5.4: Experimental Vs. Theoretical Loads at 250,000 Cycles

Table 5.9: Load Test Summary at 500,000 Cycles

Load Test Summary (N = 500,000 cycles)					
Applied Load, P (kip)	Tub Girder Moments @ Gage Locations (ft-kip)			Moment @ Midspan (ft-kip)	Back-Calculated Applied Load (kip)
	Directly-Loaded	Indirectly-Loaded	Sum		
0	0	0	0	0	0
9.08	56.96	27.26	84.22	108.28	12.55
18.16	96.88	46.23	143.11	184.00	21.33
27.23	135.05	65.00	200.05	257.20	29.82
36.31	176.47	83.71	260.18	334.51	38.78
45.39	217.08	102.54	319.62	410.94	47.64
54.47	258.22	121.82	380.03	488.61	56.65
63.55	298.77	140.91	439.68	565.30	65.54
72.62	339.96	159.54	499.50	642.21	74.46
81.7	379.52	179.14	558.66	718.28	83.28
90.78	419.42	198.63	618.05	794.63	92.13

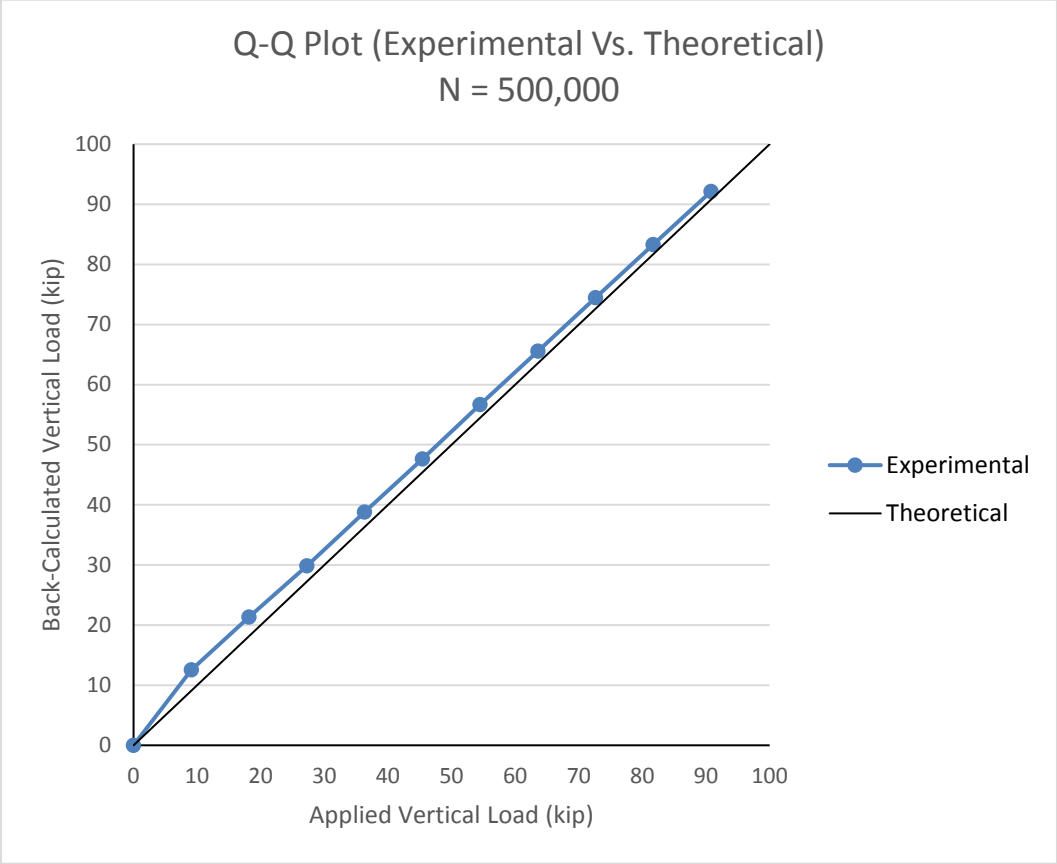

Figure 5.5: Experimental Vs. Theoretical Loads at 500,000 Cycles

Table 5.10: Load Test Summary at 1,000,000 Cycles

Load Test Summary (N = 1,000,000 cycles)					
Applied Load, P (kip)	Tub Girder Moments @ Gage Locations (ft-kip)			Moment @ Midspan (ft-kip)	Back-Calculated Applied Load (kip)
	Directly-Loaded	Indirectly-Loaded	Sum		
0	0	0	0	0	0
9.08	62.69	27.73	90.42	116.25	13.48
18.16	104.31	45.07	149.38	192.06	22.27
27.23	136.90	64.11	201.01	258.44	29.96
36.31	180.14	82.65	262.79	337.87	39.17
45.39	223.11	100.85	323.96	416.52	48.29
54.47	265.88	119.54	385.42	495.55	57.45
63.55	307.09	137.24	444.33	571.28	66.24
72.62	349.83	156.47	506.30	650.95	75.47
81.7	391.13	173.35	564.47	725.75	84.15
90.78	433.39	193.31	626.69	805.75	93.42

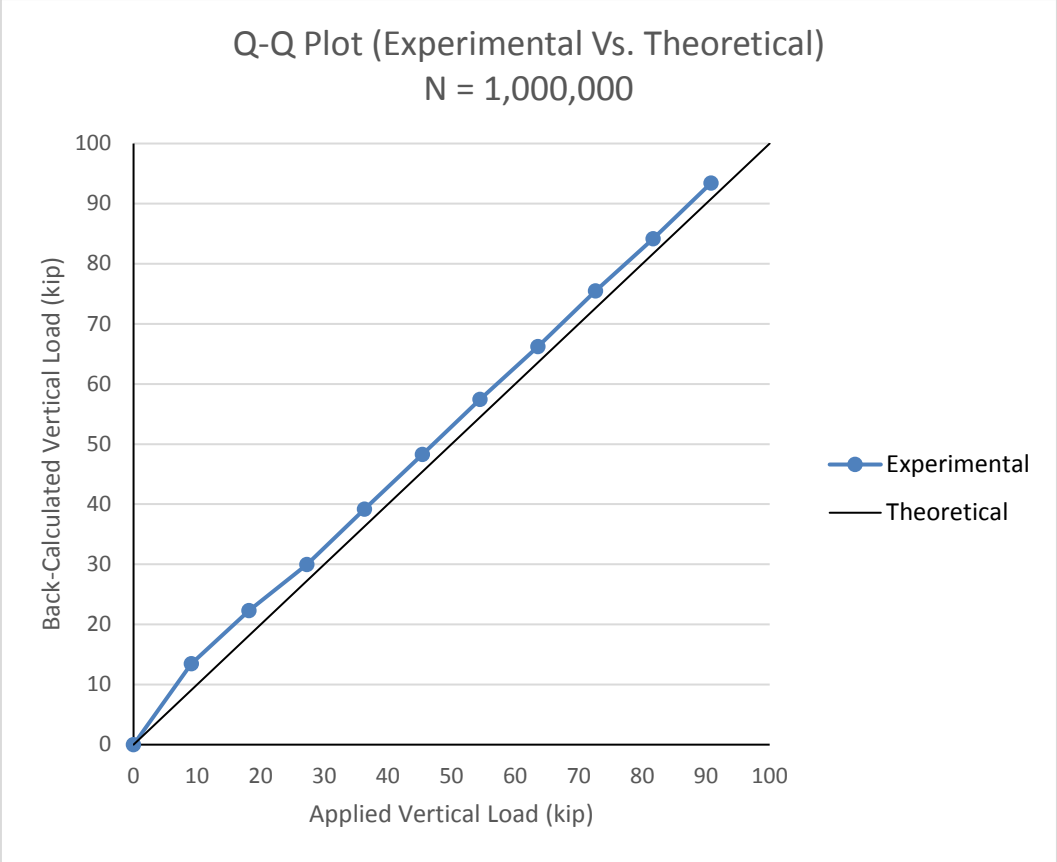

Figure 5.6: Experimental Vs. Theoretical Loads at 1,000,000 Cycles

Table 5.11: Load Test Summary at 1,500,000 Cycles

Load Test Summary (N = 1,500,000 cycles)					
Applied Load, P (kip)	Tub Girder Moments @ Gage Locations (ft-kip)			Moment @ Midspan (ft-kip)	Back-Calculated Applied Load (kip)
	Directly-Loaded	Indirectly-Loaded	Sum		
0	0	0	0	0	0
9.08	62.57	24.79	87.35	112.31	13.02
18.16	106.52	41.40	147.92	190.18	22.05
27.23	151.60	59.74	211.35	271.73	31.51
36.31	196.78	77.47	274.25	352.61	40.88
45.39	241.36	94.05	335.41	431.24	50.00
54.47	286.89	113.82	400.71	515.20	59.73
63.55	331.21	131.48	462.69	594.89	68.97
72.62	374.93	149.27	524.20	673.97	78.14
81.7	419.17	167.60	586.76	754.41	87.47
90.78	464.35	185.14	649.49	835.06	96.82

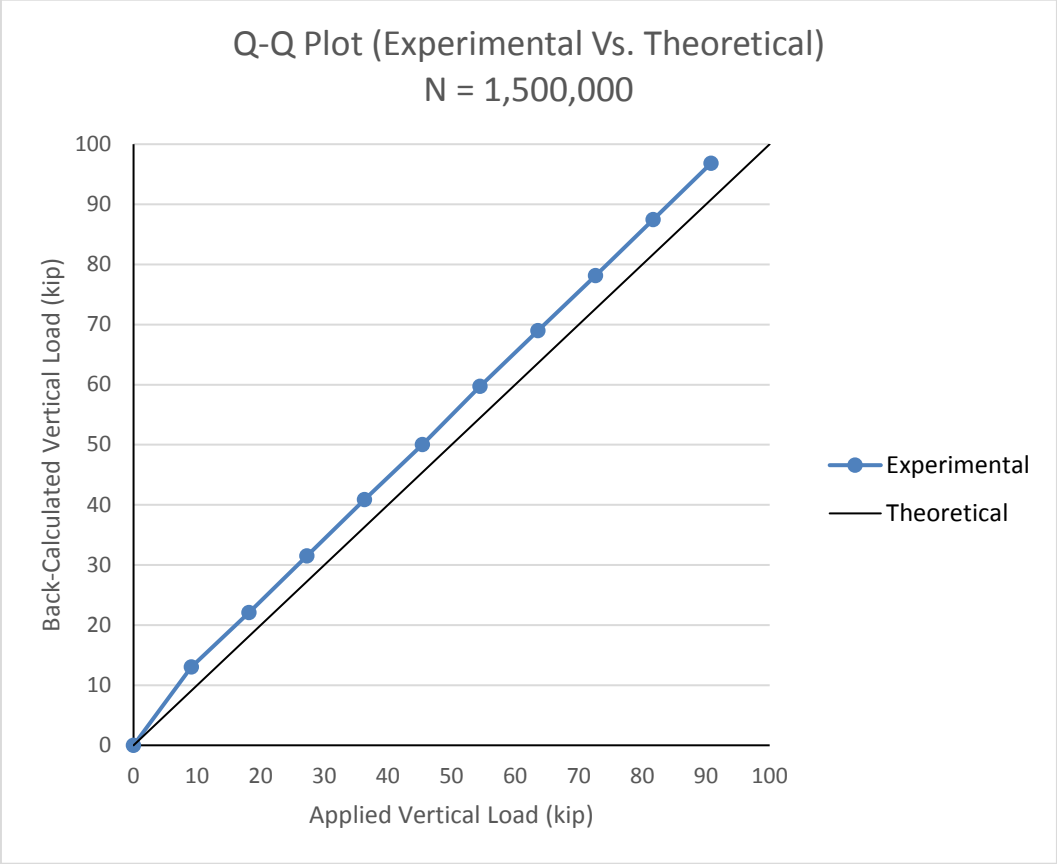

Figure 5.7: Experimental Vs. Theoretical Loads at 1,500,000 Cycles

Table 5.12: Secondary Alignment Base Test

Base Test (Secondary Alignment) Load Test Summary					
Applied Load, P (kip)	Tub Girder Moments @ Gage Locations (ft-kip)			Moment @ Midspan (ft-kip)	Back-Calculated Applied Load (kip)
	Directly-Loaded	Indirectly-Loaded	Sum		
0	0	0	0	0	0
9.08	63.91	26.89	90.80	116.74	13.54
18.16	107.55	45.17	152.72	196.35	22.77
27.23	152.63	63.31	215.94	277.64	32.19
36.31	196.15	81.01	277.16	356.35	41.32
45.39	239.79	98.07	337.86	434.39	50.36
54.47	285.97	116.18	402.14	517.04	59.95
63.55	329.92	132.29	462.20	594.26	68.90
72.62	374.27	148.18	522.45	671.72	77.88
81.7	420.73	164.77	585.51	752.80	87.28
90.78	465.77	179.88	645.65	830.12	96.25

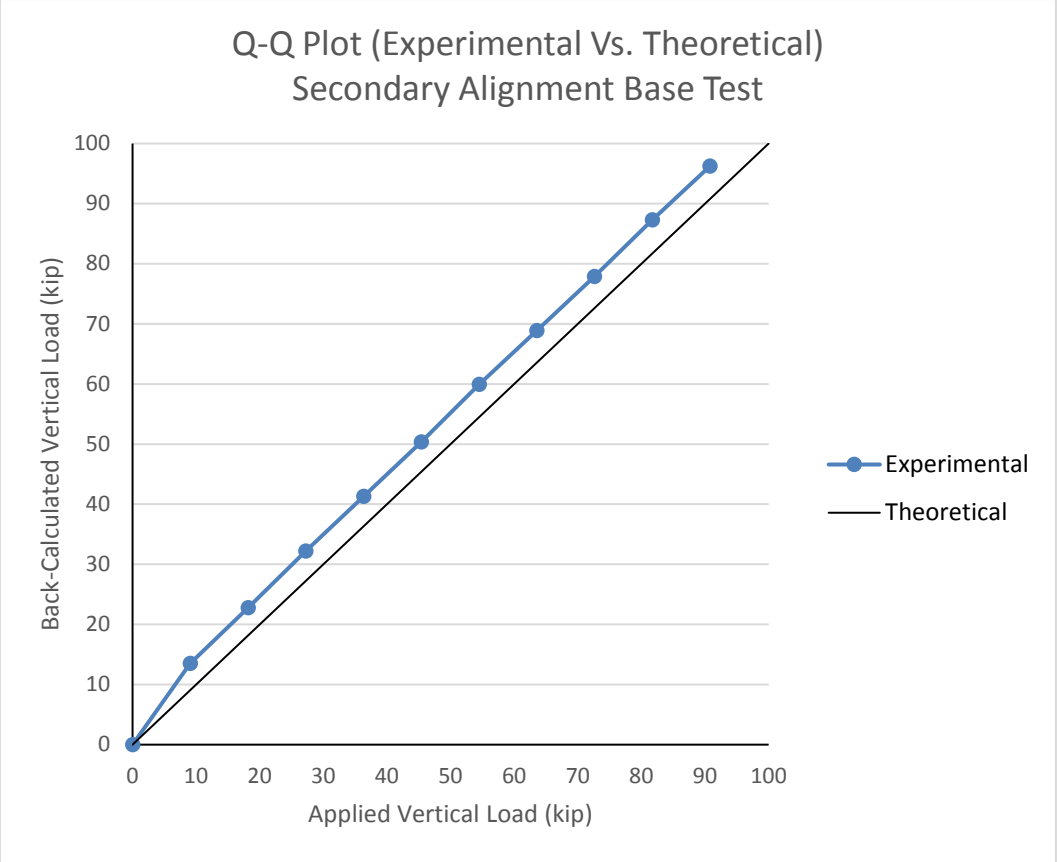

Figure 5.8: Experimental Vs. Theoretical Loads at Secondary Alignment Base Test

Table 5.13: Load Test Summary at 2,000,000 Cycles

Load Test Summary (N = 2,000,000 Cycles)					
Applied Load, P (kip)	Tub Girder Moments @ Gage Locations (ft-kip)			Moment @ Midspan (ft-kip)	Back-Calculated Applied Load (kip)
	Directly-Loaded	Indirectly-Loaded	Sum		
0	0	0	0	0	0
9.08	60.91	25.27	86.18	110.81	12.85
18.16	105.11	43.76	148.87	191.41	22.19
27.23	150.38	62.95	213.33	274.28	31.80
36.31	194.52	80.74	275.26	353.91	41.03
45.39	239.54	99.28	338.82	435.63	50.51
54.47	282.81	117.08	399.89	514.14	59.61
63.55	327.28	135.42	462.70	594.90	68.97
72.62	371.13	154.14	525.27	675.35	78.30
81.7	412.98	171.17	584.15	751.05	87.08
90.78	454.92	188.46	643.39	827.21	95.91

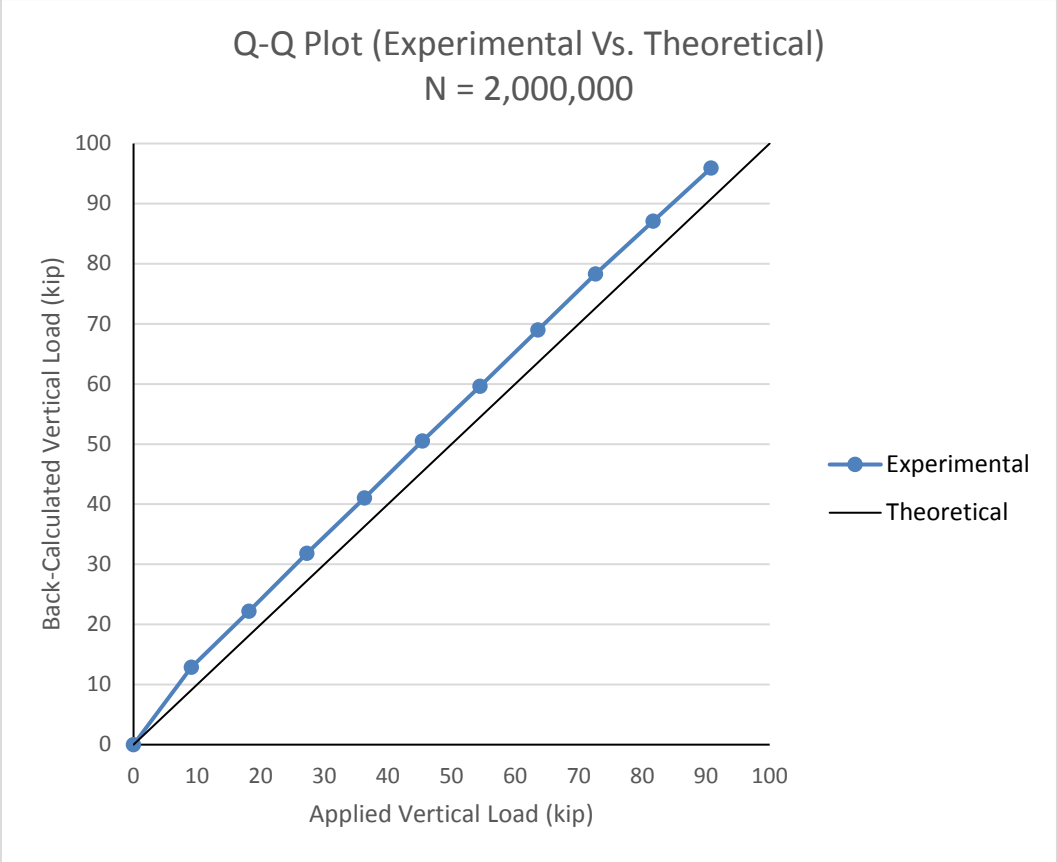

Figure 5.9: Experimental Vs. Theoretical Loads at 2,000,000 Cycles

Table 5.14: Load Test Summary at 2,100,000 Cycles

Load Test Summary (2,100,000 Cycles)					
Applied Load, P (kip)	Tub Girder Moments @ Gage Locations (ft-kip)			Moment @ Midspan (ft-kip)	Back-Calculated Applied Load (kip)
	Directly-Loaded	Indirectly-Loaded	Sum		
0	0	0	0	0	0
9.08	59.41	23.63	83.04	106.76	12.38
18.16	103.74	41.86	145.60	187.20	21.70
27.23	148.37	59.99	208.36	267.89	31.06
36.31	193.53	78.16	271.69	349.31	40.50
45.39	238.26	100.72	338.98	435.83	50.53
54.47	282.87	119.02	401.89	516.72	59.91
63.55	326.90	136.83	463.73	596.23	69.13
72.62	371.23	157.47	528.70	679.75	78.81
81.7	414.94	172.99	587.92	755.90	87.64
90.78	458.86	190.63	649.49	835.06	96.82

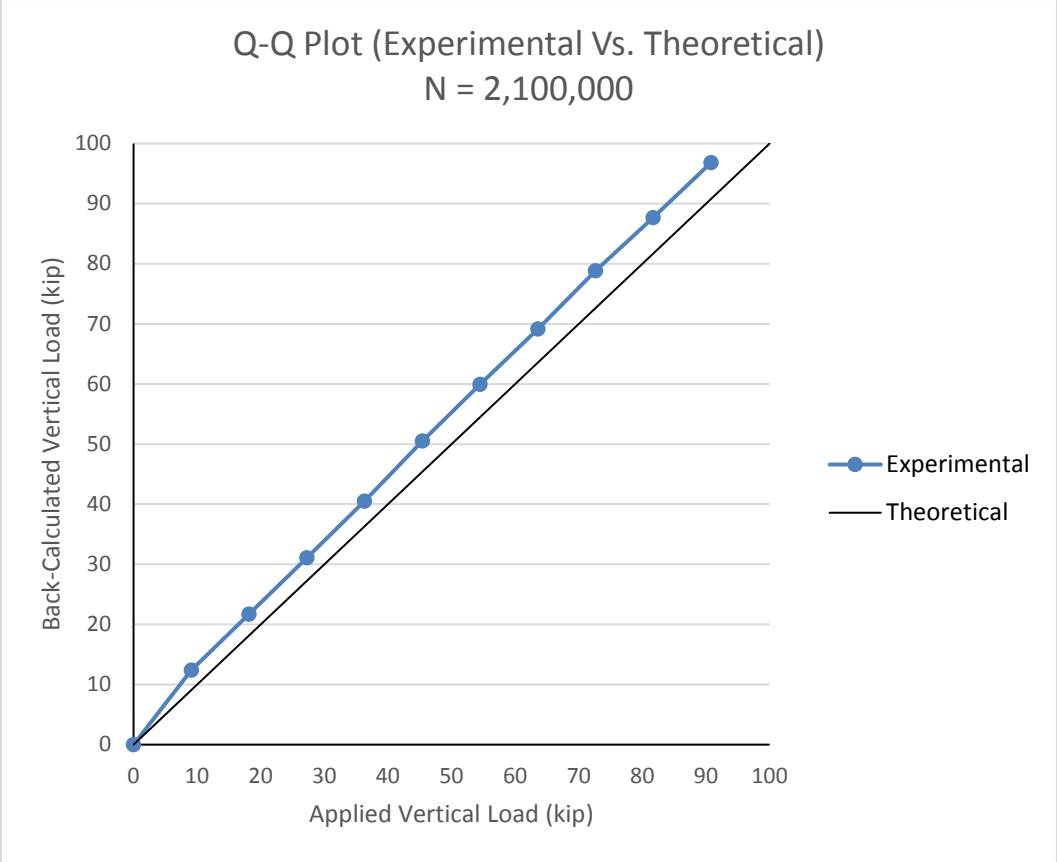

Figure 5.10: Experimental Vs. Theoretical Loads at 2,100,000 Cycles

Table 5.15: Load Test Summary at 2,200,000 Cycles

Load Test Summary (2,200,000 Cycles)					
Applied Load, P (kip)	Tub Girder Moments @ Gage Locations (ft-kip)			Moment @ Midspan (ft-kip)	Back-Calculated Applied Load (kip)
	Directly-Loaded	Indirectly-Loaded	Sum		
0	0	0	0	0	0
9.08	59.16	24.36	83.52	107.38	12.45
18.16	103.40	42.77	146.17	187.94	21.79
27.23	148.20	61.03	209.23	269.01	31.19
36.31	192.68	80.12	272.80	350.74	40.67
45.39	237.51	98.27	335.78	431.72	50.05
54.47	281.88	116.68	398.56	512.43	59.41
63.55	325.92	135.26	461.18	592.94	68.75
72.62	369.66	152.92	522.58	671.89	77.90
81.7	413.49	171.29	584.79	751.87	87.17
90.78	457.54	190.01	647.55	832.56	96.53

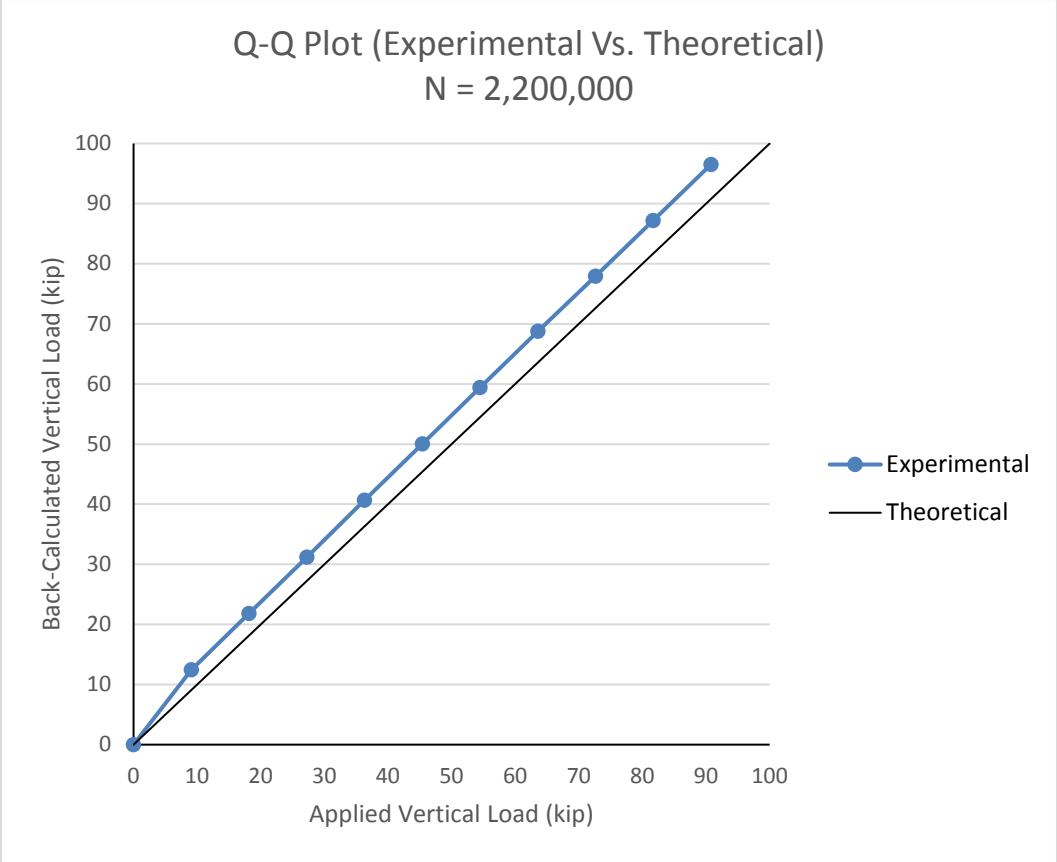

Figure 5.11: Experimental Vs. Theoretical Loads at 2,200,000 Cycles

Table 5.16: Load Test Summary at 2,300,000 Cycles

Load Test Summary (2,300,000 Cycles)					
Applied Load, P (kip)	Tub Girder Moments @ Gage Locations (ft-kip)			Moment @ Midspan (ft-kip)	Back-Calculated Applied Load (kip)
	Directly-Loaded	Indirectly-Loaded	Sum		
0	0	0	0	0	0
9.08	58.51	25.90	84.41	108.53	12.58
18.16	102.98	43.19	146.17	187.93	21.79
27.23	148.11	62.04	210.15	270.20	31.33
36.31	192.79	80.70	273.49	351.63	40.77
45.39	237.03	98.29	335.32	431.13	49.99
54.47	281.21	115.95	397.16	510.63	59.20
63.55	325.40	133.33	458.73	589.79	68.38
72.62	368.72	151.07	519.80	668.31	77.49
81.7	412.92	169.52	582.45	748.86	86.82
90.78	456.87	187.72	644.60	828.77	96.09

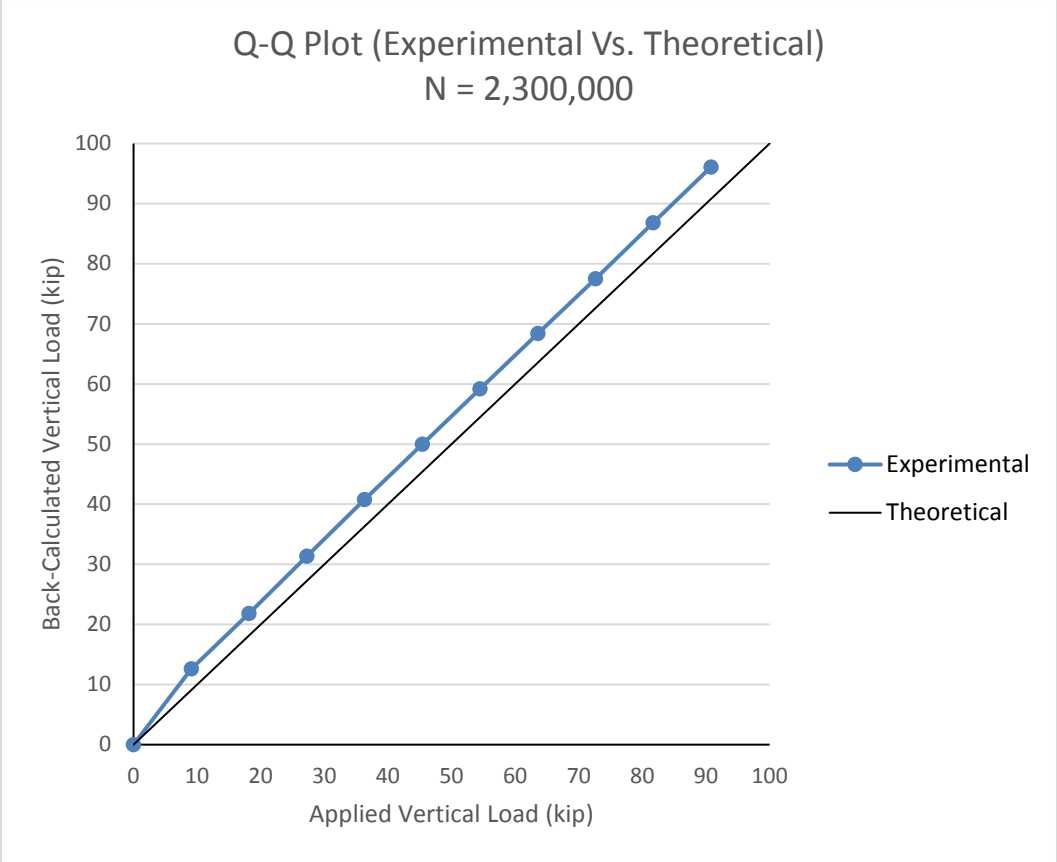

Figure 5.12: Experimental Vs. Theoretical Loads at 2,300,000 Cycles

Table 5.17: Load Test Summary at 2,500,000 Cycles

Load Test Summary (2,500,000 Cycles)					
Applied Load, P (kip)	Tub Girder Moments @ Gage Locations (ft-kip)			Moment @ Midspan (ft-kip)	Back-Calculated Applied Load (kip)
	Directly-Loaded	Indirectly-Loaded	Sum		
0	0	0	0	0	0
9.08	59.29	24.14	83.43	107.27	12.44
18.16	104.00	42.52	146.52	188.39	21.84
27.23	149.76	61.22	210.99	271.27	31.45
36.31	194.20	77.97	272.18	349.94	40.57
45.39	238.62	96.46	335.08	430.81	49.95
54.47	284.08	114.84	398.93	512.91	59.47
63.55	328.94	133.82	462.77	594.99	68.98
72.62	372.68	152.62	525.29	675.38	78.30
81.7	416.68	171.02	587.70	755.62	87.61
90.78	460.91	188.61	649.52	835.10	96.82

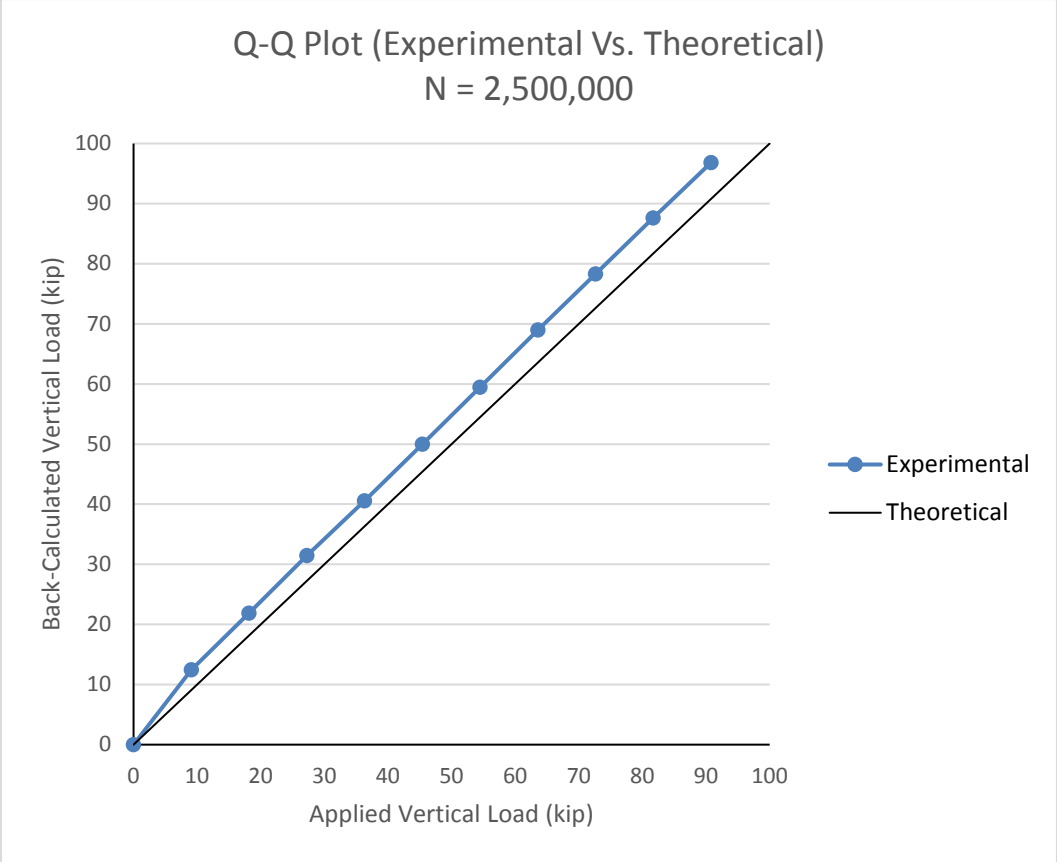

Figure 5.13: Experimental Vs. Theoretical Loads at 2,500,000 Cycles

Table 5.18: Load Test Summary at 2,700,000 Cycles

Load Test Summary (2,700,000 Cycles)					
Applied Load, P (kip)	Tub Girder Moments @ Gage Locations (ft-kip)			Moment @ Midspan (ft-kip)	Back-Calculated Applied Load (kip)
	Directly-Loaded	Indirectly-Loaded	Sum		
0	0	0	0	0	0
9.08	60.11	24.68	84.79	109.02	12.64
18.16	104.87	43.07	147.93	190.20	22.05
27.23	149.69	60.80	210.49	270.63	31.38
36.31	194.80	79.05	273.85	352.09	40.82
45.39	240.35	96.46	336.81	433.04	50.21
54.47	284.52	113.98	398.50	512.36	59.40
63.55	329.57	132.72	462.29	594.37	68.91
72.62	373.03	150.60	523.63	673.24	78.06
81.7	417.14	168.55	585.70	753.04	87.31
90.78	462.22	186.08	648.31	833.54	96.64

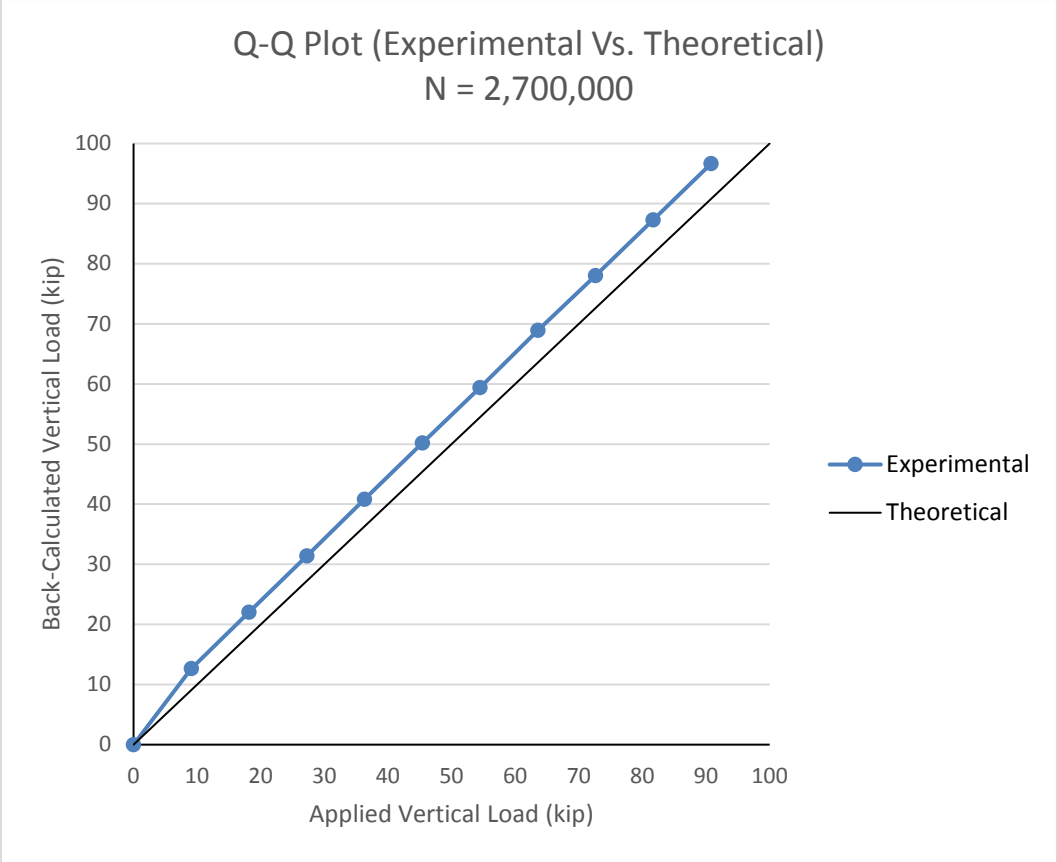

Figure 5.14: Experimental Vs. Theoretical Loads at 2,700,000 Cycles

Table 5.19: Load Test Summary at 2,800,000 Cycles

Load Test Summary (2,800,000 Cycles)					
Applied Load, P (kip)	Tub Girder Moments @ Gage Locations (ft-kip)			Moment @ Midspan (ft-kip)	Back-Calculated Applied Load (kip)
	Directly-Loaded	Indirectly-Loaded	Sum		
0	0	0	0	0	0
9.08	60.38	20.72	81.09	104.26	12.09
18.16	105.34	36.67	142.01	182.58	21.17
27.23	150.21	52.04	202.24	260.03	30.15
36.31	195.36	67.43	262.78	337.86	39.17
45.39	240.38	82.95	323.34	415.72	48.20
54.47	283.70	97.92	381.62	490.65	56.89
63.55	328.80	113.04	441.84	568.08	65.86
72.62	373.00	130.19	503.19	646.96	75.01
81.7	416.78	145.78	562.56	723.29	83.86
90.78	460.51	160.85	621.36	798.89	92.63

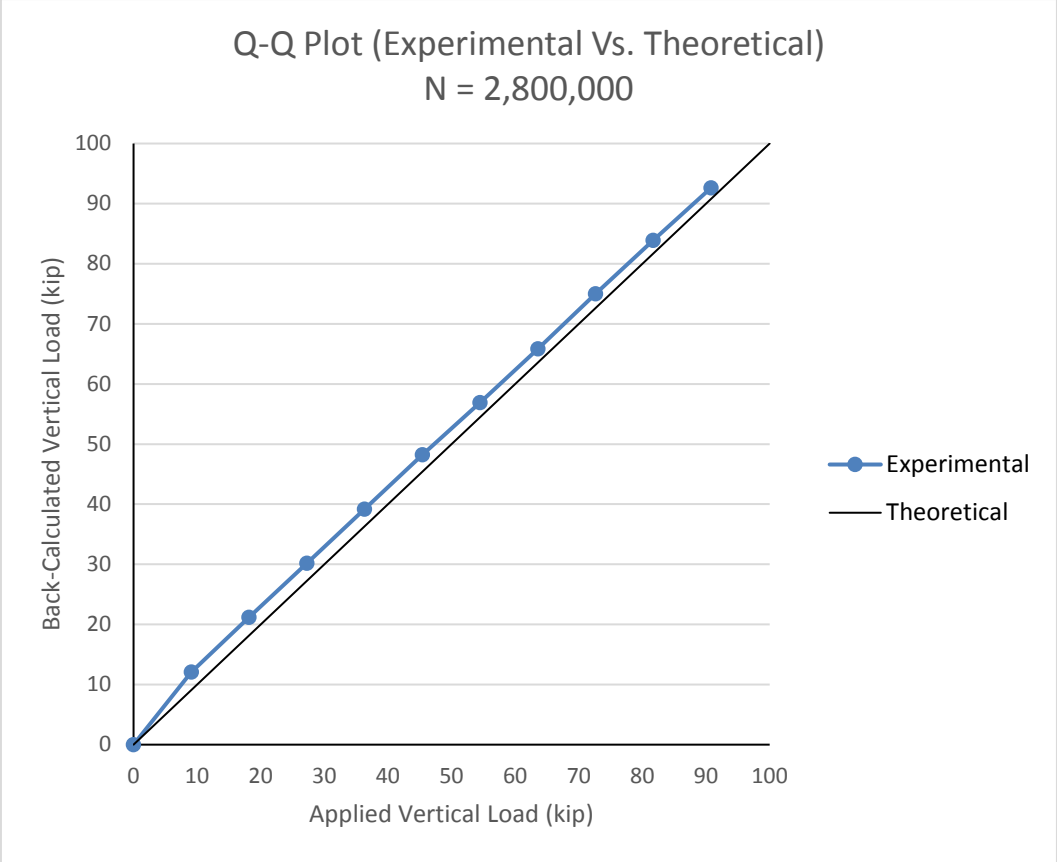

Figure 5.15*: *Experimental Vs. Theoretical Loads at 2,800,000 Cycles

Based on the results summarized in Tables 5.6 through 5.19 and Figures 5.2 through 5.15, the experimentally obtained values closely correspond to the theoretical values. Deviations summarized in Table 5.5 are minimal, and may be due to inconsistent gage readings.

5.4 DISTRIBUTION FACTORS

The Stalling/Yoo method was used to determine the live load distribution factors according to Equation 5-12:

$$DF_i = \frac{M_i}{\sum_{j=1}^{k} M_j} \qquad \text{Eq. 5-12}$$

Where M_i is the moment in individual girder, and term $\sum_{j=1}^{k} M_j$ represents the total moment in the system. Average distribution factors calculated using Equation 5-12 during the static tests are summarized in Table 5.7.

Table 5.20: Summary of Distribution Factors

Cycle Count	Average Distribution Factor	
	Directly Loaded Girder	Indirectly Loaded Girder
Initial Actuator Alignment		
0	0.691	0.309
100,000	0.631	0.369
250,000	0.676	0.324
500,000	0.678	0.322
1,000,000	0.690	0.310
1,500,000	0.717	0.283
Secondary Actuator Alignment		
1,662,000	0.711	0.289
2,000,000	0.707	0.293
2,100,000	0.708	0.292
2,200,000	0.707	0.293
2,300,000	0.706	0.294
2,500,000	0.711	0.289
2,700,000	0.712	0.288
2,800,000	0.743	0.257

The distribution factors summarized in Table 5.7 suggest that the UHPC joint effectively distributed stresses across the system throughout the testing duration. The data is consistent within each set of pre- and post- deck failure values. The variance between the sets on average is 0.033.

5.5 DEFLECTIONS

The system deflections measured by linear variable displacement transducers (LVDT) at 90.78 kips are summarized in Table 5.21. Figure 4.34 provides a visual legend regarding the location of the LVDT's.

Table 5.21: Summary of Deflections

Cycle Count	Deflection at 90.78 kips (in)							
	L7	R7	L14	R14	L21	R21	L28	R28
Initial Actuator Alignment								
0	0.269	0.099	0.427	0.178	0.441	0.179	0.280	0.112
100,000	0.273	0.098	0.434	0.179	0.447	0.180	0.283	0.112
250,000	0.282	0.100	0.447	0.183	0.461	0.184	0.293	0.114
500,000	0.285	0.098	0.452	0.181	0.467	0.183	0.296	0.113
1,000,000	0.296	0.092	0.469	0.177	0.484	0.178	0.307	0.109
1,500,000	0.301	0.090	0.477	0.173	0.492	0.175	0.312	0.107
Secondary Actuator Alignment								
1,662,000	0.120	0.300	0.210	0.484	0.208	0.486	0.114	0.320
2,000,000	0.125	0.301	0.220	0.488	0.217	0.491	0.119	0.320
2,100,000	0.128	0.301	0.222	0.487	0.219	0.490	0.122	0.319
2,200,000	0.126	0.301	0.221	0.487	0.218	0.490	0.120	0.318
2,300,000	0.128	0.304	0.223	0.493	0.219	0.495	0.122	0.322
2,500,000	0.127	0.306	0.223	0.495	0.219	0.498	0.121	0.324
2,700,000	0.128	0.309	0.225	0.499	0.221	0.502	0.122	0.328
2,800,000	0.111	0.269	0.195	0.435	0.192	0.438	0.106	0.284

5.6 SUMMARY

This chapter summarized the results obtained throughout the course of testing. The linear regression algorithm employed by Helwig and Fan along with Imhoff's procedure for induced moment calculations were effective tools in analysis of the collected data. A degree of result variation was introduced by the inconsistent strain gage performance. The results data was split into two parts: pre- and post-deck failure. The data was mostly consistent within each part. A minor difference was observed in distribution factors and deflections when the pre- and post-deck failure sets of data were compared. Overall, the UHPC joint exhibited satisfactory performance characteristics transferring the stresses from one modular unit to another.

CHAPTER 6: PROJECT SUMMARY AND CONCLUDING REMARKS

6.1 PROJECT SUMMARY

The scope of this project was to evaluate the performance of modular press-brake-formed tub girders with a UHPC joint. This was accomplished by building a full-scale 35-foot long bridge model inside a laboratory and testing it in a controlled setting. The bridge model consisted of two press-brake-formed tub girders with 6-inch concrete decks cast on top. The UHPC joint was poured between the two decks. The model was fatigue tested to simulate a 75-year period in a rural environment with an average daily traffic of 1000 vehicles, 10% of which were assumed to be truck traffic. A Service II moment was induced into the system at a predetermined numbers of cycles in order to evaluate the performance of the model. Based on the collected and analyzed strain gage data, performance of the joint was consistent throughout the test. While the low-strength concrete used to pour the decks failed under the imposed loads, the UHPC joint performed satisfactory at every stage of the testing, transferring the stresses from directly loaded girders to the adjacent ones.

6.2 RECOMMENDATIONS FOR CONTINUED RESEARCH

Based on this study, the following recommendations for future work are given:

- Use FEA modeling to replicate the system to confirm the obtained results in terms of the live load distribution factors and compare obtained results with the distribution factors specified in AASHTO LRFD.
- Model a similar system that includes a greater number of tub girders, determine live load distribution factors, and compare results with the results obtained during the lab testing.
- Validate results obtained during laboratory testing and the FEA modeling through field testing of a bridge that consists of press-brake-formed tub girder modular units connected with the UHPC concrete joints.

REFERENCES

Adams, M., & Nicks, J., & Stabile, T.,& Wu, J., & Schlatter, W., & Hartmann, J. (2011). *Geosynthetic Reinforced Soil Integrated Bridge System, Synthesis Report*. McLean, VA, Federal Highway Administration.

American Association of State Highway and Transportation Officials. (2012). *AASHTO LRFD Bridge Design Specifications, Sixth Edition.* Washington, DC, AASHTO.

Architectural Concrete Chemicals. (2014). *ACC Altus Series In-Form Retarders* [Brochure]. Capital Heights, MD. http://www.acchemicals.com/wp-content/uploads/2010/05/ACC-Altus-Brochure.pdf

ASTM C109 Standard Test Method for Compressive Strength of Hydraulic Cement Mortars (Using 2-in. or [50-mm] Cube Specimens), ASTM International, West Conshohocken, PA

ASTM C143 Standard Test Method for Slump of Hydraulic-Cement Concrete, ASTM International, West Conshohocken, PA

ASTM C39/C39M-15 Standard Test Method for Compressive Strength of Cylindrical Concrete Specimens, ASTM International, West Conshohocken, PA

Barker, M.G. & Imhoff, C.M. & McDaniel, W.T. & Frederick T.L. (1999). *Field Testing and Load Rating procedures for Steel Girder Bridges.* Jefferson City, MO: Missouri Department of Transportation

Bertoldi, A.G. (2009). *A Strength and Serviceability Assessment of High Performance Steel Bridge 10462*. Department of Civil & Environmental Engineering. Morgantown, WV, West Virginia University. Master of Science.

Burgueno, R. & Pavlich, B. S. (2008). *Evaluation of Prefabricated Composite Steel Box Girder Systems for Rapid Bridge Construction*. Landing, MI: Michigan Department of Transportation.

Culmo, M. P. (2011). *Accelerated Bridge Construction – Experience in Design, Fabrication and Erection of Prefabricated Bridge Elements and Systems.* McLean, VA, Federal Highway Administration.

Culmo, M.P. "I-93 FAST 14 Project Issues and Lessons Learned, Preliminary Designer Prospective." FHWA-MassDOT Highways for LIFE I-93 Fast 14 Showcase Presentations. Federal Highway Administration.

Culmo, M.P. "Piece By Piece." *Modern Steel Construction*, September 2014. American Institute of Steel Construction.

Davis, M. & Graybeal, B. A. (2008). Cylinder or Cube: Strength Testing of 80 to 200 MPa (11.6 to 29 ksi) Ultra-High-Performance Fiber-Reinforced Concrete. *ACI Material Journal*, November-December 2008.

Federal Highway Administration. (2015). *Every Day Counts: Building a Culture of Innovation for the 21st Century*. *EDC-2 Final Report.* Washington, DC, Federal Highway Administration.

Federal Highway Administration. (2015). *Every Day Counts: Creating Efficiency Through Technology and Collaboration. EDC-3 Progress Report #2*. Washington, DC, Federal Highway Administration.

Graybeal, B. A. (2010). *Behavior of Field-Cast Ultra-High Performance Concrete Bridge Deck Connections Under Cyclic and Static Structural Loading*. McLean, VA, Federal Highway Administration.

Graybeal, B.A. (2014). *Design and Construction of Field-Cast UHPC Connections*.

McLean, VA, Federal Highway Administration.

Graybeal, B.A., & Russell, H.G., (2013). *Ultra-High Performance Concrete: A state-of-the-Art Report for the Bridge Community*. McLean, VA, Federal Highway Administration.

Haber, Z.B. "Re: UHPC deck joint forming." Message to Karl E. Barth. 2 April 2015. E-mail

Helwig, T.A. & Fan, Z. (2000). *Field and Computational Studies of Steel Trapezoidal Box Girder Bridges.* Austin, TX: Texas Department of Transportation.

Hibbeler, R.C. (2006). Structural Analysis. Upper Saddle River, NJ, Pearson Education, Inc.

Jaber, Fouad. "IBRD, EDC and ABC Initiatives Case Study Boone County Nebraska." ABC-UTC Webinar June 30th, 2015. Nebraska Department of Roads.

Kelly, L. T. (2014). *Experimental Evaluation of Non-Composite Shallow Press-Brake-Formed Steel Tub Girders*. Department of Civil & Environmental Engineering. Morgantown, WV, West Virginia University. Master of Science.

MassDOT. "93 Fast 14 Rapid Bridge Replacement Project." 14 Aug. 2016.

https://www.massdot.state.ma.us/highway/HighlightedProjects/93Fast14RapidBridgeReplacementProject.aspx

Michaelson, G. K. (2014). *Development and Feasibility Assessment of Shallow Press-Brake-Formed Steel Tub Girders for Short-Span Bridge Applications.* Doctor of Philosophy, West Virginia University, Morgantown, WV.

Michaelson, G. K. "Base Test Evaluation." Message to Pavlo Kozhokin & Brian Gallion. 12 December 2015. E-mail.

Stallings, J. M., & Yoo, C. H. (1993). Tests and Ratings of Short –Span Steel Bridges. *ASCE Journal of Structural Engineering, 2150-2168*.

Structure Design and Rehabilitation, Inc. (2005). *Prefabricated Steel Bridge* Systems. Washington, DC: Federal Highway Administration.

West Virginia Division of Highways. (2010). *Standard Specifications Road and Bridges*. West Virginia Division of Highways.

APPENDIX A: LOADING CALCULATIONS

Gage and LVDT readings were calibrated to a zero-reading on a composite section (excluding the dead load effect), and therefore the DC and DW terms were disregarded in determination of the Service II moment. Eq. A1-1 represents this modification:

$$M_{service\ II} = 1.3\left(1.33M_{Vehicle} + M_{Lane}\right) \qquad \text{Eq. A1-1}$$

Using a load factor of 1.75 for an infinite life fatigue, and an impact factor of 1.15, the Fatigue I moment was determined according to Eq. A1-2:

$$M_{Fatigue\ I} = (1.75)(1.15)\left(M_{Fatigue\ Truck}\right) \qquad \text{Eq. A1-2}$$

Influence line analysis was used in order to determine the moments at the midspan of a simply supported beam. Eq. A1-3 displays the set of functions for the moment at the midspan:

$$f(x) = \begin{cases} x/2 & [0, L/2] \\ (L-x)/2 & [L/2, L] \end{cases} \qquad \text{Eq. A1-3}$$

The AASHTO HL-93 load model consists of either the truck and the lane or the tandem and the lane. Figure A1.1 displays an HL-93 truck placement on the simple span bridge.

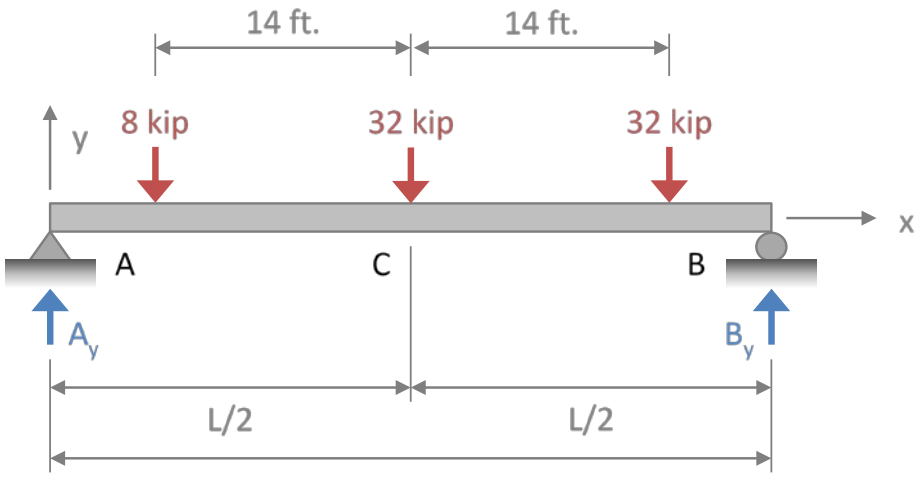

Figure A.1: HL-93 Truck Placement

Using the influence line analysis, the moment induced by the HL-93 truck is as follows:

$$
\begin{aligned}
M_{\text{Truck}} &= \sum_{i=1}^{n} P_i \times f\left(x_i\right) \\
&= 8 \times f\left(L/2-14\right) + 32 \times f\left(L/2\right) + 32 \times f\left(L/2+14\right) \\
&= 8 \times \left(L/4-7\right) + 32 \times \left(L/4\right) + 32 \times \left(L/4-7\right) \\
&= 2L - 56 + 8L + 8L - 224 \\
&\boxed{M_{\text{Truck}} = 18L - 280}
\end{aligned}
$$

Figure A1.2 displays an HL-93 tandem placement on the simple span bridge.

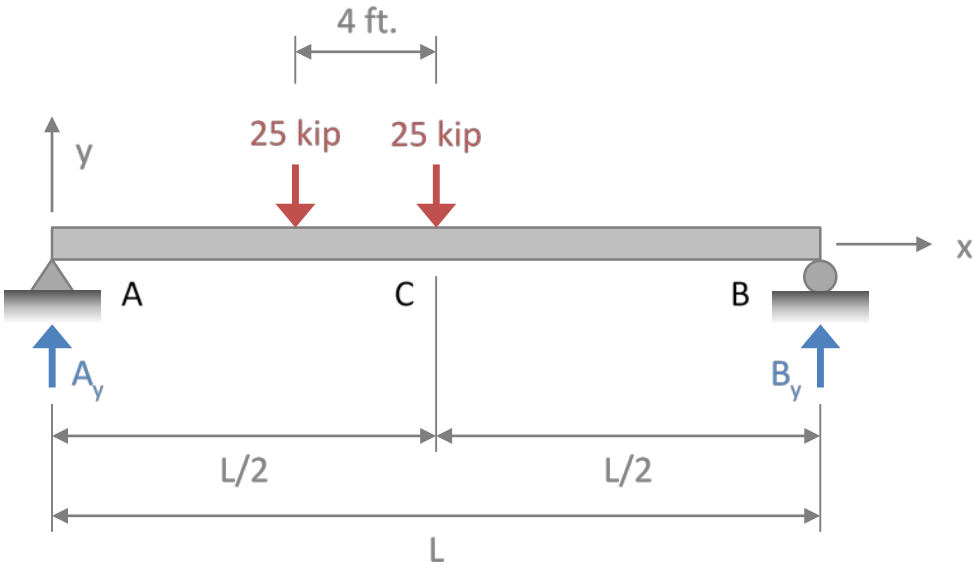

Figure A.2: HL-93 Truck Placement

Using the influence line analysis, the moment induced by the HL-93 tandem is as follows:

$$\begin{aligned} M_{\text{Tandem}} &= \sum_{i=1}^{n} P_i \times f\left(x_i\right) \\ &= 25\times f\left(L/2-4\right)+25\times f\left(L/2\right) \\ &= 25\times\left(L/4-2\right)+25\times\left(L/4\right) \\ &= 6.25L-50+6.25L \\ &\boxed{M_{\text{Tandem}} = 12.5L-50} \end{aligned}$$

Lastly, Figure A1.3 displays an HL-93 lane model.

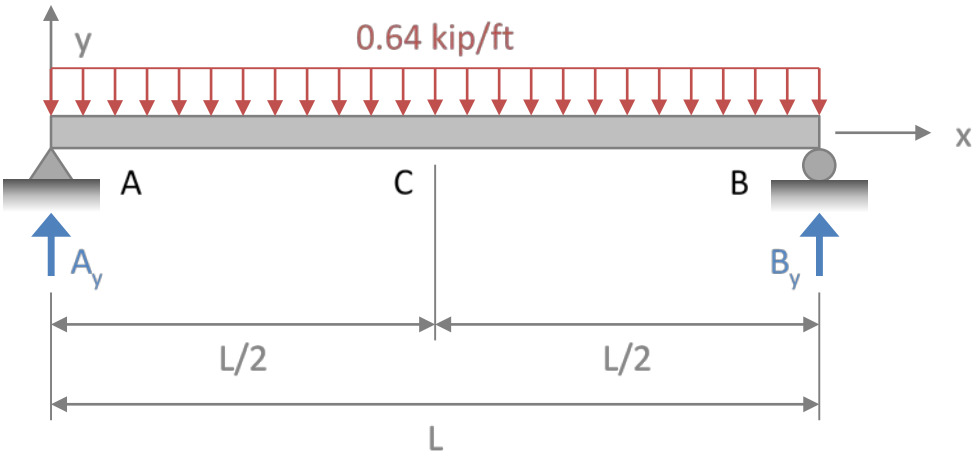

Figure A.3: HL-93 Tandem Placement

The moment at the midspan is determine as follows:

$$\begin{aligned} M_{\text{Lane}} &= \sum_{i=1}^{n} w_i \times A_i \\ &= 0.64\times\left(L^2/8\right) \\ &\boxed{M_{\text{Lane}} = 0.08L^2} \end{aligned}$$

Using a 34.5 foot clear span, moments due to the individual HL-93 truck, tandem, and the lane components were determined and are summarized in Table A1.1.

Table A.1: Summary of Moments due to Individual Components

Component	Moment (kip-ft)
HL-93 Truck	341
HL-93 Tandem	381.25
HL-93 Lane	95.22

The greater of the moments induced by either the truck or the tandem is used in Equation A1-1 as a vehicular load. Therefore, using the moments induced by the tandem and the lane components, the Service II moment was determined:

$$M_{service\ II} = 1.3\left(1.33\times 381.25 + 95.22\right) = 782.97 \text{ kip-ft}$$

To determine a point load that induces such moment, the equation for moment in a simply supported beam was used:

$$M = \frac{PL}{4}$$

$$782.97 = \frac{P\times 34.5}{4}$$

$$P = \frac{782.97\times 4}{34.5}$$

$$P = 90.78 \text{ kip}$$

A similar procedure was used to determine the Fatigue I moment. The AASHTO fatigue load model consists of a single HL-93 truck with rear axle spacing fixed at 30 feet. Since the fatigue truck is longer than the bridge span, only the front and middle axles were used to determine the highest moment induced at midspan. Figure A1.4 shows the AASHTO fatigue truck placement.

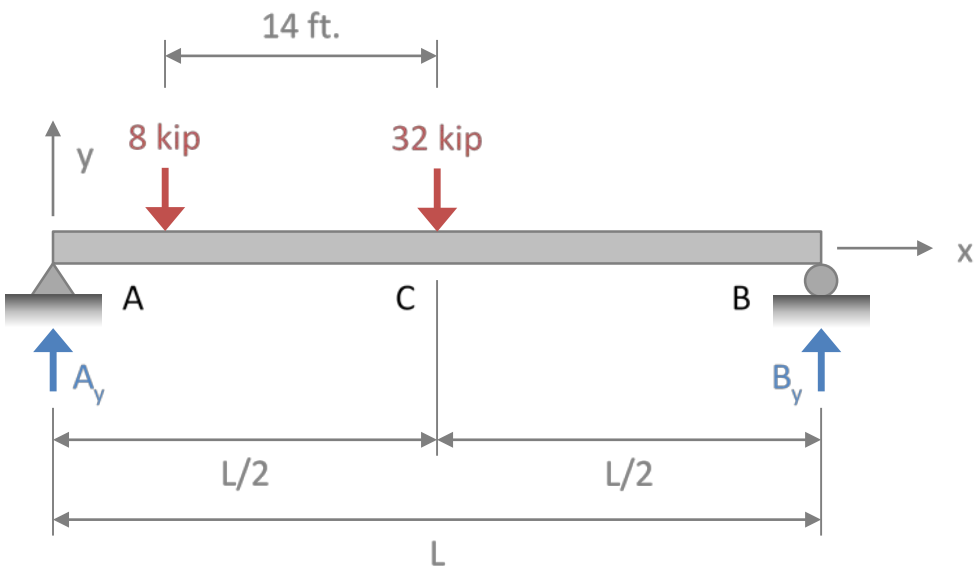

Figure A.4: HL-93 Fatigue Truck Placement

Using the influence line method, the fatigue-induced moment was determined as follows:

$$\begin{aligned} M_{\text{Fatigue Truck}} &= \sum_{i=1}^{n} P_i \times f(x_i) \\ &= 8 \times f(L/2 - 14) + 32 \times f(L/2) \\ &= 8 \times (L/4 - 7) + 32 \times (L/4) \\ &= 2L - 56 + 8L \\ &\boxed{M_{\text{Fatigue Truck}} = 10L - 56} \end{aligned}$$

Equation A1-2 was used to determine the moment:

$$\begin{aligned} M_{Fatigue\ I} = {} & (1.75)(1.15)\left(M_{Fatigue\ Truck}\right) \\ & (1.75)(1.15)(289) \\ & 581.61 \text{ kip-ft} \end{aligned}$$

To determine a point load that induced such moment, the equation for moment in a simply supported beam was used:

$$M = \frac{PL}{4}$$

$$581.61 = \frac{P \times 34.5}{4}$$

$$P = \frac{581.61 \times 4}{34.5}$$

$$P = 67.43 \text{ kip}$$

In summary, the cyclic loading was determined to be 67.43 kips and the static loading was determined to be 90.78 kips.

APPENDIX B: GAGE DATA

Gage	Original Raw Data (N = 0)								
	P = 10 k	P = 20 k	P = 30 k	P = 40 k	P = 50 k	P = 60 k	P = 70 k	P = 80 k	P = 90 k
G01	4.0699	6.4642	9.1936	10.8218	17.2862	20.4465	24.8998	29.2572	31.3645
G02	8.2257	14.4534	21.1455	27.8844	34.1587	40.6652	47.3579	53.4464	59.8139
G03	0	0	0	0	0	0	0	0	0
G04	25.5176	43.8446	61.6622	79.7128	97.949	115.7217	133.449	150.7592	167.7913
G05	29.4463	50.0641	70.3545	90.6923	111.3125	132.263	154.3415	173.978	194.6958
G06	16.431	31.9104	60.4426	91.6458	156.3513	1157.382	4860.206	3849.98	3090.584
G07	10.0246	20.2931	27.1796	38.2712	43.7866	51.557	59.998	53.8722	66.8233
G08	13.6626	22.7866	32.0044	42.3455	52.3591	62.8877	73.0423	82.4481	92.6032
G09	-9.6318	-23.5009	-35.1078	-43.3435	-48.8321	-44.8838	-40.0198	-47.3406	-48.3532
G10	4.2197	7.4653	10.804	13.5861	16.8323	19.568	22.953	25.8279	29.0275
G11	8.1428	15.076	19.2637	24.289	29.5474	35.9687	45.7407	51.697	68.1244
G12	0	0	0	0	0	0	0	0	0
G13	29.3407	50.0276	69.2408	90.0246	109.2396	129.0261	149.0035	166.6509	187.2008
G14	29.6327	50.5017	71.1866	92.0573	112.9755	133.5696	153.3764	172.7198	192.1568
G15	33.428	56.2565	79.1335	102.15	125.494	148.2345	170.185	191.5785	213.4378
G16	23.6817	39.7658	55.8965	72.0743	88.6261	105.4112	120.6582	135.9991	151.4802
G17	14.1972	23.1348	32.6308	42.919	53.1141	63.6355	73.5048	83.6075	94.0361
G18	3.7725	5.4026	8.1042	11.1317	14.5784	18.3512	20.913	23.7076	27.1079
G19	170.8759	260.8268	105.6178	228.7052	60.0738	-120.496	-531.205	-181.531	-300.203
G20	23.4962	39.9863	56.4297	72.921	89.0388	105.4843	122.8649	139.7785	156.6459
G21	0	0	0	0	0	0	0	0	0
G22	58.4404	99.1643	140.5513	182.4134	224.8914	271.0037	315.8474	362.77	405.0748
G23	70.4775	119.5454	168.7123	217.6025	267.576	318.1637	374.7579	451.0545	518.9682
G24	33.3579	39.902	83.2504	49.5209	-412.175	-1012.54	-1320.69	47566.62	47566.62
G25	46.298	78.5071	110.2506	142.2299	174.8201	207.5529	241.3183	275.8819	310.5886
G26	25.0561	43.8012	62.0728	81.2944	102.035	123.2039	147.6962	172.7122	196.2102
G27	-3.3252	-14.8418	6.7386	-23.5495	-11.0519	-5.2947	32.4774	-25.3772	134.3641
G28	9.3698	15.1214	20.8267	26.6254	32.8876	38.7786	45.7373	51.953	58.3552
G29	-41.7596	-24.5997	-85.9486	-109.843	-153.779	-214.942	-244.407	-309.709	-399.862
G30	0	0	0	0	0	0	0	0	0
G31	61.0123	103.9686	146.1329	188.7692	230.7065	273.0222	316.5582	360.3324	403.8761
G32	67.6751	115.4702	162.7134	209.0339	256.0543	302.7078	350.711	398.8579	447.2415
G33	23.0806	64.8769	112.5593	186.498	240.3435	293.6598	351.0387	398.1687	446.3279
G34	45.4525	76.9654	108.5745	141.0339	173.5423	206.0999	239.8846	273.6246	308.1209
G35	27.3632	47.0335	65.6941	88.0112	106.8654	127.9332	152.2247	175.9405	198.9357
G36	0	0	0	0	0	0	0	0	0

Gage	Original Raw Data (N = 100,000)									
	P = 9.08 k	P = 18.16 k	P = 27.23 k	P = 36.31 k	P = 45.39 k	P = 54.47 k	P = 63.55 k	P = 72.62 k	P = 81.70 k	P = 90.78 k
G01	6.334	7.3417	11.9965	10.6048	14.5398	16.459	22.4572	22.3612	25.2885	26.9682
G02	6.3685	11.7145	17.6645	23.5221	29.2865	35.1905	41.0485	45.6975	50.997	56.6688
G03	-24.823	-43.1306	-54.3729	-63.864	-70.6518	-77.0094	-78.883	-85.946	-89.7234	-87.144
G04	19.4905	35.6402	52.0231	68.5913	84.7432	101.22	117.2797	132.7361	148.6118	164.2548
G05	22.2649	40.3646	60.045	79.2957	97.3016	116.1702	136.1411	153.4306	173.2116	191.2689
G06	61.3759	88.0349	152.5615	367.52	45488.49	45488.49	45488.49	45488.49	45488.49	45488.49
G07	0	0	0	0	0	0	0	0	0	0
G08	10.1088	16.9421	24.103	32.1063	39.5012	47.8794	56.8192	66.0866	74.3719	83.1248
G09	1.6389	1.0769	1.3112	1.9199	2.4351	3.2312	5.1513	7.1181	8.8509	11.614
G10	3.8027	6.817	10.4341	13.8194	17.0659	19.8022	22.5845	24.5323	26.8974	29.4019
G11	2.4246	13.521	1.634	2.2415	25.6455	17.5346	13.946	17.9143	17.8207	29.6152
G12	0	0	0	0	0	0	0	0	0	0
G13	21.8723	41.7488	60.1511	78.9351	98.1475	115.9341	133.4356	152.1271	169.44	187.0385
G14	22.7714	41.4626	60.0149	78.8465	97.2145	115.723	134.742	152.7876	170.7878	189.2984
G15	25.2974	46.0855	66.4555	86.4073	106.686	126.8723	147.5713	167.3406	187.7622	208.3703
G16	17.717	30.6791	43.781	57.2097	70.9657	84.7217	99.5039	113.2605	127.484	142.2676
G17	9.1698	16.0133	22.9959	29.9786	37.8924	45.9462	54.6983	63.4042	72.2498	80.9092
G18	1.4912	1.3048	1.8174	2.9354	4.0998	6.29	8.8987	11.1354	13.9777	17.0992
G19	280.5819	144.0104	126.3097	307.5829	110.6215	524.9215	497.3641	282.6273	276.3598	822.8042
G20	21.1297	37.4667	46.0756	64.4678	82.8121	98.6618	124.2477	136.7721	145.1381	157.614
G21	23.6871	40.8092	67.8062	83.1784	113.3884	129.2973	151.3368	177.8529	196.8772	208.9931
G22	52.3917	93.3769	139.9768	197.7567	235.9	273.5232	312.3858	349.1104	366.1422	396.2104
G23	56.869	102.942	149.0659	194.6774	240.7162	285.8188	331.6778	375.5203	423.1258	474.7313
G24	0	0	0	0	0	0	0	0	0	0
G25	22.1687	39.71	57.9663	75.6518	93.5952	111.9675	130.0551	147.3717	165.6033	183.7785
G26	12.9603	23.0502	33.9522	44.1005	55.3509	66.7468	79.7088	90.8148	101.8053	114.6233
G27	0	0	0	0	0	0	0	0	0	0
G28	3.8835	6.5764	9.0424	11.7353	14.2299	17.1778	20.239	23.2725	26.4757	29.6224
G29	-125.196	-192.93	-230.596	-260.847	-318.465	-304.64	-316.222	-338.104	-347.252	-363.27
G30	0	0	0	0	0	0	0	0	0	0
G31	29.8747	54.142	79.0401	103.281	127.4947	151.5661	175.4957	198.5679	221.7556	245.2303
G32	33.8994	61.4517	88.6085	116.1069	143.0394	169.7471	196.2294	222.1173	248.0352	274.1244
G33	-3.1515	-80.9442	-75.0688	-137.258	-71.5965	-116.119	-69.1575	-12.7793	17.5281	-1.1449
G34	21.7513	39.504	57.4296	75.1552	93.2835	110.7798	126.8664	142.9824	159.3	178.8999
G35	13.1805	24.1549	34.1586	44.6922	55.3731	66.3778	77.1474	89.7711	102.5129	113.4009
G36	0	0	0	0	0	0	0	0	0	0

Gage	Original Raw Data (N = 250,000)									
	P = 9.08 k	P = 18.16 k	P = 27.23 k	P = 36.31 k	P = 45.39 k	P = 54.47 k	P = 63.55 k	P = 72.62 k	P = 81.70 k	P = 90.78 k
G01	1.3929	4.9475	8.9826	12.4409	15.4192	15.9958	20.4629	19.07	24.4019	27.7165
G02	7.2503	12.9668	18.9157	24.7256	31.0004	36.4846	42.1552	47.547	53.7752	59.1671
G03	-50.0245	-73.9412	-87.8308	-102.764	-112.024	-119.228	-128.303	-144.244	-146.635	-152.49
G04	22.7834	38.979	55.4994	72.16	88.7278	104.4614	120.5662	136.44	152.7782	168.699
G05	26.6289	45.9791	64.0847	81.424	100.824	120.6556	137.9016	156.5372	175.7481	194.1936
G06	23.9579	35.6977	50.2804	70.6149	75.0063	85.0208	86.0748	83.3035	100.3161	116.3508
G07	0	0	0	0	0	0	0	0	0	0
G08	11.5113	18.7643	25.6434	32.6627	39.5888	47.3099	56.1082	64.6726	74.5474	85.7326
G09	1.641	0.9844	6.47	9.0955	2.4378	-45.8008	-27.1906	15.2844	18.3319	22.6456
G10	4.2197	7.0949	10.3408	13.6796	16.6011	19.1517	21.5629	23.7426	26.479	28.6116
G11	47.1778	67.3926	61.2445	98.2349	166.1987	157.4397	146.3985	146.2126	144.3957	149.7062
G12	0	0	0	0	0	0	0	0	0	0
G13	26.063	45.2782	63.1149	81.7131	100.74	120.9096	137.9401	153.8294	171.622	190.0817
G14	26.8505	45.5404	64.323	82.9212	101.7057	119.934	138.2558	156.4855	175.3189	193.6429
G15	30.0855	50.3605	70.7295	90.8668	111.237	131.3294	151.562	171.656	192.495	213.2417
G16	20.417	33.6558	46.8017	59.8081	73.794	87.5006	101.5806	116.0336	130.674	145.6411
G17	10.8911	17.3141	24.0167	30.9057	38.4927	46.2664	54.7845	63.7685	73.1246	83.0403
G18	1.2112	1.118	1.2578	2.2364	3.8199	5.7304	7.9662	11.0416	14.2562	17.7036
G19	-615.702	-132.537	-95.6948	-713.635	-530.16	-119.151	-165.863	-166.13	-166.996	-235.943
G20	21.3729	34.8565	46.6195	59.1478	74.6888	88.3177	102.6162	114.7632	131.0715	156.8973
G21	5.57	-37.5798	-24.7886	-66.3116	-148.451	-141.63	-170.656	-200.566	-205.857	-45747
G22	54.7443	92.5543	132.5514	174.1538	218.7698	258.2425	291.843	337.586	367.9378	409.4134
G23	63.5451	108.3228	152.0713	197.3731	241.3645	286.2518	331.1429	374.723	419.1528	465.9346
G24	0	0	0	0	0	0	0	0	0	0
G25	42.2852	71.9762	101.3876	131.316	161.1993	191.5062	221.815	251.5629	281.032	311.5802
G26	31.8116	46.5826	66.9393	80.4811	55.9049	60.1637	80.5686	138.5247	299.5491	438.2903
G27	0	0	0	0	0	0	0	0	0	0
G28	7.2829	11.2727	15.3549	19.4835	23.659	28.2054	33.4015	38.2261	43.1435	48.5253
G29	2.1562	16.4384	24.852	38.746	45.8874	48.6451	65.0849	75.4441	80.5707	99.4163
G30	0	0	0	0	0	0	0	0	0	0
G31	57.327	98.045	138.4384	179.0223	219.2352	258.2804	297.4232	335.8658	373.1405	411.5892
G32	64.7284	110.1264	155.3431	200.703	245.2322	289.209	332.8181	375.4103	417.5879	460.4656
G33	3098.534	3714.274	1346.874	-710.743	-716.265	-732.41	-694.297	-669.226	-637.466	-572.595
G34	42.0117	71.1533	99.872	129.3943	155.8054	174.6242	191.5095	206.6029	220.0932	237.6408
G35	25.3382	40.8982	58.1448	75.7293	93.7961	112.0564	131.2327	150.4581	170.6478	189.6817
G36	0	0	0	0	0	0	0	0	0	0

Gage	Original Raw Data (N = 500,000)									
	P = 9.08 k	P = 18.16 k	P = 27.23 k	P = 36.31 k	P = 45.39 k	P = 54.47 k	P = 63.55 k	P = 72.62 k	P = 81.70 k	P = 90.78 k
G01	2.6897	5.5237	7.2531	11.2398	16.1874	17.965	21.9997	25.2182	26.3229	28.7248
G02	8.1797	13.9896	19.9851	26.1668	32.0699	37.8332	43.9221	48.9421	54.5665	60.0046
G03	-8.8373	-15.619	-24.0548	-28.9029	-36.7857	-41.8776	-43.7802	-44.2415	-55.987	-57.0915
G04	22.8311	39.3058	55.5024	72.3027	88.3607	104.6055	120.5719	136.3997	152.2746	168.0105
G05	26.979	45.0295	64.2747	82.9471	101.5727	121.2018	139.1123	157.5966	177.1802	195.6656
G06	-7.0149	-21.8782	-28.2802	-51.2702	-87.5389	-167.891	-246.207	-328.928	-387.21	-316.11
G07	0	0	0	0	0	0	0	0	0	0
G08	11.2683	17.7675	24.0798	30.2987	37.4994	45.168	53.5847	61.5812	71.4481	81.7356
G09	0	0	0	0	0	0	0	0	0	0
G10	3.6169	6.585	9.6918	12.6599	15.6275	18.2245	20.5895	23.2329	26.0155	28.7052
G11	12.6157	-47.472	-51.9768	146.6888	107.0781	117.9596	206.2065	182.8453	164.3918	154.9555
G12	0	0	0	0	0	0	0	0	0	0
G13	24.6404	44.5248	62.6497	80.2996	98.2354	117.2664	134.6326	150.9052	168.3678	186.5447
G14	26.942	45.6771	64.4594	82.964	101.5157	119.6506	138.0645	156.3862	174.8481	193.0319
G15	29.6195	50.3585	70.7265	90.676	110.6275	130.9045	151.09	171.09	191.4162	211.5573
G16	20.3176	33.413	46.2748	59.417	72.6534	86.4024	100.4776	114.8334	129.5157	143.9188
G17	11.1703	17.5001	23.9696	30.486	37.9336	45.5674	53.9459	62.7898	72.0064	81.5024
G18	1.4896	0.8378	0.2793	0.6983	1.6292	3.6303	5.8181	8.3779	11.2635	14.5215
G19	-221.857	14.186	84.93	-300.232	-162.025	47.4929	39.3247	-13.1379	35.0302	50.2047
G20	21.6346	38.1631	53.0206	68.0641	85.2906	102.9354	119.9308	140.8276	156.3848	172.0818
G21	0	0	0	0	0	0	0	0	0	0
G22	31.9953	58.2178	84.1441	110.4885	134.3038	161.0379	183.0097	206.8877	231.6904	253.6056
G23	66.2904	112.5443	157.7279	203.6636	249.8836	297.8374	344.0194	387.4007	427.6065	472.1173
G24	54.1471	92.0443	129.5728	167.4755	204.8234	241.8959	278.8316	315.1657	352.2464	389.0042
G25	38.5969	65.532	82.1161	123.2015	152.5776	182.6114	212.0846	242.0752	277.41	307.4981
G26	29.7453	45.8065	68.5691	92.9967	116.8548	140.6655	166.9978	191.0022	219.7613	252.7502
G27	0	-46219.2	0	0	0	0	0	0	0	0
G28	4.1663	6.3772	8.7013	10.8839	13.4064	16.0425	18.8771	22.0232	25.3966	28.8263
G29	95.9769	119.5296	121.5552	121.3426	97.5789	97.0045	122.1886	134.01	130.8656	135.4003
G30	0	0	0	0	0	0	0	0	0	0
G31	46.3346	79.2607	111.9634	145.0824	177.4501	209.1417	240.7593	271.5502	302.7201	333.703
G32	39.7288	67.5582	95.4737	123.3626	150.6861	177.6424	204.3736	230.823	257.1881	283.6403
G33	40.456	48.6282	70.0273	124.2944	141.653	157.0479	181.8026	212.162	242.3791	270.229
G34	42.4255	71.0702	100.3263	130.006	159.547	189.324	219.572	249.8679	280.3075	310.326
G35	25.6808	41.2919	58.9273	75.3108	92.7545	111.5483	130.536	149.0901	167.5001	188.0322
G36	0	0	0	0	0	0	0	0	0	0

Gage	Original Raw Data (N = 1,000,000)									
	P = 9.08 k	P = 18.16 k	P = 27.23 k	P = 36.31 k	P = 45.39 k	P = 54.47 k	P = 63.55 k	P = 72.62 k	P = 81.70 k	P = 90.78 k
G01	4.1808	6.4391	5.2379	11.0042	9.5145	14.0796	14.8962	18.9327	18.1638	22.5848
G02	7.5325	11.763	17.3895	23.573	28.874	34.918	38.8705	45.148	49.0075	55.0515
G03	53.2677	81.9572	-261.433	-197.719	-156.239	-109.617	-55.1067	-26.2347	12.6783	51.0381
G04	23.5298	38.9389	55.5087	71.1045	86.6539	102.9471	117.5692	133.8163	147.3719	164.0845
G05	29.5857	45.9806	66.2483	84.5089	102.6739	122.4183	140.4892	159.4697	172.7607	193.9418
G06	25.1553	60.2344	164.3836	193.6208	315.1483	465.9098	554.0485	788.1065	921.6124	1009.056
G07	0	0	0	0	0	0	0	0	0	0
G08	10.6256	15.7278	21.8137	27.7584	33.5163	40.9128	47.7007	56.4082	64.8352	73.73
G09	-44.3989	-53.2537	37.4499	6.8945	2.7451	-1.6945	-2.5046	-1.8815	-0.3131	-0.4521
G10	3.3393	5.2413	7.9776	10.668	12.8942	15.2597	16.9759	19.2485	21.1504	23.4698
G11	0.9795	6.7109	19.7106	16.9158	17.5692	17.9889	48.7882	50.8388	66.17	139.2939
G12	0	0	0	0	0	0	0	0	0	0
G13	24.6469	41.3484	60.2869	78.0366	96.1676	111.7294	128.957	146.6142	162.6533	180.5018
G14	26.7578	44.7511	63.2558	81.5753	99.2001	117.6603	134.8687	153.0515	170.4005	188.2137
G15	29.7085	49.98	70.4855	90.34	110.056	129.587	149.0255	168.744	187.998	208.3225
G16	20.3682	33.1858	46.0503	58.8688	71.3146	84.5531	97.7452	111.5906	125.3895	139.8884
G17	11.0317	16.7574	22.8087	29.0925	35.7026	42.7322	50.1802	57.8614	65.7754	74.5739
G18	1.1171	-0.2329	-0.9309	-1.3497	-1.2101	-0.0002	0.7911	3.3049	5.1201	7.9594
G19	133.1029	209.8029	102.6102	341.9306	245.9699	492.6672	377.8161	321.9014	360.4272	562.3645
G20	28.725	42.9025	31.0951	49.4556	65.5859	80.6006	95.2906	110.725	125.3695	141.316
G21	0	0	0	0	0	0	0	0	0	0
G22	4.7949	-62.4374	-2464.77	-2428.17	-2426.17	-2234.54	-2247.43	-2310.25	-2342.27	-2344.65
G23	67.1447	113.2097	161.2946	206.4767	253.2574	301.1214	343.7849	390.3439	434.4221	478.7855
G24	55.3169	94.5673	133.5418	172.7983	211.0356	250.1588	287.6116	326.8339	364.5252	403.0561
G25	43.129	72.7733	102.6066	133.0975	163.9652	196.6613	227.6734	261.264	292.1392	322.7355
G26	21.5104	39.9138	58.8035	70.4583	89.252	109.3578	125.8219	148.6976	168.3199	190.0801
G27	6205.086	19.8662	4261.496	-32940.8	1407.738	4689.39	3642.508	50179.35	50179.35	7025.805
G28	6.4455	9.645	13.6792	17.0184	21.2846	25.8294	30.3739	35.1504	39.9736	45.4922
G29	13.038	30.0444	43.0837	58.8668	66.1255	88.577	97.3554	115.6717	124.8727	133.6091
G30	0	0	0	0	0	0	0	0	0	0
G31	36.4008	62.1287	87.7148	113.5602	138.9488	163.9377	188.7559	213.5188	237.395	261.6731
G32	67.0703	113.9229	160.3154	207.1764	253.2072	299.3807	344.2131	389.6061	433.4713	477.8975
G33	0	0	0	0	0	0	0	0	0	0
G34	42.0623	71.7747	100.8335	131.3914	161.0148	191.8575	222.3741	253.8761	285.2858	316.9788
G35	23.8549	40.2892	57.9288	74.4604	95.572	113.9363	133.4105	151.7767	171.8785	192.8973
G36	0	0	0	0	0	0	0	0	0	0

Gage	Original Raw Data (N = 1,500,000)									
	P = 9.08 k	P = 18.16 k	P = 27.23 k	P = 36.31 k	P = 45.39 k	P = 54.47 k	P = 63.55 k	P = 72.62 k	P = 81.70 k	P = 90.78 k
G01	1.8761	1.9243	6.2541	9.0442	11.8344	13.8551	17.8483	17.3191	22.6591	25.8826
G02	4.6017	8.9251	15.2468	20.3137	25.3806	32.5398	37.3276	41.8371	46.9508	51.6926
G03	0	0	0	0	0	0	0	0	0	0
G04	20.4215	35.5528	51.1947	66.7908	81.4592	98.4953	113.6287	128.391	143.6184	158.0104
G05	22.4701	39.2992	58.2807	77.1195	92.3247	114.9901	133.783	150.4728	169.3627	187.201
G06	-14.9583	-66.9132	-238.666	-411.211	-524.881	-403.565	-341.942	-146.165	189.3246	618.5557
G07	0	0	0	0	0	0	0	0	0	0
G08	10.6246	15.3982	21.4832	27.5682	32.9507	40.5801	47.2267	55.3251	63.6097	71.5209
G09	-1.2134	-4.2469	-6.0671	-8.0738	-10.0805	-8.2605	-7.467	-6.4869	-5.1802	-3.6403
G10	3.1077	5.288	7.9318	10.622	12.6631	16.2348	18.0904	20.2238	22.45	24.7236
G11	2.002	9.6401	16.7656	40.4711	67.2521	82.0177	96.0384	97.6222	101.8143	106.8921
G12	0	0	0	0	0	0	0	0	0	0
G13	25.836	42.2039	59.8571	77.654	94.9756	112.488	129.3825	147.1815	164.2196	179.831
G14	26.3411	44.104	62.0528	79.8629	96.7925	114.6505	131.9061	149.0693	166.4189	183.7229
G15	29.0605	48.729	68.7705	88.5343	106.857	126.5293	145.365	164.806	184.1075	203.3179
G16	19.7629	31.5558	44.328	56.3078	67.6822	80.9213	93.7413	106.9814	120.5944	134.0681
G17	9.6351	14.336	20.0146	25.1346	30.6276	37.8424	44.778	52.4121	60.2324	67.6808
G18	0.326	-2.002	-3.5381	-4.6088	-5.7259	-4.6554	-3.4917	-1.6295	0.6518	2.3276
G19	-118.956	-21.958	-291.526	-260.924	-37.1072	-69.109	137.565	-269.683	-141.238	342.4763
G20	20.27	34.4497	49.9785	65.5082	80.991	97.266	112.6565	128.0955	143.2545	159.0656
G21	0	0	0	0	0	0	0	0	0	0
G22	0	0	0	0	0	0	0	0	0	0
G23	53.7219	92.0272	131.0973	168.6854	205.6665	244.3262	281.3511	317.3883	354.1518	391.4898
G24	56.1185	95.223	134.936	174.3255	213.5795	253.3945	291.1655	329.7308	368.2985	406.8697
G25	42.6676	72.9999	104.3156	135.1188	166.1111	198.5543	230.0183	261.2034	293.3255	325.7305
G26	0	0	0	0	0	0	0	0	0	0
G27	50031.7	50031.7	50031.7	50031.7	50031.7	50031.7	50031.7	50031.7	50031.7	50031.7
G28	5.8447	8.1173	11.4569	14.7501	18.5072	22.5429	26.764	31.4489	36.366	41.4685
G29	20.6248	32.061	47.7914	64.5257	86.7583	100.0822	115.4937	136.3241	142.9867	156.7538
G30	0	0	0	0	0	0	0	0	0	0
G31	60.0509	102.5541	145.7632	188.4613	230.6004	272.6967	313.8129	354.3238	395.0251	436.1983
G32	67.311	114.9257	162.9158	210.4931	257.4258	304.5482	350.5156	395.6522	440.6533	486.5863
G33	145.9077	84.963	145.9686	49.4389	75.2742	-45103	-45485.2	-45356.7	-46008.8	-46710.8
G34	41.251	71.5291	101.052	133.1315	162.9892	194.9782	225.7387	253.0459	283.7151	318.5044
G35	25.8419	41.7047	58.773	77.7227	96.9143	114.949	135.1548	156.615	177.5455	197.175
G36	0	0	0	0	0	0	0	0	0	0

Gage	Original Raw Data (Secondary Alignment Base Test)									
	P = 9.08 k	P = 18.16 k	P = 27.23 k	P = 36.31 k	P = 45.39 k	P = 54.47 k	P = 63.55 k	P = 72.62 k	P = 81.70 k	P = 90.78 k
G01	7.0336	7.6116	12.67	18.8846	21.5826	30.7842	32.6151	37.0956	45.0448	48.9474
G02	22.8722	37.9817	54.6718	69.6887	85.5432	103.1657	119.8117	136.8762	155.3377	172.3103
G03	0	0	0	0	0	0	0	0	0	0
G04	61.8484	104.6176	148.7834	192.3959	235.8263	280.6079	324.4175	367.6273	412.188	455.963
G05	57.175	98.1029	141.0402	175.9057	202.9873	173.3117	230.5899	-124.462	259.6874	-1470.69
G06	-117.935	-167.473	-178.004	-77.5076	-64.1444	246.8733	50096.75	50096.75	50096.75	50096.75
G07	0	0	0	0	0	0	0	0	0	0
G08	22.7858	36.8985	52.512	65.2658	78.77	95.182	109.3907	125.0533	141.7012	156.4743
G09	0	0	0	0	0	0	0	-46057.1	-91341.8	0
G10	1.2997	1.9029	3.3883	4.5485	7.6585	11.1395	14.6664	17.869	21.8145	25.4347
G11	19.1094	32.3468	45.6774	59.3818	74.7643	94.0632	109.6333	123.5254	139.3765	155.6473
G12	0	0	0	0	0	0	0	0	0	0
G13	67.9252	114.7691	162.332	209.3748	255.327	304.7123	349.9108	395.6854	442.6545	490.105
G14	61.4416	104.0145	147.6114	190.284	233.0538	276.5688	319.1138	361.3373	405.0027	447.9297
G15	58.9987	100.1955	141.9065	182.7845	224.177	265.8985	306.2749	346.7935	389.0373	430.2606
G16	35.1103	58.9375	83.3728	107.1097	130.7542	155.659	179.679	203.98	230.2416	255.1045
G17	20.0702	33.2027	46.242	58.8626	71.0181	85.1296	98.6829	112.7954	128.7249	143.304
G18	3.6784	5.4479	6.3326	6.9379	7.2639	8.8006	11.0357	13.7365	17.2756	20.5816
G19	30.1236	81.3364	121.0945	-31.3821	-90.6125	-131.08	-76.776	159.6984	26.0402	74.5329
G20	7.9077	12.8854	17.9564	23.4921	28.3767	33.727	38.4256	43.4965	49.5907	55.3131
G21	0	0	0	0	0	0	0	0	0	0
G22	0	0	0	0	0	0	0	0	0	0
G23	31.9441	54.6685	75.7939	96.4029	115.9303	136.7762	154.6111	172.9174	192.6831	208.449
G24	22.0018	37.7245	53.0755	68.055	82.2439	97.4569	110.8558	125.046	138.911	150.9615
G25	13.1227	22.4627	31.2895	39.7894	47.7289	56.7892	64.4957	72.2022	80.9829	88.6898
G26	0	0	0	0	0	0	0	0	0	0
G27	-5.0719	-14.1058	80.0326	69.698	320.3415	316.5698	288.507	291.9533	284.5321	304.2823
G28	-1.7573	-3.004	-3.5426	-4.4496	-4.7894	-4.8746	-5.2148	-5.5832	-5.7533	-6.0651
G29	0	0	0	0	0	0	0	0	0	0
G30	0	0	0	0	0	0	0	0	0	0
G31	27.5724	46.3896	65.3757	83.8155	101.6669	119.5604	136.1493	152.697	169.0345	184.9096
G32	30.0838	50.9907	71.4814	91.7408	111.2593	130.9641	149.3248	167.5012	185.9099	202.6494
G33	-70.047	-123.541	-212.613	-189.508	-105.152	-246.808	-294.224	-364.768	-347.944	-244.573
G34	13.8425	23.3359	33.0634	42.37	51.8645	61.5457	70.5725	80.2073	89.5618	98.4488
G35	9.0333	13.381	19.0814	23.3807	28.8396	36.2311	42.0285	44.1541	46.5212	49.7582
G36	0	0	0	0	0	0	0	0	0	0

Gage	Original Raw Data (N = 2,000,000)									
	P = 9.08 k	P = 18.16 k	P = 27.23 k	P = 36.31 k	P = 45.39 k	P = 54.47 k	P = 63.55 k	P = 72.62 k	P = 81.70 k	P = 90.78 k
G01	1.5421	0.3373	2.1206	3.3736	7.7591	9.4463	17.6396	24.5313	29.7368	34.4604
G02	19.619	32.962	47.933	62.4855	79.085	95.2195	113.0755	131.257	148.1375	164.8325
G03	0	0	0	0	0	0	0	0	0	0
G04	61.6672	105.6004	151.9526	196.7764	241.1395	283.5551	326.4856	368.7692	409.7082	450.9766
G05	59.2571	102.7259	147.0375	190.1881	232.9233	274.4496	315.56	356.3006	396.1593	435.8341
G06	71.0188	123.0634	178.6325	241.6077	310.5354	398.7021	713.5187	1648.292	3707.72	6019.051
G07	0	0	0	0	0	0	0	0	0	0
G08	19.495	33.976	48.5513	61.9556	77.1407	90.5926	107.2321	123.1685	135.6841	148.9029
G09	0	0	0	0	0	0	0	0	0	0
G10	-1.5776	-4.2688	-5.8464	-7.2384	-6.2176	-3.712	0.7424	6.3573	10.8586	15.2202
G11	17.016	28.6712	40.5596	53.101	66.8552	81.6824	97.6287	114.2282	130.5023	146.2635
G12	0	0	0	0	0	0	0	0	0	0
G13	65.4037	116.2474	165.0493	213.427	261.857	308.5768	354.5387	399.6478	443.4745	486.8286
G14	61.2168	105.8351	151.3391	195.5019	239.3439	281.5649	323.4197	364.8589	405.1421	445.5675
G15	59.053	101.929	145.832	188.5755	230.7185	271.1899	311.6647	351.1194	389.7858	428.3156
G16	34.132	58.0069	82.3962	106.4599	131.1315	154.9644	179.4982	203.6602	226.4238	249.7481
G17	17.6479	29.0567	40.9312	52.9457	66.0781	78.9777	93.7873	107.9457	121.2659	134.866
G18	1.1642	-1.0246	-2.4682	-3.2602	-2.142	-0.6521	2.6082	6.3342	9.8742	12.9945
G19	67.6375	113.2531	117.1802	21.1317	36.351	25.7827	216.7906	41.8982	22.8988	-66.3611
G20	5.5366	8.7004	12.9346	16.7033	21.4024	25.8691	32.011	38.3858	44.2019	49.6924
G21	0	0	0	0	0	0	0	0	0	0
G22	0	0	0	0	0	0	0	0	0	0
G23	29.9581	51.5929	73.8873	95.1476	116.315	137.6713	156.8177	177.6111	196.147	214.872
G24	21.6096	37.3051	53.9325	69.9083	85.419	100.9303	115.9296	130.6494	145.0441	158.554
G25	12.1387	20.9968	30.2304	39.2763	47.9943	56.572	64.3059	73.3524	80.1494	87.3211
G26	-14.382	-22.2598	-34.1058	-38.4412	-40.1814	-43.8451	-46.5929	-50.012	-53.7671	-55.2325
G27	0	0	0	0	0	0	0	0	0	0
G28	-5.6144	-10.2534	-14.3366	-17.6774	-19.5798	-20.1366	-19.951	-18.9302	-17.863	-17.4918
G29	0	0	0	0	0	0	0	0	0	0
G30	0	0	0	0	0	0	0	0	0	0
G31	29.018	50.9702	71.9864	92.5828	113.0861	133.0286	153.0187	173.5246	192.3457	211.6828
G32	28.741	50.2977	71.5307	92.0229	112.3771	132.2678	151.9742	171.542	190.3689	209.3355
G33	-701.356	-721.287	-604.356	1118.789	1242.922	-489.549	-883.275	-965.462	-988.004	333.161
G34	13.806	24.3828	34.632	44.7418	54.4304	64.6806	73.7608	82.9814	92.3428	101.4704
G35	7.049	12.6981	20.4233	23.6583	30.8525	34.522	42.4406	49.0074	53.4982	60.0167
G36	0	0	0	0	0	0	0	0	0	0

Gage	Original Raw Data (N = 2,100,000)									
	P = 9.08 k	P = 18.16 k	P = 27.23 k	P = 36.31 k	P = 45.39 k	P = 54.47 k	P = 63.55 k	P = 72.62 k	P = 81.70 k	P = 90.78 k
G01	3.9042	3.7114	4.82	8.9652	11.7126	16.7746	22.0766	30.8977	37.0196	41.7435
G02	18.784	32.546	46.402	61.6075	77.556	94.204	111.8281	129.7785	147.962	166.193
G03	0	0	0	0	0	0	0	0	0	0
G04	59.2657	104.4626	150.0819	195.287	239.3345	282.5962	325.3038	367.829	409.893	452.1931
G05	57.3666	101.1762	145.0834	188.9941	232.0234	274.1233	315.8542	356.2823	397.4603	437.8019
G06	61.9421	102.5405	150.3719	199.7635	248.6746	298.6567	351.4051	441.8377	778.8089	1379.562
G07	0	0	0	0	0	0	0	0	0	0
G08	20.1573	33.424	47.6285	62.1152	77.399	93.5269	109.0462	125.0818	141.4456	157.6231
G09	717.5173	1136.961	1392.258	46463.29	46463.29	46463.29	46463.29	46463.29	46463.29	46463.29
G10	-1.4843	-4.0353	-6.5863	-7.5602	-6.6326	-3.5718	1.0663	6.5857	12.4761	18.32
G11	15.807	26.9514	39.0286	52.272	66.6345	81.0446	96.4809	113.1769	130.1998	146.8505
G12	0	0	0	0	0	0	0	0	0	0
G13	66.1119	115.2381	164.7496	214.8376	262.4065	310.4086	355.7002	403.7588	447.5822	493.315
G14	58.91	103.7693	149.0043	193.5937	237.6303	280.4638	322.1408	363.6358	404.7622	445.6606
G15	57.3711	100.7986	144.6021	187.9906	230.4994	271.6162	311.9922	351.6738	391.1256	430.4879
G16	32.8214	57.0192	80.9387	105.1856	130.2262	154.5686	179.2855	203.0239	227.2301	251.4372
G17	16.9017	28.7751	40.0899	52.4297	65.2352	79.0189	92.9428	107.4261	121.8633	136.3937
G18	0.4657	-1.3969	-3.3527	-3.958	-3.1198	-1.071	1.8626	5.4943	9.8712	13.5967
G19	-87.2729	19.3401	47.4458	6.5593	164.7339	-55.3139	38.6436	143.919	140.8689	171.1703
G20	5.2104	8.932	12.1889	16.2833	32.8459	39.173	44.9889	58.0628	56.4341	61.6921
G21	0	0	0	0	0	0	0	0	0	0
G22	10.0423	22.488	33.1083	50.2416	58.7929	71.6054	86.3962	99.4527	110.1964	124.3188
G23	28.4127	50.6173	72.2112	94.2296	194.3652	215.5416	235.7305	255.7791	276.0171	295.5026
G24	20.2834	35.707	51.0375	66.6492	82.2611	97.5927	111.8031	126.4816	141.0671	155.1851
G25	10.3871	18.9962	28.5413	37.1975	46.1811	55.8203	64.8045	72.9467	81.3697	89.8863
G26	0	0	0	0	0	0	0	0	0	0
G27	0	0	0	0	0	0	0	0	0	0
G28	-6.1623	-11.2587	-15.3823	-18.6717	-20.7567	-21.3126	-20.9422	-19.5518	-18.0229	-16.6797
G29	0	0	0	0	0	0	0	0	0	0
G30	0	0	0	0	0	0	0	0	0	0
G31	28.5716	49.9778	71.7126	92.5115	113.5923	134.0184	154.0702	174.1697	194.6922	214.8869
G32	28.3998	49.6658	70.8867	91.5058	111.6623	131.7736	151.4221	170.9323	190.5361	210.0478
G33	-785.596	-2352.52	-2356.16	-2952.26	-3760.1	-3418.5	-3988.88	-1402.99	-2195.53	-2285.36
G34	12.5623	23.3967	33.8108	43.8046	53.706	63.4673	73.0418	82.4295	92.1914	101.5328
G35	6.1185	12.427	18.3559	25.9451	32.8228	36.8546	42.4517	50.0415	57.4414	64.0351
G36	0	0	0	0	0	0	0	0	0	0

Gage	Original Raw Data (N = 2,200,000)									
	P = 9.08 k	P = 18.16 k	P = 27.23 k	P = 36.31 k	P = 45.39 k	P = 54.47 k	P = 63.55 k	P = 72.62 k	P = 81.70 k	P = 90.78 k
G01	6.4618	6.8957	4.5328	11.3323	9.0658	12.2967	17.6496	26.8601	35.0099	41.2793
G02	18.7375	32.3145	46.2645	61.004	77.3255	94.1595	111.5524	129.457	147.5475	166.1515
G03	0	0	0	0	0	0	0	0	0	0
G04	59.2587	104.1253	149.7391	194.7071	238.8425	282.4241	324.9875	366.9968	409.3345	451.7691
G05	57.781	101.6802	145.8166	189.3509	232.0499	273.8196	315.0338	355.552	396.2131	436.6445
G06	59.081	99.9938	128.8091	163.7487	209.918	210.4002	231.1028	266.6427	515.4974	831.8274
G07	0	0	0	0	0	0	0	0	0	0
G08	19.2658	33.2352	46.9702	61.2216	75.9422	90.8506	106.3688	122.0284	137.8761	153.8179
G09	-34.3275	-88.241	-108.76	-114.804	-122.552	-145.947	-169.097	-163.055	-156.526	-154.966
G10	-2.1803	-4.8714	-7.5155	-8.8609	-8.4433	-5.7066	-1.1595	4.0363	9.6497	16.1921
G11	15.4017	26.1364	36.4977	48.3996	61.1424	75.659	91.2493	106.747	123.1789	139.938
G12	0	0	0	0	0	0	0	0	0	0
G13	64.7461	113.9774	163.6897	212.3115	260.9857	307.8068	353.1557	399.1275	444.4845	490.5125
G14	59.2508	104.2628	149.6954	194.2514	238.1607	280.8204	322.7878	363.8763	404.8291	445.9242
G15	57.3705	100.844	145.0195	188.036	230.219	271.847	312.223	351.4851	391.3556	430.6708
G16	32.8713	56.9313	81.1794	105.1018	129.5854	154.3499	178.9291	202.8093	226.6912	250.6678
G17	16.9941	28.0755	39.623	51.403	64.3945	78.0847	93.0322	107.5613	121.998	136.2485
G18	0.4656	-1.5839	-3.7732	-4.5183	-3.9595	-1.9098	1.071	4.5181	8.5704	12.8556
G19	8.3849	29.539	-32.3816	-59.4014	-72.1189	-83.7654	-65.6437	-69.7897	-45.3794	-75.1474
G20	5.025	8.9334	12.5626	16.8432	21.5894	26.5678	33.0354	39.1774	45.7849	52.9043
G21	0	0	0	0	0	0	0	0	0	0
G22	15.3996	30.3739	37.4656	48.879	58.4057	69.6677	80.5038	91.2182	107.4122	111.8567
G23	28.3894	49.9058	71.188	94.2601	115.0735	135.4159	154.9594	173.7498	193.7654	211.8978
G24	20.2005	35.3517	50.8304	66.6371	81.9765	97.1294	111.4874	125.6124	140.3453	154.6582
G25	11.8855	21.2445	30.604	39.8699	48.6683	57.4189	66.7789	74.8753	84.1427	92.7071
G26	13.2235	15.8193	22.2637	26.6919	30.9981	36.1902	41.9625	43.2454	47.8878	52.8966
G27	0	0	0	0	0	0	0	0	0	0
G28	-5.9391	-11.135	-15.543	-18.4188	-20.646	-21.5276	-21.2492	-19.6252	-18.6044	-17.1204
G29	0	0	0	0	0	0	0	0	0	0
G30	0	0	0	0	0	0	0	0	0	0
G31	28.6763	49.9971	71.2714	92.1725	112.2777	132.7582	152.6773	173.2535	192.9399	213.002
G32	27.861	48.9086	69.9106	90.7279	110.8042	130.3256	149.8469	169.1373	188.5215	207.7672
G33	-618.033	-3075.48	-3990.05	-4468.52	-4069.52	-5034.35	-5106.37	-5543.8	-2760.28	-2276.57
G34	12.83	23.3188	33.6206	44.2972	54.2718	63.9651	72.7692	82.6509	91.8299	101.7579
G35	7.6877	12.8131	17.8416	24.9495	30.607	38.4405	46.4191	49.9005	55.6549	64.4075
G36	0	0	0	0	0	0	0	0	0	0

Gage	Original Raw Data (N = 2,300,000)									
	P = 9.08 k	P = 18.16 k	P = 27.23 k	P = 36.31 k	P = 45.39 k	P = 54.47 k	P = 63.55 k	P = 72.62 k	P = 81.70 k	P = 90.78 k
G01	1.4958	1.1581	-2.4607	0.7719	5.3557	12.9309	18.2383	25.8136	36.1875	35.6567
G02	18.32	31.5725	45.662	60.4035	76.0285	92.5375	109.931	127.3715	145.8357	164.161
G03	0	0	0	0	0	0	0	0	0	0
G04	58.9917	104.5639	150.2333	195.7211	239.9581	283.2694	326.306	368.6954	410.9485	453.5314
G05	57.7524	102.5507	147.2136	190.9479	233.6136	276.0495	317.4629	358.0405	398.6211	439.2517
G06	55.559	92.7628	135.9944	167.3224	182.8915	227.8721	304.4068	344.7798	320.8073	320.7981
G07	0	0	0	0	0	0	0	0	0	0
G08	19.691	33.5689	47.9632	62.4982	76.9868	91.7104	107.1849	122.5656	139.1662	154.6422
G09	0	0	0	0	0	0	0	0	0	0
G10	-2.7381	-5.801	-8.4464	-9.8388	-9.0031	-6.4975	-2.2741	2.6453	8.1683	14.1555
G11	-16.4567	462.7177	589.6113	445.4121	328.3553	603.6122	580.5571	559.7408	516.8578	483.3631
G12	0	0	0	0	0	0	0	0	0	0
G13	61.8569	110.6238	161.3008	209.3154	255.6668	302.3563	348.9067	392.5549	438.6373	484.4379
G14	59.153	104.5312	149.868	194.651	238.5573	281.3058	323.223	364.7257	405.5823	446.8132
G15	57.4172	101.403	145.392	188.8744	231.29	272.5465	313.2015	353.162	392.7071	432.2089
G16	32.5645	57.0589	81.4617	105.8187	130.1767	154.8163	179.3168	203.2119	227.7615	251.8457
G17	17.0491	28.229	39.549	51.4288	64.6127	78.0297	91.7735	105.9369	120.5207	134.6851
G18	0.6062	-1.5854	-3.8233	-4.8025	-4.103	-2.3314	0.4662	4.0097	7.6465	12.0297
G19	-32.6109	-83.8432	-116.217	-111.227	-163.513	-151.527	-140.986	-165.985	-157.823	-193.872
G20	4.7442	8.0003	11.0703	15.0708	18.978	23.9089	29.165	35.0727	41.3525	48.0049
G21	0	0	0	0	0	0	0	0	0	0
G22	15.0963	28.3971	40.7547	51.6212	63.7966	76.9771	86.8397	101.7559	114.7241	123.8265
G23	28.2463	49.7616	71.1836	92.418	112.4292	132.724	151.4653	171.1494	191.0697	209.9077
G24	20.16	36.185	52.023	67.72	82.618	97.611	112.041	126.3296	141.136	155.3315
G25	12.3988	21.3821	31.1148	40.7538	50.1586	58.956	67.5194	76.4572	85.2078	94.0052
G26	40.6001	49.2965	55.084	53.2772	56.9212	58.9425	61.3921	65.8017	70.0582	68.6498
G27	0	0	0	0	0	0	0	0	0	0
G28	-5.8944	-11.6499	-15.9197	-18.8438	-21.1642	-22.0925	-21.9533	-21.5355	-20.0969	-18.8901
G29	5.4186	9.2348	11.1668	16.2556	22.3339	28.6008	34.9149	40.6634	47.4017	54.4699
G30	0	0	0	0	0	0	0	0	0	0
G31	30.9407	50.597	74.3927	95.1791	113.9446	133.1805	153.3582	172.9251	193.6688	213.3785
G32	27.6833	48.4121	68.7242	89.1303	108.6092	127.8106	146.4565	164.8708	183.7034	202.3975
G33	0	0	0	0	0	0	0	0	0	0
G34	13.9228	23.8144	34.2688	44.9106	54.6624	64.0856	74.0251	82.7924	92.3103	101.7349
G35	14.2236	16.3039	22.932	30.2861	37.6883	43.2041	47.4617	53.4129	59.7996	67.009
G36	0	0	0	0	0	0	0	0	0	0

Gage	Original Raw Data (N = 2,500,000)									
	P = 9.08 k	P = 18.16 k	P = 27.23 k	P = 36.31 k	P = 45.39 k	P = 54.47 k	P = 63.55 k	P = 72.62 k	P = 81.70 k	P = 90.78 k
G01	2.9468	1.4494	2.9468	2.1256	6.0385	6.0867	14.7824	17.8259	25.9902	31.5939
G02	18.3685	31.5755	45.2011	59.339	74.78	91.616	109.1974	126.872	144.966	163.2934
G03	0	0	0	0	0	0	0	0	0	0
G04	59.3673	105.3146	151.6378	196.8963	241.1369	285.3811	328.5134	370.6736	413.3951	455.7481
G05	57.4322	102.375	147.6954	191.7604	231.8654	276.5445	318.802	360.0833	400.9482	442.2362
G06	50.8535	95.0566	135.9098	180.7431	222.1297	265.9151	347.6997	513.6158	763.7605	1284.917
G07	0	0	0	0	0	0	0	0	0	0
G08	19.2683	33.0048	48.0079	61.1825	76.421	92.9258	108.9616	124.8113	139.6762	156.4644
G09	0	0	0	0	0	0	0	0	0	0
G10	-2.5984	-6.2176	-8.9552	-10.9968	-10.9504	-8.2592	-3.5728	1.6704	7.0997	13.0394
G11	-156.97	-272.785	-317.416	-439.507	-680.126	-629.563	-526.745	-532.319	-525.861	-518.465
G12	0	0	0	0	0	0	0	0	0	0
G13	65.6533	115.5055	168.9345	216.8443	266.1401	314.2495	361.4585	406.9089	453.0783	498.8229
G14	59.7492	105.1698	150.6862	195.9756	240.108	283.1309	325.6934	366.6813	407.9972	449.4092
G15	57.751	101.6965	146.111	189.785	232.0675	273.9812	315.0149	354.7951	394.4859	433.9004
G16	33.02	57.2266	81.3415	106.0169	130.6938	155.2785	180.2843	204.4049	228.6666	252.6027
G17	16.903	28.3118	39.4414	51.456	64.123	78.2806	92.6245	106.5965	121.0347	135.5666
G18	0.2796	-2.0977	-4.2885	-5.7338	-5.2678	-3.3562	-0.233	3.1698	6.9458	11.1414
G19	-4.433	-6.5794	14.5125	5.647	11.9936	4.4814	-6.6718	5.787	52.4559	37.3806
G20	4.6527	7.8163	11.0266	14.3768	18.6107	23.5894	28.94	38.897	46.0628	53.0425
G21	0	0	0	0	0	0	0	0	0	0
G22	12.1124	26.477	43.7336	47.7509	64.6124	77.0306	93.4058	100.5285	112.7649	124.0275
G23	27.79	49.9751	73.1513	91.8059	114.277	136.7493	158.8452	177.6446	197.2452	214.8676
G24	18.2691	34.1501	50.6878	61.6499	76.5484	93.1338	109.064	120.8244	135.3498	146.783
G25	12.6798	21.0557	30.6479	37.5734	48.5697	57.9752	68.6446	76.6937	85.4443	92.2771
G26	3.3744	4.0736	6.2624	7.2048	9.3637	12.5253	15.3834	17.2378	18.3626	21.3722
G27	0	0	0	0	0	0	0	0	0	0
G28	-6.263	-11.9692	-16.5154	-20.1336	-22.0824	-23.2887	-22.732	-21.804	-20.7368	-19.4845
G29	6.8334	7.6818	8.4831	20.6422	23.3759	34.027	39.9655	47.6483	53.4455	58.1588
G30	0	0	0	0	0	0	0	0	0	0
G31	27.9969	50.0023	70.6508	91.8148	111.9967	132.273	152.7845	172.6408	192.9666	212.6841
G32	27.5837	48.9564	70.2833	90.6377	110.8075	130.236	149.8509	169.0956	188.5727	208.19
G33	-0.3674	-18.8431	-45.0425	9009.86	-45222.4	-45149.9	9094.57	50.1008	-45070.6	-45074.4
G34	13.4583	23.9629	34.5613	44.4093	54.5865	64.2001	74.1429	83.6167	93.4188	102.6112
G35	9.4799	14.3167	20.2177	26.1188	31.5848	35.6478	41.8391	47.1118	51.4168	58.3338
G36	0	0	0	0	0	0	0	0	0	0

Gage	Original Raw Data (N = 2,700,000)									
	P = 9.08 k	P = 18.16 k	P = 27.23 k	P = 36.31 k	P = 45.39 k	P = 54.47 k	P = 63.55 k	P = 72.62 k	P = 81.70 k	P = 90.78 k
G01	1.6445	2.3217	0.7741	1.6928	-0.0967	6.7711	12.478	18.1368	23.4085	32.4531
G02	18.5108	31.4413	44.976	59.3489	74.8854	91.3986	108.8894	126.2415	144.152	162.5755
G03	0	0	0	0	0	0	0	0	0	0
G04	59.8881	105.796	151.8476	197.6246	242.2904	286.1701	329.7282	372.1738	415.0419	459.8659
G05	58.2285	102.9416	147.4724	191.774	234.8668	277.0305	318.4045	359.5958	400.1368	441.6612
G06	30.3293	56.5571	84.7494	97.7567	151.2098	280.2186	1633.677	3988.624	48674.62	48674.62
G07	0	0	0	0	0	0	0	0	0	0
G08	21.2757	35.272	50.302	65.1447	81.4907	97.18	114.8425	130.2976	146.9749	164.3101
G09	0	0	0	0	0	0	0	0	0	0
G10	-3.0174	-5.9416	-9.6087	-11.4657	-11.5121	-9.2839	-5.1059	0.0465	5.1526	11.3731
G11	-245.792	-367.522	-394.267	-414.398	-426.332	-49175	-49747.8	-50011.7	-50283.1	-52001.3
G12	0	0	0	0	0	0	0	0	0	0
G13	66.1862	116.6647	164.9573	214.3504	265.1292	310.4822	357.0782	401.6769	447.8523	494.5084
G14	59.9408	105.319	151.3508	196.2736	240.55	283.2989	326.0047	367.1359	408.1775	449.7334
G15	58.26	102.808	147.4531	191.5905	234.6155	276.2952	317.792	357.6641	397.5391	437.4175
G16	33.3474	57.7878	81.9961	106.5789	131.4895	155.9344	181.1274	205.3417	229.2775	253.8671
G17	17.4174	28.4083	39.6326	51.6021	64.7363	78.1505	92.8224	106.4701	120.8169	135.2574
G18	0.746	-1.3524	-3.9639	-5.6428	-4.7569	-2.9844	-0.2332	2.9843	6.762	10.8662
G19	145.6411	-176.157	-397.62	-564.266	-371.009	-191.46	-196.632	-297.728	-284.82	-218.693
G20	5.1176	8.0019	10.9331	14.2359	18.3304	22.5639	28.2399	34.1021	40.1505	46.7104
G21	0	0	0	0	0	0	0	0	0	0
G22	19.6233	31.0809	42.1122	58.9336	71.3976	83.9535	97.8202	111.809	125.5848	136.4048
G23	28.9657	49.7846	70.9343	90.3886	110.8805	129.6294	152.2899	171.7002	190.4519	207.932
G24	21.6632	37.5593	53.2689	68.932	85.3455	99.7898	115.595	129.5243	143.736	157.9008
G25	12.7693	21.7505	30.4043	40.9291	50.8461	60.7169	70.0729	80.3644	89.9081	98.142
G26	-1.7649	-5.2032	-7.3635	-6.7854	-7.0288	-10.1932	-10.2846	-7.7593	-8.0938	-10.7411
G27	0	0	0	0	0	0	0	0	0	0
G28	-5.8015	-10.953	-15.5006	-19.3528	-21.3021	-22.6018	-21.9986	-21.3487	-20.1416	-19.4456
G29	17.0159	39.6043	60.7139	59.0866	82.6638	105.4528	117.2922	136.4325	149.3583	168.4012
G30	0	0	0	0	0	0	0	0	0	0
G31	28.6599	49.9097	70.5502	91.6611	112.5848	132.7121	152.8868	172.9219	193.3329	213.1817
G32	27.6415	48.3274	68.5965	88.1711	107.607	126.7653	144.6253	163.043	181.2289	199.6013
G33	-46277.5	-46287	-46556	-46104.5	-46907.3	-47757.7	-47920.4	-46372.6	-47880.6	-47979.6
G34	13.0095	24.0463	34.7548	44.665	54.7166	64.4393	73.9273	83.5093	92.6693	101.5469
G35	7.0734	14.8253	19.9125	28.5854	29.1668	35.3201	42.4911	47.6271	53.9745	59.6436
G36	0	0	0	0	0	0	0	0	0	0

Gage	Original Raw Data (N = 2,800,000)									
	P = 9.08 k	P = 18.16 k	P = 27.23 k	P = 36.31 k	P = 45.39 k	P = 54.47 k	P = 63.55 k	P = 72.62 k	P = 81.70 k	P = 90.78 k
G01	0.4356	2.7588	2.2748	4.2108	2.5652	7.7921	9.2442	16.8422	29.1842	32.6209
G02	18.1385	31.0685	44.1384	58.4179	73.5816	89.816	107.1668	125.0769	143.0805	160.8059
G03	0	0	0	0	0	0	0	0	0	0
G04	60.1205	106.2149	151.8951	197.8116	242.5706	285.1949	329.311	372.4079	414.9969	457.2644
G05	58.8294	104.1909	148.9507	193.3411	236.3835	277.4238	320.2866	361.3807	400.8919	440.9191
G06	0	0	0	0	0	0	0	0	0	0
G07	0	0	0	0	0	0	0	0	0	0
G08	21.4376	36.1525	50.022	64.9259	80.6767	95.9109	111.8978	128.5437	144.9545	161.6016
G09	5.5786	7.5109	8.6413	10.0268	12.8706	17.246	21.6944	27.492	33.5811	38.0295
G10	-2.9711	-6.685	-10.6307	-12.8588	-12.8124	-10.4914	-6.685	-1.0213	4.178	9.9343
G11	-80.2954	-38.3866	-182.931	416.2429	1194.955	1106.262	1260.823	1390.793	1343.84	1478.818
G12	0	0	0	0	0	0	0	0	0	0
G13	67.6605	117.5189	169.0012	217.7742	266.7896	312.1892	358.8316	403.9537	449.0318	494.6383
G14	59.8934	105.3634	151.1158	196.6871	240.9163	282.8284	325.9979	367.4532	408.726	449.956
G15	58.026	102.6205	146.9855	191.029	233.8204	274.5689	316.437	356.2615	395.9031	435.5012
G16	33.3979	57.9349	81.6798	106.499	131.6461	155.5812	180.5908	204.9947	229.4467	253.3397
G17	17.5075	28.8691	39.812	51.9657	64.9581	77.9505	92.2011	106.8709	121.1218	135.187
G18	0.7923	-1.8185	-4.8492	-6.0146	-5.4085	-3.8235	-0.6531	2.8437	6.7135	10.63
G19	-51.3954	62.55	-23.2262	22.0431	-45.1331	-49.6005	26.8805	-221.732	-174.271	-211.048
G20	4.9772	7.8147	10.5593	14.048	17.8624	22.0489	27.7242	33.5855	40.0054	46.1923
G21	382.9426	600.2486	45897.2	45983.39	46135.01	46170.23	46274.61	46309.48	46361.14	46369.7
G22	0.4881	8.7925	15.723	22.2571	32.3328	40.1493	51.2334	62.6533	69.188	73.6769
G23	17.4497	30.9906	43.4968	55.7155	68.4809	80.3265	91.0225	104.6802	116.0953	127.5107
G24	13.0737	22.9939	32.8284	42.1468	52.2968	61.5871	70.1031	80.3973	89.2294	98.1474
G25	7.6855	13.5427	19.1719	24.8578	30.8297	36.4302	40.5447	47.6884	52.7746	58.0042
G26	-2.4106	-1.5563	-3.265	-1.0374	-1.251	2.4718	0.885	5.5537	5.523	6.2248
G27	-59.2139	-249.875	-230.83	-45563.6	-222.49	-220.183	-7851.01	-43686.9	48170.23	-42371.2
G28	-3.8548	-6.8593	-9.8354	-12.0745	-13.1513	-13.8317	-13.9735	-12.6979	-11.9892	-11.2243
G29	0	0	0	0	0	0	0	0	0	0
G30	0	0	0	0	0	0	0	0	0	0
G31	28.8843	49.7987	71.0424	91.8171	112.5938	132.0573	151.8501	173.0509	193.3611	212.734
G32	27.723	48.6786	68.754	88.9231	108.4902	127.0843	146.1428	166.1756	185.1891	202.9977
G33	-46733.5	-48721.8	-49308.1	-50020.1	-50637.9	-50953.2	-51114.7	-51247	-51492.5	-51518.3
G34	13.3396	23.6265	34.759	44.9524	55.1928	64.3063	74.1714	84.4126	94.043	102.969
G35	5.2304	13.7548	19.9544	26.5898	32.4505	39.6189	45.8671	54.2953	59.5751	65.0485
G36	0	0	0	0	0	0	0	0	0	0